SYNTHESIS AND CHARACTERIZATION OF HYBRID MATERIALS AND THEIR APPLICATION FOR DECONTAMINATION OF GROUNDWATER FROM HEAVY METEALS AND RADIONUCLIDES

By

Hirakendu Basu

(CHEM 01201204013)

Bhabha Atomic Research Center, Mumbai

A thesis submitted to the

Board of Studies in Chemical Sciences

In partial fulfillment of requirements

For the Degree of

DOCTOR OF PHILOSOPHY

of

HOMI BHABHA NATIONAL INSTITUTE

October, 2016

Homi Bhabha National Institute

Recommendations of the Viva Voce Committee

As members of the Viva Voce Committee, we certify that we have read the dissertation prepared by **Hirakendu Basu** titled "**Synthesis and characterization of hybrid materials and their application for decontamination of groundwater from heavy metals and radionuclides**" and recommend that it may be accepted as fulfilling the thesis requirement for the award of Degree of Doctor of Philosophy.

Chairman - Prof. B. S. Tomar		**Date:** 1/11/2016
Guide / Convener – Dr. R. K. Singhal		**Date:** 27/10/2016
Examiner - Prof. S. Chidambaram		**Date:** 27/10/16
Member 1- Prof. R. M. Tripathi		**Date:** 27/10/2016
Member 2- Prof. A. K. Tyagi		**Date:** 27/10/2016

Final approval and acceptance of this thesis is contingent upon the candidate's submission of the final copies of the thesis to HBNI.

We hereby certify that we have read this thesis prepared under our direction and recommend that it may be accepted as fulfilling the thesis requirement.

Guide

Date: 27-10-2016
Place: Mumbai

STATEMENT BY AUTHOR

This dissertation has been submitted in partial fulfillment of requirements for an advanced degree at Homi Bhabha National Institute (HBNI) and is deposited in the Library to be made available to borrowers under rules of the HBNI.

Brief quotations from this dissertation are allowable without special permission, provided that accurate acknowledgement of source is made. Requests for permission for extended quotation from or reproduction of this manuscript in whole or in part may be granted by the Competent Authority of HBNI when in his or her judgment the proposed use of the material is in the interests of scholarship. In all other instances, however, permission must be obtained from the author.

Hirakendu Basu.

Hirakendu Basu

DECLARATION

I, hereby declare that the investigation presented in the thesis has been carried out by me. The work is original and has not been submitted earlier as a whole or in part for a degree / diploma at this or any other Institution / University.

Hirakendu Basu

List of Publications arising from the thesis

Publications in refereed journals

a. Published:

1. Highly efficient removal of TiO_2 nanoparticles from aquatic bodies by silica microsphere impregnated Ca-alginate. **H.Basu**, R.K.Singhal, M.V.Pimple; New Journal of Chemistry, **2016**, 40, 3177—3186.
2. Arsenic removal from ground water by goethite impregnated calcium alginate beads. **H.Basu**, R.K.Singhal, M.V.Pimple, A.V.R.Reddy. Water, Air, and Soil pollution, **2015**, 226:22.
3. Synthesis and characterization of silica microsphere and their application in removal of Uranium and Thorium from water. **H.Basu**, R.K.Singhal, M.V.Pimple, A.V.R.Reddy. International Journal of Environmental Science and Technology, **2015**, 12 (6), 1899-1906.
4. Development of natural sorbent for decontamination of drinking water from low level of transuranic and other long-lived radionuclides. R.K.Singhal, **H.Basu,** A.V.R.Reddy. Journal of Environmental Analytical Chemistry, **2014**, 1:2.
5. Synthesis and characterization of alumina impregnated alginate beads for fluoride removal from potable water. **H.Basu**, R.K.Singhal, M.V.Pimple, A.V.R.Reddy. Water, Air, and Soil pollution, **2013**, 224:1572.
6. Removal of environmental level of $^{239+240}$ Pu and ^{241}Am from groundwater by using humic coated colloidal suspension of goethite (α-FeO(OH)). R.K.Singhal, **H.Basu**, A.V.R.Reddy. Journal of Radioanalytical and Nuclear Chemistry, **2013**, 295, 1345-1351.

7. Removal of low level americium-241 from potable water originated from different geochemical environments by calcium alginate. R.K.Singhal, **H.Basu**, V.Manisha, A.V.R. Reddy, T. Mukherjee. Desalination 280, **2011**, 313–318.

b. Communicated:

1. Chitosan impregnated Ca-alginate: A new hybrid material for removal of uranium from potable water. **H. Basu**, R.K.Singhal, S.Saha, and M.V.Pimple.

c. **Other Publications:**

1. Association and Migration of Uranium and Thorium with Silica Colloidal Particles in Saturated Subsurface Zone. **H. Basu**, R.K. Singhal, M.V. Pimple, A. Kumar, A.V.R. Reddy. Journal of Radioanalytical and Nuclear Chemistry, 2014, 303, 2283–2290.
2. Influence of molecular assembly and NaCl concentration on gold nanoparticles for colorimetric detection of cysteine and glutathione J.Bhamore, Karuna A.Rawat, **H.Basu**, R.K.Singhal, S.K.Kailasa. Sensors and Actuators B, 2015, 212, 526–535.
3. Simultaneous colorimetric detection of four drugs in their pharmaceutical formulations using unmodified gold nanoparticles as a probe Karuna A.Rawat, **H.Basu**, R.K.Singhal, S.K.Kailasa. RSC Advances, 2015, 5, 19924-19932.
4. One-step hydrothermal approach to fabricate carbon dots from apple juice for imaging of mycobacterium and fungal cells V.N.Mehta, S.Jha, **H.Basu**, R.K.Singhal, S.K.Kailasa. Sensors & Actuators: B. Chemical, 2015, 213, 434–443.
5. One-step synthesis of fluorescent carbon dots for bacteria and fungus cells imaging B.S.B.Kasibabu, S.L.D'souza, S.Jha, **H.Basu**, R.K.Singhal, S.K.Kailasa. Analytical Methods, 2015, 7, 2373.

6. Physical speciation of thorium in aquatic environment having elevated levels of dissolved humus materials. R.K.Singhal, **H.Basu**, M.V.Pimple, ManishaV., M.K.T.Bassan, A.V.R.Reddy. Journal of Radioanalytical and Nuclear Chemistry, 2014, 301, 805–810.
7. Spectroscopic determination of U(VI) species sorbed by the Chlorella (Chlorella pyrenoidosa) a fresh water algae. R.K.Singhal, **H.Basu**, M.K.T.Bassan, M.V.Pimple, V. Manisha, M.K.T.Bassan, A.V.R.Reddy. Journal of Radioanalytical and Nuclear Chemistry, 2013, 298, 587-592.
8. Remediation of malathion contaminated soil using zero valent iron nano-particles. R.K. Singhal, B. Gangadhar, **H.Basu**, ManishaV., G.R.K.Naidu, A.V.R.Reddy. American Journal of Analytical Chemistry, 2012, 3, 76-82.
9. Development of naturally occurring siliceous material for the preferential removal of thorium from U–Th from aquatic environment. **H.Basu**, R.K.Singhal, M.V.Pimple, V. Manisha, M.K.T.Bassan, A.V.R.Reddy, T.Mukherjee. Journal of Radioanalytical and Nuclear Chemistry, 2011, 289, 231–237.

d. Conference publications:

1. Arsenic removal from ground water by goethite impregnated calcium alginate beads. **H.Basu**, R.K.Singhal, M.V.Pimple, and A.V.R.Reddy. Proceedings of the International Conference on Environmental Pollution and Remediation. Toronto, Ontario, Canada, July 15-17, 2013.
2. Synthesis and characterization of silica microspheres and its use to remove traces of U, Th from potable water; **H.Basu**, R.K.Singhal, M.V.Pimple and A.V.R.Reddy. Proceedings of Nuclear and Radiochemistry Symposium. Govt. Model Science College, Jabalpur, India. Feb, 19-23, 2013.

Dedicated to my family

ACKNOWLEDGEMENTS

First of all, I would like to express my deepest appreciation and sense of gratitude to my mentor and guide **Dr. R.K. Singhal**, Analytical Chemistry Division for introducing me to present area of research. The present thesis work would not have been possible without his endless support, valuable guidance and constant encouragement. His contagious enthusiasm and uninterrupted motivation has driven me to carry out timely submission of this dissertation.

Further, I am extremely grateful to **Prof. B. N. Jagatap**, Head, Analytical Chemistry Division and Director, Chemistry Group, BARC for providing me valuable advise with lots of constructive criticisms which served as a vital source of inspiration.

I sincerely thank **Smt. M.V. Pimple** and **Ms. Sudeshna Saha,** Analytical Chemistry Division for helping me in conducting the laboratory experiments, analyzing samples and providing enormous assistance during my experimental works. I express my sincere thanks to my colleagues **Smt. Manisha Venkatesh, Dr. M.K.T. Bassan**, Analytical Chemistry Division for their valuable advice and help during my experimental works. I am also thankful to all other colleagues of Analytical Chemistry Division for providing countless assistance over the years.

I am highly grateful to the doctoral committee members, **Prof. B.S. Tomar,** chairman, **Prof. R.M. Tripathi,** member, **Prof. A.K.Tyagi**, member, for constant guidance and encouragement not only during the progress review meetings but also whenever I approached.

My deepest gratitude goes to my family for their unflagging love and support throughout my life; this dissertation is simply impossible without them. I am indebted to my

parents (**Maa** and **Baba**), my wife **Ranita** and sister **Nabaruna** for their care, dedication and love. Words fail me to express my appreciation for my little son **Bhumit**, playing and talking to him after a hard working day was the best way to be relaxed. I would also like to thank all my friends for their backing and encouragement during the dissertation work.

Further, I would like to thank the **Almighty**, without Him I could do nothing.

Finally, I would like to thank everybody who was important to the successful realization of this dissertation, as well as expressing my apology that I could not mention personally one by one.

Hirakendu Basu

CONTENTS

Synopsis

The contamination of groundwater by heavy metals originating either from natural soil sources or from anthropogenic sources is a matter of utmost concern to the public health. Remediation of contaminated groundwater is of highest priority since billions of people all over the world use it for drinking purpose. Depending on local geology, groundwater contains heavy metals (including radioactive elements) in low levels, but sometimes in concentrations which are not acceptable for drinking water. These heavy metals may be radioactive or even nanoparticles. They are not biodegradable and tend to accumulate in living organisms, causing various diseases and disorders. Treatment processes for contaminated ground water include filtration, centrifugation, chemical precipitation, coprecipitation, micro- and ultra filtration, sedimentation and gravity separation, flotation, coagulation, oxidation, solvent extraction, evaporation, distillation, reverse osmosis, ion exchange, electrolysis, adsorption etc. Adsorption is considered as one of the suitable water treatment methods due to the availability of a wide range of adsorbents and its ease of operation. Adsorption can be applied for the removal of organic, inorganic, and biological pollutants both in soluble and insoluble forms. Generally, packed bed columns, with a stable, porous material that has a specific grain size, are used. In spite of these facts, adsorption has certain limitations such as it could not achieve a good status at commercial levels. Probably, it is due to the lack of suitable adsorbents of high capacity to prepare commercial scale columns and a single adsorbent cannot be used for all kind of contaminants. Moreover, tailored materials must be stable and resistant to the medium that is investigated so that there is no release of constituent components. Therefore cost effective alternative technologies or sorbents for treatment of contaminated groundwater are need of the modern days. The high

sorption capability exhibited by many biogenic material such as algae, bacteria, and yeasts or geological materials like silicate and aluminate could be exploited to develop a cost effective method for treating such waters. These geogenic and biogenic matrices can be tailored by chemical modification or by incorporation of suitable material in the matrix. This will not only make them specific to some metal ions or radionnuclides but will also enhance their sorption capacity. Composites consisting of two different components are called hybrid materials. Normally one component is inorganic in nature and the other is organic. Combining a inorganic matrix with biological systems offers important advantages. Algae appear to be one of the very promising materials in this regard. Dried algae or even algal extraction residues can be used as sorption material or for immobilizing the specific sorbent. The hybrid materials synthesis by impregnating inorganic material in organic matrices or vice versa shows enhances applicability in wastewater treatment. Hybrid materials could not only be effective in the removal of inorganic pollutants but also show fair affinity towards the radioactive and nanoparticle impurities as well. In general, these materials possess two different sorption sites enabling enhanced capability for removal. Another major advantage associated with these hybrid materials is that they will not leach into experimental solution as they do not have sufficient solubility in ground water in the pH range of 5-8. In view of this they can easily be separated from the process water. This can be verified by quantifying various drinking water quality parameters after decontamination. This will ensure the safe consumption of drinking water by human beings. During this thesis work displacement reaction was used for immobilizing different materials in biogenic matrices. The porosity and the degree of immobilization of the embedded materials was controlled over a wide range of concentration. Core-shell types of hybrid materials were synthesized using sol-gel route. A

third category of hybrid material i.e. organic coating on inorganic substrate was also prepared. The resultant hybrid materials were characterized by using various techniques like Zeta-sizer for size characterization, SEM-EDS, FTIR, BET surface area analysis and XRD for the surface and structural characterization. The stability of the prepared hybrid material and changes in the properties were observed with time. The structure and binding capacity of different types of hybrid material was investigated with regard to their practical use for the selective and reversible accumulation of heavy metals and radionuclides. Detailed analysis of various metal ions was done by using absorption/emission spectroscopy while the ultra trace level of radionuclides was measured by using gamma and alpha spectrometry.

This thesis aims at: (i) Development of highly efficient hybrid materials of different types (impregnation of suitable inorganic material into alginate matrix as well as core shell types), (ii) characterization of the newly developed hybrid material, (iii) removal of contaminants (conventional, radionuclides and nanoparticales) using the hybrid materials, (iv) practical field application of the developed hybrid materials. The hybrid materials developed and investigated in this thesis are: chitosan impregnated calcium alginate (for uranium); silica microspheres (for uranium, thorium); pure calcium alginate beads (for americium) and humic coated goethite (for americium and plutonium); silica microsphere impregnated calcium alginate (for titanium oxide nanoparticle); goethite impregnated calcium alginate (for arsenic); alumina impregnated calcium alginate (for fluoride). The work done and the obtained results are organised in following seven chapters.

Chapter 1: Introduction

In this chapter, concept of hybrid materials was introduced along with their unique advantage for the selective uptake of metal ions from aquatic medium. Categorization of hybrid

materials based on types of formation and interaction among the components are discuseed in details. It also includes a brief discussion about the possible natural and anthropogenic reasons for elevated level of certain conventional and radioactive elements in groundwater. Advantages of present work for remediation of groundwater over the existing techniques are discussed. Literature pertaining to the decontamination of groundwater from different conventional and radioactive pollutants and earlier work carried out by various researchers in understanding the interaction of metal ions with hybrid materials are summarized. Finally the scope of the thesis is presented in brief.

Chapter 2: Synthesis and characterization of hybrid materials

This chapter describes the details of experimental methods used for the synthesis and characterization of different types of hybrid materials along with optimisation of different parameters and composition of the hybrid materials. Three different categories of hybrid materials were mainly dealt with in this thesis. Inorganic material impregnated calcium alginate were synthesised by ionotropic geletion method. Core-shell type hybrid material silica microspheres were synthesized based on a polyvinylpyrrolidone involved emulsion polymerization and subsequent sol–gel process. Details of the process of the synthesis as well as the composition, morphological and structural characterization are discussed. Various characterization techniques used in the thesis work include Fourier transformed infra red spectroscopy (FTIR), X-ray fluorescence (XRF), X-ray diffraction (XRD), scanning electron microscope (SEM) and energy dispersive X-ray analysis (EDX) etc. The techniques used for determination of the concentration of the metal ions [flame atomic absorption spectroscopy (FAAS) and inductively coupled plasma optical emission spectroscopy (ICP-OES)] and radionuclides [alpha and gamma spectrometry] are also briefed in this section.

Chapter 3: Decontamination of groundwater from radionuclides (U, Th, Pu, Am) using hybrid materials

Wide spread drinking water resources contamination by radioactive constituents can result either from catastrophic incidents (Chernobyl in 1986 and Fukishima in 2012) or natural geological processes like uranium in groundwater of certain district of Punjab, India. In this chapter, the uptake studies of the radionuclides are described. All three categories of the hybrid materials [alginate based; core-shell type; organic coating on inorganic substrate] were utilised for the removal of radioactive contaminants. The results obtained are summarized below.

Uranium (U) and thorium (Th) removal: Alginate based hybrid material chitosan impregnated calcium alginate (Cal-Alg-Chi) bead [7% loading of chitosan into 4% Ca-alginate] was used to sorb uranium from potable water without compromising primary water quality parameters. Results from the uptake study, carried out in batch mode, showed more than 98% sorption of uranium in the concentration range of 0.1–50 $\mu g mL^{-1}$. Optimum pH for sorption was 3-5. The sorption capacity was evaluated as 36.04 $mg g^{-1}$ from Langmuir model. The sorption kinetics was also tested. The FTIR spectra were used as a tool for understanding the interaction between uranium and chitosan impregnated into Ca-alginate.

Silica microspheres (SM) were also used to remove the traces of U and Th in different water. Ultra-filtration technique was used to isolate the SM from the water samples. The results of batch sorption experiments suggest that SM is very effective at pH 3, and sorption is more than 99 %. The maximum U and Th uptake were 30 and 36 mg g^{-1}, respectively.

Plutonium (Pu) and americium (Am) removal: Humic coated colloidal suspension of goethite (α-FeO(OH)) followed by ultrafiltration were used to decontaminate the water having $^{239+240}$Pu and ^{241}Am in the concentration range of 10–100 Bq L^{-1}. Experimental results clearly indicate preferential association of Pu and Am with goethite suspension dominated with 30 nm colloids. The impact of humus material on selectivity of Pu and Am by goethite was studied in the concentration range of 10–100 µg mL^{-1} of humic acid. This selectivity was further enhanced linearly with the increase in concentration of humic acid from 10 to 60 µg mL^{-1} and thereafter it remained constant. Laboratory simulated experiments were also carried out for the removal of low level of ^{241}Am using calcium alginate (Ca-Alg) beads followed by treatment with activated charcoal. It was observed that the variation of carbonate, bicarbonate, does not influence the sorption capacity of calcium alginate whereas the dissolved organic carbon (DOC) decreased the sorption capacity. 98-99% of Am is recovered from Ca-Alg beads by using 0.6 M HNO3.

Chapter 4: Removal of TiO_2 nanoparticles (TiO_2 NP) from aquatic medium using hybrid materials

Concerns have been raised in recent times that TiO_2 NP may throw challenges to human health because of its unique bioactivity as many in vitro and in vivo toxicological studies showed adverse effect of TiO_2 NPs on living organisms. This chapter discussed about the utilization of the core-shell type of hybrid material silica microspheres for the isolation of nanoparticles from aquatic medium. Calcium–alginate–silica microsphere (Cal-Alg-SM) bead [10 % (wt/vol) SM loaded in 4% calcium alginate] was developed by calcium alginate impregnation of silica microspheres prepared through sol-gel route. These beads were highly efficient in the removal of TiO_2 NP from aquatic bodies. Uptake studies carried out in batch

mode, showed that Cal-Alg-SM beads are very effective for removal of TiO_2 NP in the pH range of 3-5 and the sorption was more than 90% in the concentration range of 10–500 µg mL^{-1}. Sorption isotherm was seen to follow Langmuir model and the uptake capacity evaluated was 29.9 mg g^{-1}. Mechanism of sorption was proposed based on the zeta potential values of the silica microspheres and TiO_2 NP at different pH.

Chapter 5: Hybrid materials for decontamination of groundwater from conventional pollutants (As, F)

In recent years, arsenic and fluoride contamination of drinking water has become a major concern on a global scale. In this Chapter, the uptake studies of arsenic and fluoride are described. The results obtained are summarized below.

Arsenic (As) uptake: Goethite (α FeO(OH)) impregnated calcium alginate (Cal-Alg-Goe) beads [18% goethite loaded in 4% calcium alginate] were used to sorb the arsenic from groundwater without disturbing its physicochemical characteristics. The results of batch sorption experiments suggest that Cal-Alg-Goe beads are very effective for removal of arsenic in the concentration range of 10 – 10000 ng mL^{-1}. The sorption at different pH was explained based on the species of arsenic present and the zeta potential values of goethite. Isotherm and kinetic models were tested and the sorption capacity was 30.4 mg g^{-1}.

Fluoride (F) uptake: The feasibility of alumina impregnated calcium alginate (Cal-Alg-Alu) beads [22 % (wt/vol) alumina loaded in 2% calcium alginate] was tested to sorb the excess fluoride ions from the potable water without disturbing the drinking water qualities. The results of batch sorption experiments suggest that Cal-Alg-Alu beads is very effective for defluoridation in the pH range of 3.5 to 9.0 and sorption is more than 99% in the concentration range of 1 – 100 mg L^{-1}. Equilibrium sorption follows Langmuir isotherms

well and the maximum fluoride uptake calculated was 17.0 mg g^{-1}. Equilibrium time was 300 minutes and both the pseudo-first-order and pseudo-second-order kinetic models were tested.

Chapter 6: Application of the hybrid materials developed under this study for decontamination of Uranium, Fluoride and Arsenic contaminated groundwater under field conditions

This chapter discusses the effectiveness of the newly developed hybrid materials for contaminated water samples collected from the various parts of India. In case of uranium, samples were from the state of Punjab; while fluoride and aersenic contaminated samples were collected from Andhra Pradesh and the state of West Bengal, India respectively. Various measured physicochemical parameters of groundwater before and after the treatment with hybrid material were studied and presented in details. It is clear from the result that there is no elevated level of concentration of any particular property after the treatment assuring the drinkability of the water. Special care had been taken to check the leachability of the constituent from the hybrid materials.

Integrity of the hybrid materials were checked by studying the morphological, structural characteristics, reusability and quantification of various constituents of the hybrid material after the decontamination processes. Various experimental results clearly indicate that the newly developed materials in field condition are as effective as in case of laboratory spiked samples. In all three cases a flow process diagram was proposed for effective online removal of U, F and As.

Chapter 7: Work summary

In this chapter, we summarize the main conclusions of the thesis. It has been conclusively demonstrated that specificity of the material can be enhanced by incorporation of geogenic or

biogenic materials into the biogenic matrix. Core-shell hybrid materials showed enhanced sorption because of the higher surface area. Evaluation of composite structure and metal-binding capacity of different types of immobilized materials with regard to their use for the selective and reversible accumulation of metal ions were carried out. In addition, we have emphasized that the leaching of the components doesn't take place and also there is no uptake of essential elements from potable water and suitable for human consumption. Demonstration of the newly developed hybrid materials for efficient removal of the contaminants in the field conditions was successfully carried out. This Chapter is concluded with future scope of the work which stress the needs for strengthening the certain areas for highly efficient use of hybrid materials.

LIST OF FIGURES

Note: Abbreviation used for Figure: **Fig.**

LIST OF TABLES

Chapter 1

Introduction

1.1 Chemistry of hybrid material:

Hybrid materials are composites consisting of two or more different components in one polymeric matrix. Hybrid materials have been receiving increased attention by researchers in recent years due to their unique properties and superior performance compared to that of conventional inorganic and organic polymeric materials. Hybrid materials used in treatment of wastewater or groundwater are materials obtained from the addition of effective components into the original material to enhance the removal power. It is logical to introduce functional chemical groups or components into the initial chemical which can strengthen the removal power [1,2]. Traditional materials, such as polymers and ceramics, can be combined with substances of a dissimilar type, such as biological molecules and other diverse chemical functional groups to form novel hybrid materials using the building block approach. The resultant compounds that are formed tend to possess exciting new properties for future functional materials and resultant technological applications. Due to the synergetic effect of hybrid components in one material, hybrid materials hence pose a superior performance than that of individual components [3,4]. They differ from traditional composites where the constituents are at the macroscopic (micrometer to millimeter) level. Mixing at the microscopic scale leads to a more homogeneous material that either show characteristics in between the two original phases or even new properties. A number of terminologies have been used to address hybrid materials used for coagulation and flocculation processes, such as composite coagulant [5], composite polymer [6], hybrid coagulant [7], hybrid flocculant [8], hybrid polymer [9,10] and so forth. A standardized terminology system is yet to be established. Researchers tend to use the terms ‘‘hybrid’’ and ‘‘composite’’ interchangeably regardless of the macroscopic and microscopic properties of the materials. Compared to

individual chemical components, hybrid materials, which have combined functional components into one prescription, would be a convenient alternative material for the operation of water treatment facilities because of various advantages [1,11].

1.1.1 Classification of hybrid materials based on interaction

The hybrid materials can be categorized based on two major criteria. First is the categorization based on the interaction among the components of the hybrid material and second is based on their construction pattern. According to Nanko [12], the following three primary groups of hybrid materials have been proposed:

(a) Structurally-hybridized or class I hybrid material

Structurally-hybridized materials, also known as composites, refer to the combination of materials where they are designed based on the rule of mixture at macroscopic or microscopic level [12]. This is usually practiced in preparing inorganic–organic hybrid materials through physical blending at ambient temperature or elevated temperature [13,14] (Fig. 1.1A). The components of this type of hybrid material show weak interactions like Vander Waal force, hydrogen bonding or weak electrostatic interactions among themselves. The properties of structurally-hybridized materials can be understood from the rule of mixture where it combines the properties of the component materials. As such, the performance of the structurally-hybridized materials in sorption can be enhanced with the synergetic effect of the component materials.

(b) Chemically-bound-hybridized or class II hybrid material

Unlike structurally-hybridized materials, chemically-bound hybridized materials contain special combination and mixture of atoms and molecules at molecular level. The components of this type of hybrid material show strong chemical interactions like covalent or coordinate

bonding among themselves (Fig. 1.1B). Gibbs free energy (ΔG) and enthalpy of formation (ΔH) of this type of hybrid materials are higher compared to the ΔG and ΔH of class I hybrid materials. There are some hybrid materials with excellent properties and performance due to some particular chemical-bonds at the interface between the component materials. Such

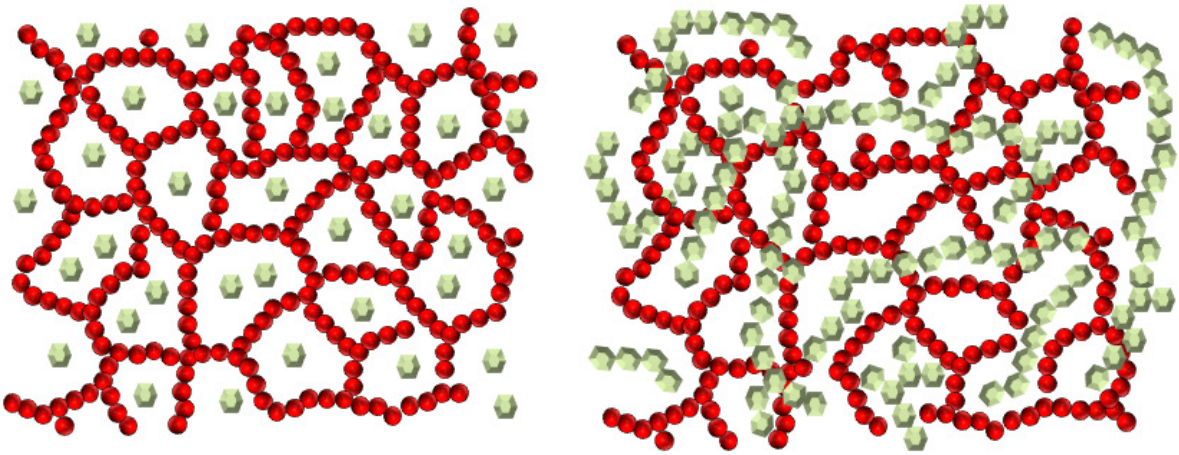

Blend Interpenetrating networks

Fig. 1.1A: Class I hybrid material

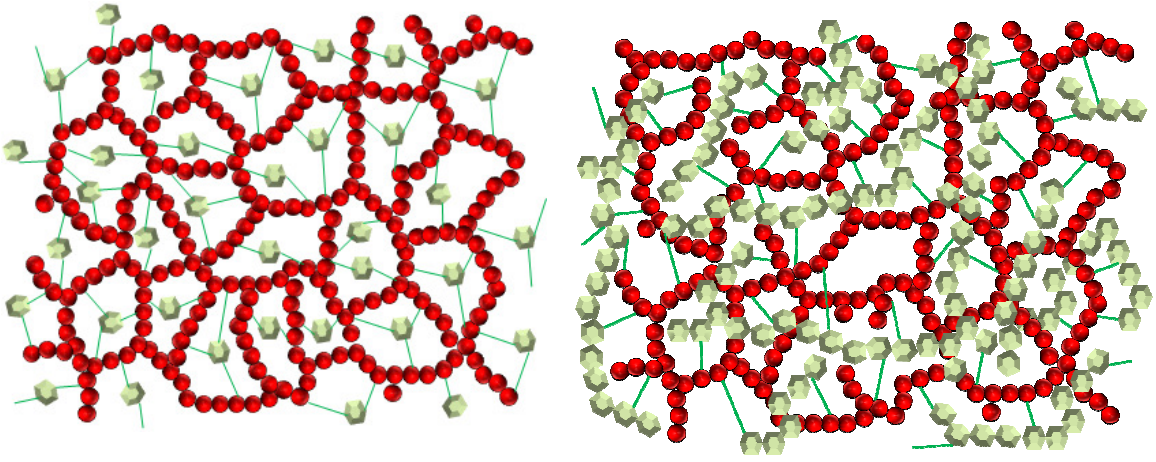

Covalently connected building blocks Covalently connected polymers

Fig. 1.1B: Class II hybrid material

materials are produced under hybridization through chemical modification where a new chemical group is introduced into the molecular chain of materials to produce new chemically-hybridized materials [12]. To produce chemically bound hybridized materials, chemical modification method such as hydroxylation–prepolymerization, copolymerization and chemical grafting or crosslinking can be used.

(c) Functionally-hybridized material

Compared to class I and class II hybrid materials, the concept of the hybridization of functions is relatively ambiguous and yet to be established. However, Nanko [12] has tried to define functionally hybridized materials as the materials that have harmonizing function and utilization of interface functions, which results in new functions or super functions. As such, structurally-hybridized materials and chemically-bound-hybridized materials which combine the functions or utilize the interface functions of the component materials, can be considered as functionally-hybridized materials. Class I and class II hybrid materials are the subsets of functionally-hybridized materials.

1.1.2 Classification of hybrid materials based on structural pattern

Based on construction type or structural pattern of the developed hybrid material which may depend on the route of synthesis followed; the hybrid material can be further classified into the following three categories.

(a) Homogenize impregnation of one material into another matrix

Normally an inorganic material is impregnated in another material (normally organic) homogonously or vice versa and hybrid material of the desired shape is formed [15-17]. Most common organic matrix used for this purpose is the alginate details of which are discussed in the subsequent sections. The high sorption capability exhibited by many biogenic material

such as algae, bacteria, and yeasts or geological materials like silicate and aluminate could be exploited to develop such hybrid material for treating contaminated waters [18,19]. These geogenic and biogenic matrices can be tailored by chemical modification to make them specific to some metal ions or radionnuclides and to enhance their sorption capacity. Alginate based hybrid material dealt in this thesis fall under this category.

(b) Core-shell type

In recent years, core-shell particles (solid core and porous shell or superficially porous) have been increasingly used for highly efficient sorption [20,21]. It is basically a solid core surrounded by a porous shell or vice versa [Fig. 1.2]. The solid core plus the porous shell

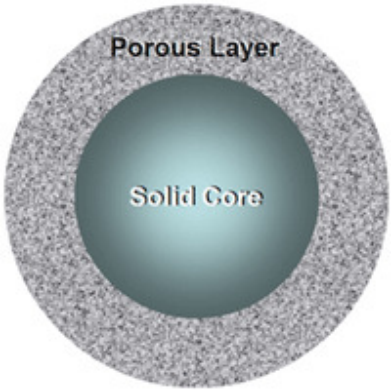

Fig. 1.2 : Core-shell type of hybrid material

gives a larger particle while the porous shell and small solid core can provide higher surface area for the separation to occur [22]. Principally composite organic/inorganic particles can be divided into systems with an organic core and an inorganic shell or vice versa according to the nature of the precursor particles. Both polymer encapsulation of inorganic particles and coating of polymer particles with minerals can be used to modify the properties of the precursor particles and lead nanocomposite particles with tailored structures and morphologies [23,24-26]. They are very effective in removal as they have large surface area,

narrow distribution of the pore size, well-defined and adjustable pore structure. Silica microsphere discussed in this thesis fall under this category of hybrid material.

(c) Coating of a material on another substrate

Sometimes a porous substrate (normally inorganic ceramic) is used as a base for providing a coating of suitable organic material over it to make its specific for uptake of some metal ion [27, 28]. Schematic is given in Fig. 1.3. For this type of hybrid material the interaction of the metal ion will be mainly with the coating material although the metal ions from solution may penetrate deep into the substrate material and can interact. Humic acid coated goethite particles which are discussed in this thesis is an example of this type of hybrid material.

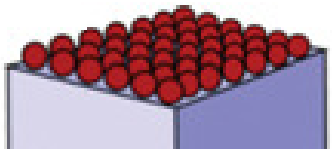

Fig. 1.3 : Coating of a material on another substrate

To further elaborate the classifications of hybrid materials, the hybrid materials that are used for sorption purposes can be classified into four secondary groups after the three primary groups in which they can be composed to form new hybrid materials [15] using combination among each other resulting a number of different types:

i. Inorganic.

ii. Organic.

iii. Natural polymer.

iv. Biopolymer.

1.1.3 Alginate as a biogenic medium for impregnation

Alginate has been used extensively in this thesis work for impregnation of inorganic materials and subsequent synthesis of hybrid materials. Combining a ceramic like oxide matrix with biological systems offers important advantages. Alginate is an extremely important family of polysaccharides because of their utility in preparing hydrogels at mild pH and temperature conditions. Alginates are unbranched polysaccharides consisting of 1-4 linked b-D-mannuronic acid (M) and its C-5 epimer a-L guluronic acid (G). It is comprised of sequences of M (Mblocks) and G (G-blocks) residues interspersed with MG sequences (MG-blocks) [29]. A representative structure of the alginate backbone is shown in Fig. 1.4 where (a) shows the chain conformation and (b) shows the typical block distribution. Computer driven mathematical models were also used in understanding the alginate microstructure [30-32]. The clearest understanding of alginate backbone structure was however achieved only using ^{1}H and ^{13}C NMR spectroscopy [33,34].

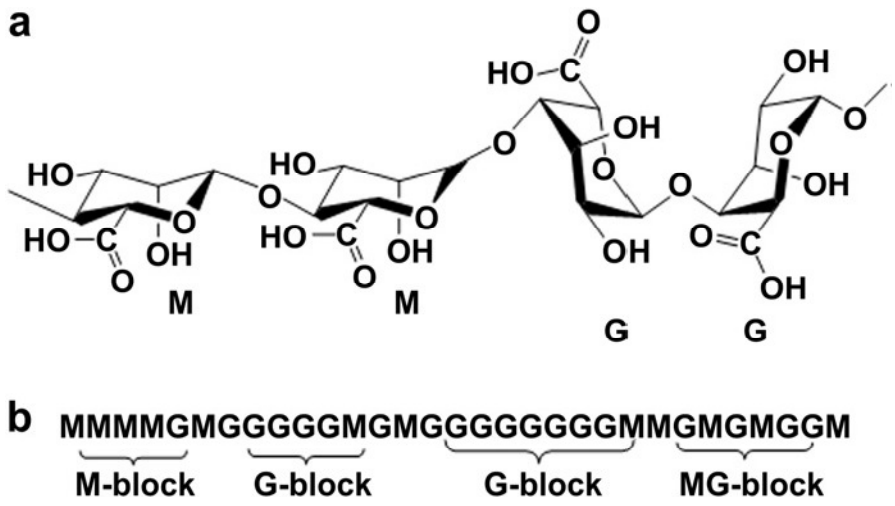

Fig. 1.4: Representative alginate structure: (a) chain conformation and (b) block distribution. Reprinted with permission from Siddhesh N. Pawar, Kevin J. Edgar; Alginate derivatization: A review of chemistry, properties and applications; Biomaterials 33 (2012) 3279-3305; Elsevier License No. 3797060440699.

While it is possible to obtain alginates from both algal and bacterial sources, commercially available alginates currently come only from algae (Fig. 1.5). Due to the abundance of algae in water bodies, there is a large amount of alginate material present in nature. Current commercial production of alginate is based entirely on algal sources.

Fig. 1.5: Brown marine algae

Alginates occur in brown algae in the intracellular matrix as gels containing sodium, calcium, strontium, magnesium and barium ions, such that the counter ion composition is determined by the ion-exchange equilibrium with seawater. The copolymer composition, sequence and molecular weights vary with the source and species that produce the copolymer. Industrial alginate production is estimated to comprise about 10% of the biosynthesized alginate material [35]. Therefore there is significant additional potential to design sustainable biomaterials based on alginates. Alginates are currently used as wound dressing materials for the treatment of wounds [36]. Chemical modification of alginates is a tool to attain enhance existing properties (example: improvement of ionic gel strength by additional covalent crosslinking, improve biodegradation, increase hydrophobicity of the backbone, etc.) and introduce completely new properties. In short, alginate derivatization is very convenient way to achieve both inherent property enhancement and new property introduction. The solubility of alginates in water is governed by pH of the solvent, ionic

strength of the medium and presence of gelling ions in the solvent. To make alginates soluble it is essential that the carboxylic acid groups be deprotonated therefore the pH above a certain critical value. Changing the ionic strength of the medium affects solubility as properties such as polymer conformation, chain extension, viscosity may get altered. Alginates gel is formed in the presence of divalent cations. It is therefore necessary to enable dissolution to have an aqueous solvent free of crosslinking ions. The solubility of alginates highly depends on the state of the backbone carboxylic acid groups. Alginic acid with its carboxylic acid groups in their protonated form is not fully soluble in water and any other solvent system. Na-alginate is dissolved in water, but was not entirely soluble in organic medium.

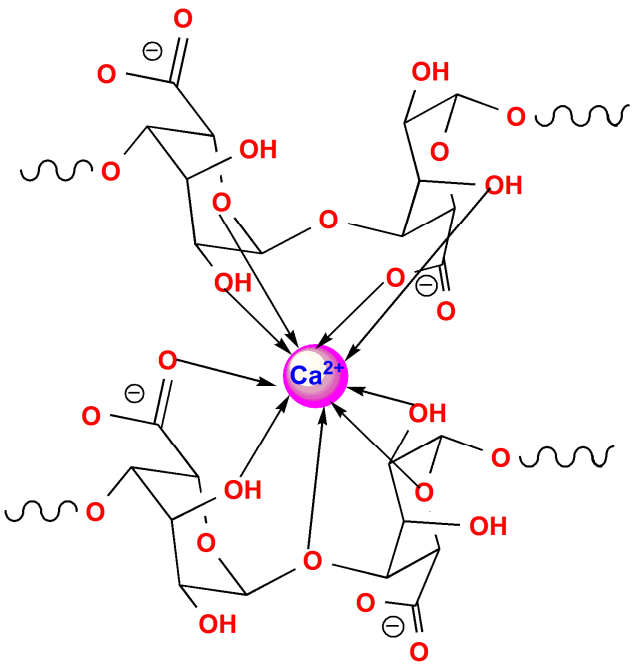

Fig. 1.6 : Crosslinking of G block of alginate with Ca^{2+}

Alginate chelates with divalent metal ions to form hydrogels. This gel formation enables us for impregnation of suitable material into it during the formation process. Gel

formation is driven by the interactions between G-blocks which associate in the presence of divalent cations to form tightly held junctions [37]. In addition to G-blocks, MG blocks also

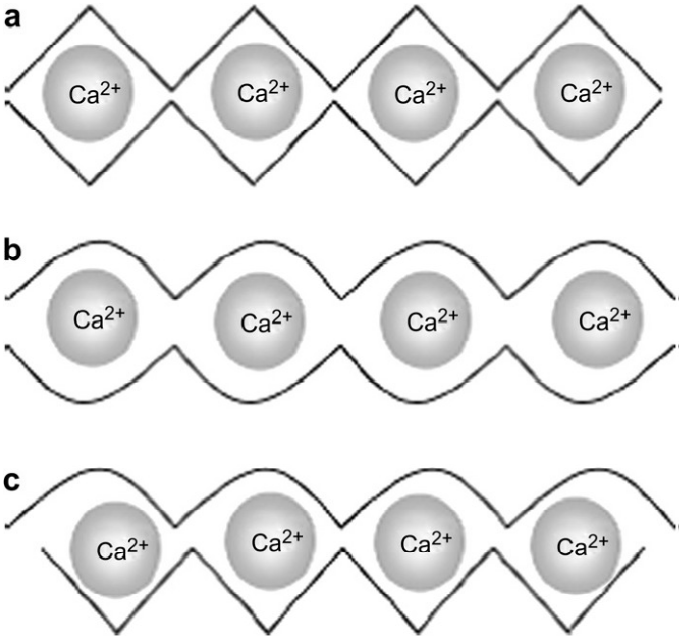

Fig. 1.7 : Possible junction points in alginates. (a) GG/GG junctions, (b) MG/MG junctions, and (c) GG/MG junctions. Reprinted with permission from Donati I., Holtan S., Mørch Y.A., Borgogna M., Dentini M., Skjåk-Bræk G.; New hypothesis on the role of alternating sequences in calcium-alginate gels; Biomacromolecules 2005; 6(2); 1031-1040. Copyright Clearance centre, ACS Publications.

form weak junctions [38]. Ca^{2+} is the most commonly used cation to induce alginate gel formation (Fig.1.6 & Fig. 1.7) however other divalent cations like Pb, Cu, Sr, Ba, Zn etc. can also be used. Calcium crosslinking of alginates along with the impregnation can be performed by two methods [29]. The first is a "diffusion" method, wherein crosslinking ions diffuse into the alginate solution. The ions are in an outside solution in contact with the alginate. The second is the "internal setting" method, where the ion source is located within

the alginate solution and a controlled trigger sets off the release of crosslinking ions into solution. Typically this is done by variation of pH or solubility of the ion source.

The diffusion method yields gels may have a Ca^{2+} ion concentration gradient across the thickness, while internal setting gives gels with uniform ion concentrations throughout [39]. Diffusion set gels are typically made by dropping Na-alginate solution into $CaCl_2$ solution. Impregnation of certain material is obtained by suitably premixing the component with the Na-alginate. Internal set gels typically use insoluble calcium salts such as $CaCO_3$ as a calcium source.

1.1.4 Advantages of hybrid materials over conventional sorbents

The hybridmaterials covered in this thesis had several advantages over the conventional single component materials used as a sorbent for contaminant removal. The advantages are as follows:

- Leaching of the component can be avoided, hence drinking water qualities are not affected.
- A relatively inert aqueous environment exists within the matrix.
- Inorganic material or nano particles with specific properties can be incorporated in organic polymer matrices.
- Reduction of operation time as a result of the application of these hybrid materials in a single operation is favorable to the industries that are discharging large volumes of wastewater.
- Synthesis process is free of organic solvents.
- A high gel porosity allows high diffusion rates of macromolecules.

- Contrary to pure solid state inorganic materials that often require a high temperature treatment for their processing, hybrid materials show a more polymer-like handling [29,40].

1.2 Contaminants in drinking water

Drinking water is derived from two basic sources: surface waters, such as rivers and reservoirs and groundwater. All water contains natural contaminants, particularly inorganic contaminants that arise from the geological strata through which the water flows and to a varying extent, anthropogenic pollution by both microorganisms and chemicals. In general, groundwater is less vulnerable to pollution than surface waters. There are a number of possible sources of man-made contaminants, some of which are more important than others. [41-46]. Pollutants reported as water contaminants can be of divided into three major categories like organic, inorganic and biological contaminants. Some of them have serious side effects and toxicities with a few being carcinogenic and lethal [47-49].

1.2.1 Groundwater contamination

Groundwater is the main source of drinking water for the human being [36]. More than 60% of irrigated agriculture and 85% of drinking water supplies are dependent on groundwater. Urban residents increasingly rely on groundwater due to unreliable and inadequate municipal water supplies. Groundwater can become contaminated from natural sources or numerous types of human activities. Naturally occurring substances in rocks like iron, manganese, chlorides, fluorides, sulfates or radionuclides are dissolved in groundwater. Organic matter can move in groundwater as particles. Some of these substances in higher concentrations may pose a threat to human health, while others may result in poor taste, odour or colour. Some of these substances can often be removed from groundwater by common treatment methods.

Waste from residential, commercial, industrial and agricultural activities can seriously affect groundwater quality. These contaminants may reach groundwater from activities on the land surface, such as industrial waste storage or spills; from sources below the land surface but above the water table, such as septic systems; from structures beneath the water table, such as wells or from contaminated recharge from the aquifers. Kinds of heavy metals which are of concern, include toxic elements (Hg, Cr, Pb, Zn, Cu, Ni, Cd, As, Co, Sn, F etc.), precious metals (Pd, Pt, Ag, Au, Ru etc.) and radionuclides (U, Th, Ra, Am, Pu etc.) [50,51].

1.2.2 Surface water contamination

Surface water is water on the surface of the planet such as in a river, lake or reservoir. Sources of surface water pollution are generally grouped into two categories based on their origin.

(a) Point sources

Point source water pollution refers to contaminants that enter a waterway from a single, identifiable source, such as a pipe or ditch. Examples of sources in this category include discharges from a sewage treatment plant, a factory or a city storm drain.

(b) Nonpoint source

Nonpoint souce (NPS) pollution refers to diffuse contamination that does not originate from a single discrete source. NPS pollution is often the cumulative effect of small amounts of contaminants gathered from a large area. A common example is the leaching out of nitrogen compounds from fertilized agricultural lands. Nutrient runoff in storm water from "sheet flow" over an agricultural field or a forest are also cited as examples of NPS pollution. With the growth of industry and development of nanotechnology, there has been a tremendous growth in the application of nanoparticles (NP) for various uses like antibacterial

materials, drug delivery systems, cosmetics, sunscreens and electronics [52-55]. NPs are defined as objects with at least one of its three dimensions in the range of 1–100 nm [56,57]. The smaller size of NPs ensures a large surface area per unit mass. Compared to fine particles, NPs of the same composition generally possess dramatically different physicochemical properties. Since surface properties, such as energy level, electronic structure, and reactivity are quite different from bulk, the bioactivity of NPs will be different from that of the bulk analogue [41,58]. As a consequence of indiscriminate use of nanoparticles (TiO_2, Graphene etc.), poses a risk to contaminate aquatic bodies therefore exposure to the human population. This is the latest kind of inorganic pollutants. Organic pollutants have also been found in different water resources. These belong to various classes such as pesticides, hydrocarbons, plasticizers, fertilizers, phenols, biphenyls, detergents, oils, pharmaceuticals etc. [59-61].

The above discussed pollutants have great risk to human health, and the ecosystem of the earth as a whole. Many of them are not biodegradable and tend to accumulate in living organisms, causing various diseases and disorders. The side effects and toxicities of these contaminants are discussed in literature. Contaminants studied in this thesis ranges from heavy elements, radionuclides, nanoparticles as well as non metal conventional pollutants. A brief description of all the studied contaminants are given below.

1.2.3 Radioactive contaminants studied in this thesis

Radioactive constituents of drinking-water can result from

- Naturally occurring radioactive species (e.g., radionuclides of the thorium and uranium decay series in drinking-water sources), in particular radium (^{226}Ra and ^{228}Ra) and a few others.

- Technological processes involving naturally occurring radioactive materials (e.g., the mining and processing of mineral sands or phosphate fertilizer production).
- Radionuclides discharged from nuclear fuel cycle facilities.
- Manufactured radionuclides (produced and used in unsealed form), which might enter drinking-water supplies as a result of regular discharges and, in particular, in case of improper medical or industrial use and disposal of radioactive materials.

Wide spread drinking water resources contamination can also be caused by Catastrophic incident like Daiichi Nuclear Power Plant (NPP) Fukushima, Japan (11 March 2011) and Industrial nuclear accidents like Chernobyl, USSR (March 1986). In 2008, WHO published a third edition of the Guidelines for Drinking Water Quality. These guidelines are not intended to provide a control on amounts of activity which may be discharged into drinking water sources, but are guidelines from which drinking water suppliers can determine whether action is necessary to reduce radioactivity levels in the water supply [62]. These levels relate to natural and artificially enhanced radioactivity in drinking water. Screening levels of 0.1 and 1 Bq L^{-1} for gross alpha and gross beta activity respectively have been retained from the first edition. If activity of drinking water are below this level, no further action is required and the water is drinkable [63,64]. Uranium and thorium are important elements not only in industrial application but also in energy and environmental problems. In view of the extensive usage of uranium and thorium for various industrial purposes and their sub trace level releases through liquid effluents which in turn reflects into the various aquatic medium [65]. Uranium and thorium are omnipresent in terrestrial and aquatic environment. World average concentration of uranium in soil is about 3 µg g^{-1} except the areas rich with uranium ore. Fresh water system contains uranium in the range of 1 ng mL^{-1} to few tens of ng mL^{-1}

whereas seawater contain in the range of 1-10 ng mL^{-1}. These natural variation in terrestrial and aquatic environment is mainly due to the impact of local geo-chemical environment. Elevated levels of uranium in groundwater in the range of tens of ng mL^{-1} to 600 ng mL^{-1} were observed in many parts of the world [65,66]. In some of the recent studies carried out in India, groundwater samples originated from northern states (Punjab and Haryana) showed elevated levels of uranium [67,68]. The reason for elevated levels of uranium in this part of India, is still a matter of further investigation although various investigation indicates localized mineralization process or use of localized phosphate fertilizer etc. Change in redox potential at mineral-water interface, which in turn accelerates the leaching of uranium in water from the host rock. Concentration of uranium in the rock depends on its type e.g. granite rocks are enriched in U with an average concentration of 5 µg g^{-1} whereas basaltic rocks are having an average concentration of 1 µg g^{-1}. However some studies in north and western region of India also pointed out large scale use of phosphate fertilizer which contains uranium bearing minerals responsible for elevated level U in groundwater [67,68]. Under natural circumstances, thorium is not expected in aquatic bodies because its high particle reactive nature but can be present in soil, rock, sediment etc. Allowable concentration of $^{239+240}Pu$ and ^{241}Am in drinking water as per guidelines of WHO issued in 2008 is 0.1 Bq L^{-1} [64]. In natural environments such as soils, iron oxides (i.e. oxides, hydroxides, oxyhydroxides) are generally present in small quantity (which could be lower than g kg^{-1}), even though their presence and distribution depend on the availability of iron and on environmental conditions.

1.2.4 Nanoparticle contaminant (TiO_2) studied in this thesis

Traditionally, TiO_2 is considered as poorly soluble, low toxicity particles [69,70] and TiO_2 nanoparticles (TiO_2 NP) have been widely used in industrial and consumer products due to their stronger catalytic activity when compared to bulk TiO_2. TiO_2 NP is a white pigment. Because of its brightness and very high refractive index it is widely used [71-73]. TiO_2 NP are used in the industries like paints, pharmaceuticals, coatings, food products, cosmetics, plastics, papers, inks, toothpaste etc. [74-76]. In recent times, concerns have been raised that these same properties of TiO_2 NP may throw challenges to human health because of its unique bioactivity [77,78]. Many in vitro and in vivo toxicological studies showed adverse effect of TiO_2 NP on living organisms [79,80]. Different animal models employing multiple exposure routes of administration, including inhalation, oral intake, dermal exposure, intravenous injection etc. have been intensively used. [81,82]. Studies have also revealed that TiO_2 NP are more toxic than bulk [83,84]. TiO_2 has been classified as a Group 2B carcinogen by the International Agency for Research on Cancer (IARC) [85]. Wide applications of TiO_2 NP pose potential for environmental release which inevitably allows for a potential health risk to the eco-system and to the humans [86].

1.2.5 Conventional pollutants studied in this thesis

In recent years, arsenic contamination of water has become a major concern on a global scale. The most common and serious route of arsenic exposure for humans is through drinking water contaminated with arsenic compounds. Arsenic occurs in natural waters in a variety of forms like soluble, particulate and organic bound [87]. Depending on the redox conditions, arsenic occurs in nature as trivalent As(III) and pentavalent As(V) oxidation states and due to the relatively slow arsenic redox transformations, both oxidation states are often observed, As(III) being more toxic than As(V) [88-90]. Redox potential (Eh) and pH

control arsenic speciation. Arsenic species (H_3AsO_3, $H_3AsO_3^{2-}$, H_3AsO_4, $H_3AsO_4^{-}$, $H_3AsO_4^{2-}$, AsO_4^{3-}etc.) predominating in various pH ranges have been discussed extensively in literature [91-93].

Several areas of the world have relatively high arsenic concentrations in their groundwater used for drinking purpose [94,95]. High arsenic concentrations have been reported recently from the USA, China, Chile, Bangladesh, Taiwan, Mexico, Argentina, Poland, Canada, Hungary, Japan and India. Among 21 countries in different parts of the world affected by groundwater arsenic contamination, the largest population at risk is in Bangladesh followed by West Bengal in India [96]. Since arsenic is highly toxic and carcinogenic, the World Health Organization (WHO) has set the guideline for arsenic in drinking water at 10 μg L^{-1} [64, 97]. Daily consumption of water with greater than 0.01 mg L^{-1} of arsenic, less than 0.2 % of the fatal dose, can lead to problems with the skin, circulatory and nervous systems.

Fluoride is an essential constituent for humans and animals depending on the total amount ingested or its concentration in drinking water. The presence of fluoride in drinking water, within permissible limits of 0.5 –1.0 mg L^{-1}, is beneficial for the production and maintenance of healthy bones and teeth, while excessive intake of fluoride causes dental or skeletal fluorosis which is a chronic disease [64]. As there is no treatment for fluorosis, prevention is the only means of controlling the disease [98]. Fluorosis is a disease that causes mottling of the teeth, calcification of ligaments, crippling bone deformities and many other physiological disorders.

Fluoride exists naturally in water sources and is derived from fluorine, the thirteenth most common element in the Earth's crust. Fluoride is found in all natural waters at some

concentration. Seawater typically contains about 1 mg L^{-1} while rivers and lakes generally exhibit concentrations of less than 0.5 mg L^{-1}. In groundwater, however, low or high concentrations of fluoride can occur, depending on the nature of the rocks and the occurrence of fluoride-bearing minerals [99,100]. Concentrations in water are limited by fluoride solubility, so that in the presence of 40 mg L^{-1} calcium it should be limited to 3.1 mg L^{-1}. It is the absence of calcium in solution which allows higher concentrations to be stable. High fluoride concentrations may therefore be expected in groundwater from calcium-poor aquifers and in areas where fluoride-bearing minerals are common [101]. Fluoride concentrations may also increase in groundwater in which cation exchange of sodium for calcium occurs [102]. Many countries have regions where the water contains more than 1.5 mg L^{-1} of fluoride due to its natural presence in the earth's crust, or discharge by agricultural and industrial activities, such as steel, aluminium, glass, electroplating. Excessive exposure to fluoride in drinking-water, or in combination with exposure to fluoride from other sources, can give rise to a number of adverse effects as discussed above. Drinking-water is typically the largest single contributor to daily fluoride intake. For a given individual, fluoride exposure (mg kg^{-1} of body weight per day) via drinking-water is determined by the fluoride level in the water and the daily water consumption (litres per day). However, from several studies, a rough estimate of total daily fluoride exposure in a temperate climate would be approximately 0.6 mg per adult per day in an area in which no fluoride is added to the drinking-water and 2 mg per adult per day in a fluoridated area [103-106].

1.3 Remediation techniques and sorbents

To address the undeniable need of contaminant free drinking water, various water treatment methodologies have been proposed and applied at both experimental level and field

conditions. Methods for removing contaminants from aqueous solution consist of physical, chemical and biological technologies. Various techniques and sorbent generally used for water treatment are discussed in this section.

1.3.1 Methodologies in use

The technologies conventionally used for removing metal ions from aqueous solution commonly are screening, filtration, centrifugation, separation, evaporation, sedimentation,

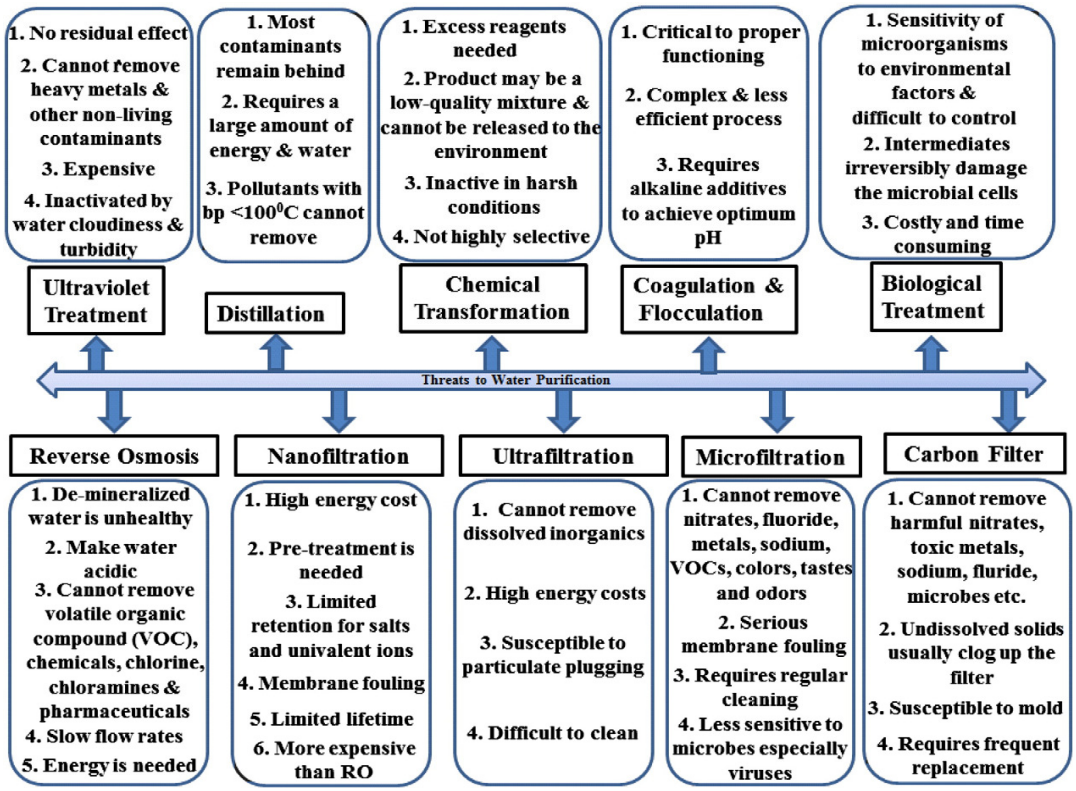

Fig. 1.8: Desalination methodologies and related issues; Reprinted with permission from Rasel Das, Md. Eaqub Ali, Sharifah Bee Abd Hamid, Seeram Ramakrishna, Zaira Zaman Chowdhury; Carbon nanotube membranes for water purification: A bright future in Desalination 336 (2014) 97–109; Elsevier License No. 3862480972193.

coagulation and flocculation, distillation, crystallization, evaporation, solvent extraction, oxidation, precipitation, ion exchange, reverse osmosis (RO), nanofiltration (NF), ultrafiltration (UF), microfiltration (MF), adsorption, electrolysis and electrodialysis [107]. The advent of membrane technologies has given immeasurable facilities and opportunities to purify water even at the ionic levels. Membrane filtration allows the passes of water solvent but rejects solutes, gases, fluids and various particles present in the polluted water. around 19% of the world's desalination plants have successfully installed the RO membrane [108]. However, the most of these techniques have one or another disadvantages. Some methods are energy and operationally intensive and therefore are not affordable at a commercial scale. Chemical precipitation and electrochemical treatment become ineffective when metal ion concentration in aqueous solution is high and also produce large quantity of sludge required to treat with great difficulty. Ion exchange, membrane technologies (RO, NF, UF, MF) are extremely expensive when treating large amount of water and wastewater containing heavy metal or other contaminants in low concentration, therefore difficult to be used at large scale [109].

Energy consumption costs approximately one half of the total cost in the RO process and thus contribute significantly to the emission of greenhouse gases [110]. Additionally, membrane technologies are less robust and incapable of self-cleaning function, necessitating the chemical treatments for cleaning and recycling [111,112]. Adsorption is considered as the best wastewater treatment method due to its universal nature, inexpensiveness and ease of operation. Adsorption is the accumulation of a substance at a surface or interface. In case of water treatment, the process occurs at an interface between solid adsorbent and contaminated water. The pollutant being adsorbed is called as adsorbate and the adsorbing phase as

adsorbent. Adsorption techniques are easy and simple but cannot desalinate salty water [113]. The main advantages of adsorption are that it is versatile, it does not require high amounts of energy, large amounts of water or additional chemicals, thus it is most frequently used desalination method [114-116]. Major issues related to common water purification systems are summarized in Fig. 1.8. It clearly reflects that no single method is sufficient to remove all pollutants from water.

1.3.2 Sorbents

A large quantity of materials has been investigated as sorbents for the removal of inorganic, organics and biological pollutants extensively. In recent years, applying biotechnology and nanotechnology in controlling and removing metal pollution has been paid much attention.

Table 1.1: Widely used low cost adsorbents

	House hold wastes	Agricultural products	Industrial wastes	Sea materials	Soil and ore materials
	• Fruit waste • Coconut shell • Scrap tyres	• Bark and other tannin-rich materials • Sawdust and other wood type materials • Rice husk	• Fertilizer wastes • Fly ash • Petroleum wastes • Sugar industry wastes • Blast furnace slag	• Chitosan and seafood processing wastes • Seaweed and algae • Peat moss	• Geolite • Clay • Sediment and soil • Ore minerals • Metal oxides and hydroxides

Large quantities of metals can be accumulated by both living and dead biomass as well as cellular products such as polysaccharides. A variety of biosorbents including bacteria, fungi, yeast, algae, etc. which have metal-sequestering property can be used for metal removal

[50,117]. The various nanostructured materials fabricated with features such as high aspect ratio, reactivity, tuneable pore size, electrostatic, hydrophilic and hydrophobic interactions have been applied for water treatment. Adsorption has been used for the removal of a variety of pollutants from various contaminated water sources. Table1.1 gives various low cost materials which are widely used as adsorbent apart from the synthetic materials.

1.3.3 Sorbents used as a component of hybrid material in this thesis

Various geogenic and biogenic materials as well as synthetic materials have been used in this thesis to synthesize hybrid materials. A brief overview of them are given below.

(a) **Alginate:** A large number of studies has already been conducted to exhibit excellent adsorption ability for multivalent metal ions by calcium alginate [118-120]. The ability of alginate to form gels by ionexchange reaction with multivalent metal ions suggests its use as a metal adsorbent. Many recent studies have addressed the collection of heavy metals such as Co, Cu, Cd and Zn by alginic acid [121-124]. The alginic acid and alginates are thus likely to be potentially useful as adsorbents for the removal of heavy metals and radionuclides from waste solutions. However, a limited amount of information is available concerning the uptake behavior of radioactive nuclides on these polymer gels from potable water. In this thesis it was applied as a sorbent for radionuclides or as impregnating medium for other inorganic materials. The use of alginate as an immobilizing agent in most applications rests in its ability to form heat-stable strong gels which can be developed and stable at room temperature. It is the alginate gel formation with calcium ions which has been of interest in most applications.

(b) **Chitosan:** A large number of studies have been reported by using chitosan [125-127] for decontamination of various pollutants from aquatic streams flocculants for protein

recovery etc. Chitosan is the N-deacetylated products of chitin manufactured from shrimp or crab shells. It is inexpensive, non-toxic, hydrophilic, biocompatible, and biodegradable. Chitosan is a linear polysaccharide soluble in acidic aqueous medium. It is composed of β-(1-4)-linked D-glucosamine and N-acetyl-D-glucosamine (Fig. 1.9). These acetylated and deacetylated units are randomly distributed. It is very effective in removal because of its unique character like it is the only pseudo natural cationic polymer [128]. Chitosan could provide an excellent binding capacity with heavy metal ions since it has active primary amino groups in the polyaminoglucosan chain, which could provide sufficient amount of chelating sites for metal ions [129-131]. It can be produced commercially by deacetylation of chitin. Chitin can be derived from exoskeleton of crabs, shrimp and cell walls of fungi. Although chitosan can be selective towards uranium, separation of the sorbent after uptake may be an issue, therefore immobilising the sorbent in a suitable medium is practised by many researchers [132-133].

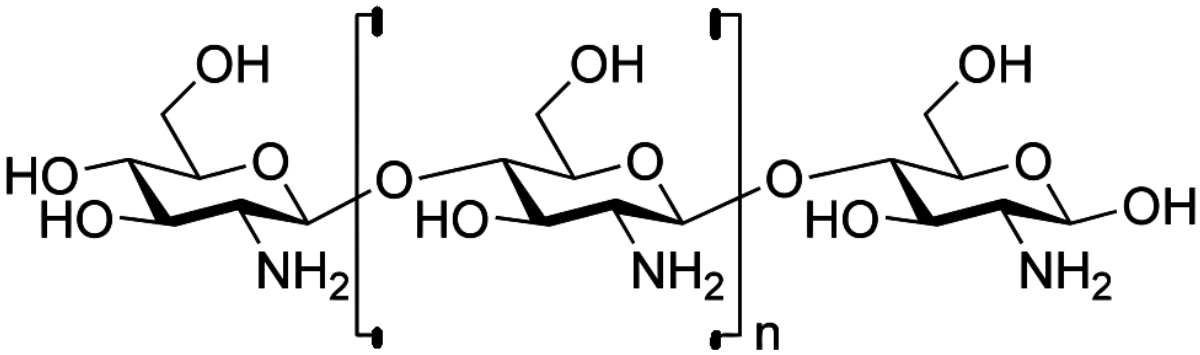

Fig. 1.9: Structure of chitosan

(c) **Silica microspheres:** The advent of nanotechnology has given immeasurable opportunities to purify water even at ionic state. Silica microspheres nanoparticles [134-136] have been used for removal of various pollutants from aquatic environments including dyes,

heavy metals and radionuclides [137-139]. They are very effective in removal as they have large surface area, well-defined and adjustable pore structure, narrow distribution of the pore size. These spheres can be obtained by the synthesis of core–shell type particles. These core–shell particles often exhibit properties that are substantially different from those of the template core because of higher surface area, different surface chemical compositions, increased stability and different optical and magnetic properties [140-142]. Such particles can be applied in various fields including catalysis, coatings, capsule agents for drug delivery, composite materials [143-146]. Although silica microspheres (SM) can be selective towards certain elements, sufficiently high sorption capacity could be achieved by high specific surface areas i.e. smaller size and hollow or porous nature of the microspheres. SM was used in this thesis as hybrid material either as powder form or as impregnated into Ca-alginate for the removal of U, Th and TiO_2 NP.

(d) **Goethite:** Goethite (α-FeO(OH)) is one of the magnetic carriers commonly found in natural environments [147-149]. The sorption of As(III) and As(V) onto iron oxides has been studied previously, actually iron oxides seem to be responsible for the attenuation of arsenic in soils, lacustrine and marine sediments [150-152]. Although many iron oxides are selective towards arsenate, goethite was used as a component of hybrid material in this thesis for the removal of arsenic.

(e) **Alumina:** Alumina (Al_2O_3) is significant in its use as a refractory material, electrical insulator and ceramic material due owing to its high melting point. Recent trend shows its use (particularly γ Al_2O_3) as sorbent for various elements such as fluoride [153]. A large number of materials such a sclay [154], soil [155], bone char [156], zeolites [157], granular ferric hydroxide [158], nano alumina have been tested for fluoride removal from

ground water. Decreasing the fluoride concentration to less than 2 mg L^{-1}, most of the tested materials displayed a very low capacity of fluoride removal therefore, not suitable for drinking water, especially as some of them can only work at an extreme pH value and leaves its chemical constituents in water which are difficult to remove from water [159-161]. In this thesis we have used alumina for synthesis of alginate based hybrid material which was used for fluoride removal.

1.4 Scope of the thesis

The development of hybrid materials with extraordinary properties is currently an area of extensive research, particularly with regard to their potential applications in decontamination of drinking water. Research and development of novel hybrid materials has been undertaken by various groups throughout the world in most recent years. It is evident from the earlier discussions that there are several issues in synthesis and application of highly efficient hybrid material for decontamination of potable water from a wide range of contaminants without disturbing the water quality. These materials can bridge the various scientific disciplines while concurrently co-bridging the best attributes of the two material systems into one system. In a truly interdisciplinary manner, inorganic and organic chemistry, material sciences, physical sciences and biological sciences are united in the search for novel recipes to create unique materials. Therefore, the motivation of the present thesis is many folds:

(i) Synthesis and characterization of new hybrid materials with improved capacity. For this purpose, development of highly efficient hybrid materials of different types like impregnation of suitable inorganic material into alginate matrix, core shell types, organic coated oxides have been synthesized and tested for their capability to remove various contaminants (conventional, radionuclides and nanoparticales).

(ii) Practical field application of the developed hybrid materials. It's important to take care of the practical applicability of the sorbent during the design of a hybrid material. From this point of view the developed hybrid materials in this thesis were tested in field conditions. We have demonstrated the decontamination of actual ground water samples from U, As, F without disturbing the water quality parameters. Nanoparticles which can be a new potential threat to aquatic bodies, was also decontaminated using newly developed hybrid material.

The experimental work and the obtained results during the thesis work are organized as follows.

In chapter 2, we discuss the details of the synthesis and characterization of different types of hybrid materials along with optimisation of different parameters and composition of the hybrid materials. The hybrid materials investigated were mainly of three types. Inorganic material impregnated in calcium alginate were synthesised by ionotropic geletion method. Core-shell type hybrid material silica microspheres were synthesized through sol–gel route. Details of the process of the synthesis as well as the composition, morphological and structural characterization using various techniques like FTIR, SEM-EDS, XRF, XRD, BET etc. are discussed. The techniques used for determination of the concentration of the metal ions and radionuclides are also described in this chapter.

In chapter 3, the uptake studies of the radionuclides (U, Th, Am, Pu) are described. For the decontamination of U and Th from potable water silica microspheres and chitosan impregnated calcium alginate (Cal-Alg-Chi) bead [7% loading of chitosan into 4% Ca-alginate] were used to sorb uranium without compromising primary water quality parameters. Humic coated colloidal suspension of goethite (a-FeO(OH)) followed by ultrafiltration were

used to decontaminate the water having $^{239+240}Pu$ and ^{241}Am in the concentration range of 10–100 Bq L^{-1}. Results from the uptake study, carried out in batch mode, showed more than 90% sorption of the radionuclides. Optimization of pH, time, isotherm, kinetics studies were carried out and discussed in this chapter.

In chapter 4, we describe the utilization of the core-shell type silica microspheres for the isolation of nanoparticles from aquatic medium. Calcium–alginate–silica microsphere (Cal-Alg-SM) bead was developed by calcium alginate impregnation of silica microspheres. Cal-Alg-SM beads were very effective for removal of TiO_2 NP in the pH range of 3-5 and the sorption was more than 90% in the concentration range of 10–500 μg mL^{-1}.

In chapter 5, the uptake studies of conventional pollutants (As, F) using hybrid materials are discussed. Goethite (α FeO(OH)) impregnated calcium alginate (Cal-Alg-Goe) beads [18% goethite loaded in 2 % calcium alginate] and alumina impregnated calcium alginate (Cal-Alg-Alu) beads [22 % (wt / vol) alumina loaded in 2 % calcium alginate] were utilized for arsenic and fluoride removal respectively.

In chapter 6, we demonstrate the effectiveness of the newly developed hybrid materials for real water samples under field condition. Groundwater samples collected from ambient environment having elevated levels of F, As and U were successfully decontaminated using the developed hybrid materials. No change of the physicochemical characteristics of groundwater due to the treatment was ensured. Process flow diagrams and ready to use kits made out of the developed hybrid materials were demonstrated for the successful decontamination of U, F and As under field condition.

In chapter 7, we summarize the conclusions of the works carried out in the thesis. It has been conclusively demonstrated that enhanced sorption could be achieved without

compromising the water quality by incorporation of specific material into the biogenic matrix alginate and by core-shell type of hybrid materials.

Chapter 2

Synthesis and characterization of hybrid materials

2.1 Synthesis of alginate based hybrid materials

The general method used for synthesis of alginate based material is the ionotropic gelation method. This includes the formation of the hydrogel beads by treating the alginate solution with the solution containing polyvalent (mostly divalent) ions (ionotropic gelation method). This is the commonest method employed and it can be modified in many different ways to bring about the desired shape, size and effects. In brief the solution of the sodium alginate is prepared (different concentration) and the sorbent in different concentrations is added to that solution if impregnation is required. The mixture is stirred and allowed to stand for required time. The mixture is then dropped into the solution containing Ca^{2+} ion and if required at different concentration and pH conditions. The method of bringing the sodium alginate in contact of Ca^{2+} ion can be of three types which are as follows:

Fig. 2.1: Synthesis of alginate beads using dropper

Fig. 2.2: Synthesis of alginate beads using peristaltic pump

i. **Syringe or dropper method** where the mixture is passed through the syringe or dropper of uniform diameter and allowed to drop into calcium chloride solution to form the beads.

ii. **Extrusion method** where the mixed materials is pushed through a die (a certain dimension) of the desired cross-section to get desired shape.

iii. **Laminar jet break-up or prilling method** where beads are formed by allowing drops of the liquid prill substance to congeal or freeze in mid-air after being dripped from the top of a tall prilling tower.

Depending on the tools and method used the material obtained can be of desired shape. The alginate based hybrid materials discussed in this thesis had spherical shape beads with desired diameter. Fig. 2.1 and Fig. 2.2 show typical setup used in the laboratory for synthesis of alginate beads. The formation of alginate and impregnated alginate beads are discussed here.

2.1.1 Chemical and reagent

All the reagents used in this study were obtained from Sigma Aldrich. MILLIQ water having resistivity 0.01 cm^{-1} and Dissolved Organic Carbon (DOC) less than 5 ng mL^{-1} was used throughout the experiment for the preparation of the reagents. All other chemicals were of analytical grade and used without pre-treatment.

2.1.2 Pure calcium alginate beads

A 2% solution (wt. / vol.) of Na alginate in water was prepared with deionized water. This solution was taken in syringe and added to 0.2 M $CaCl_2$ solution drop-wise. Na alginate reacted with $CaCl_2$ to form beads of Ca alginate. These beads were stored in 0.2 M CaCl2 solution and were thoroughly washed with deionized water until free from CaCl2. Calcium alginates beads so formed are stable in the temperature range 20–50 °C. The beads were permeable to water and had enough mechanical strength to be held in water column for 3–4

weeks. The size of the spherical beads was 2±0.2 mm as shown in the Fig. 2.3A and Fig. 2.3B.

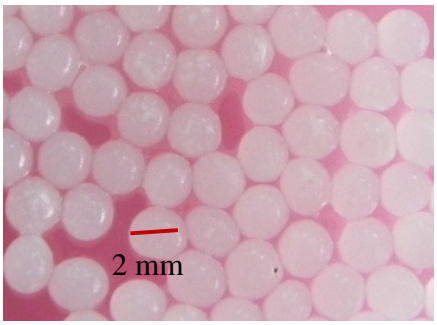

Fig. 2.3A: Digital image of pure Ca-alginate beads

Fig. 2.3B: Size measurement of the Ca-alginate beads

2.1.3 Chitosan impregnated calcium alginate beads (Cal-Alg-Chi)

Chitosan (sigma-aldrich cat. no.448877) was dried under infrared lamp for two hours and grinded well before mixing with 4% solution of sodium alginate. A 7% (wt./vol.) of chitosan powder was mixed thoroughly in the sodium alginate solution. In order to homogenise, the mixture was stirred at 700 rpm for 3 h with the help of a magnetic stirrer. Under stirring conditions, the mixture was added dropwise into 4% calcium chloride ($CaCl_2$) solution with

the help of a peristaltic pump (Fig. 2.2). Sodium alginate reacted with the $CaCl_2$ and formed beads of calcium alginate, entrapping the chitosan within it. Calcium alginate immobilization involves a simple displacement reaction. The beads were further kept in $CaCl_2$ solution for 1 h and then washed with deminerised water until free from $CaCl_2$ (verified with silver nitrate solution). A digital image of the beads is given in Fig. 2.4.

2.1.4. Alumina impregnated Calcium Alginate beads (Cal-Alg-Alu)

A 4% solution (wt. / Vol.) of Na alginate in water was made. Weighed alumina was mixed thoroughly in the solution to make 22% (wt./ Vol.). Then the mixture was taken in syringe and was added drop by drop into 0.5 M $CaCl_2$ solution. Na alginate reacted with $CaCl_2$ to form beads of Ca alginate, entrapping the alumina within it. The beads of immobilized alumina were stable upto $80^{O}C$ and permeable to water (Fig. 2.5).

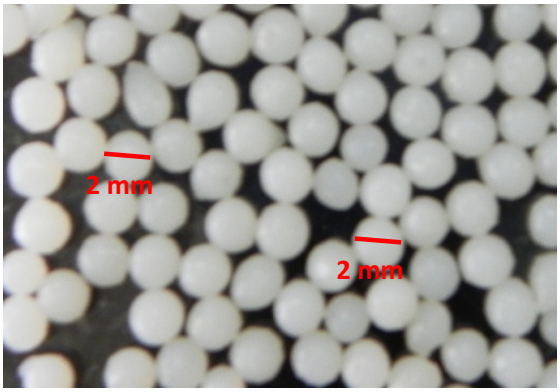

Fig. 2.4: Digital image of Cal-Alg-Chi beads

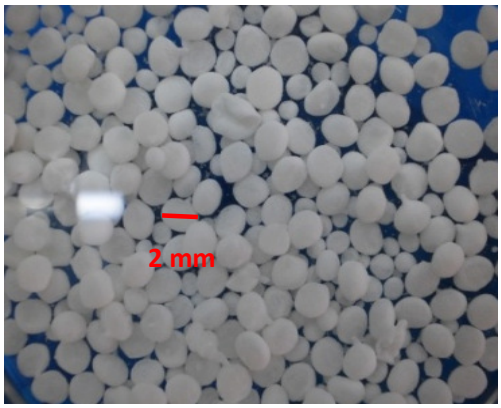

Fig. 2.5: Digital image of Cal-Alg-Alu beads

2.1.5 Goethite impregnated calcium alginate (Cal-Alg-Goe) beads

Goethite was first synthesized using ferrous sulphate and NaOH maintaining a proper molar ratio and stirring speed at 60°C. 200 mL of suspension were prepared by mixing 100 mL of FeSO4, 7H2O solution with 100 mL of NaOH solution. The rotation speed of the magnetic

stirrer was set at 760 rpm. The reaction was carried out at room temperature (T = 25ºC) keeping the ratio (R) of [FeSO4]/ [NaOH] at 0.2 [FeSO4,7H2O = 0.15 M; NaOH= 0.75 M]. The goethite thus prepared was in suspension form. It was separated using ultracentrifuge (20000 rpm for 1h) and powder was washed with water and dried. Weighed goethite [18% (wt./vol.)] was mixed thoroughly in the 4% Na-alginate solution to make it homogeneous. Then the mixture was stirred (400 rpm) for 3 h taken in polypropylene bottles and was added dropwise into 0.5 M calcium chloride ($CaCl_2$) solution using dropper method. Na alginate reacted with $CaCl_2$ to form beads of Ca alginate, entrapping the goethite within it. The beads of immobilised goethite were stable, homogenous and permeable to water. Fig. 2.6 shows set up for goethite synthesis and the digital image of the Cal-Alg-Goe beads.

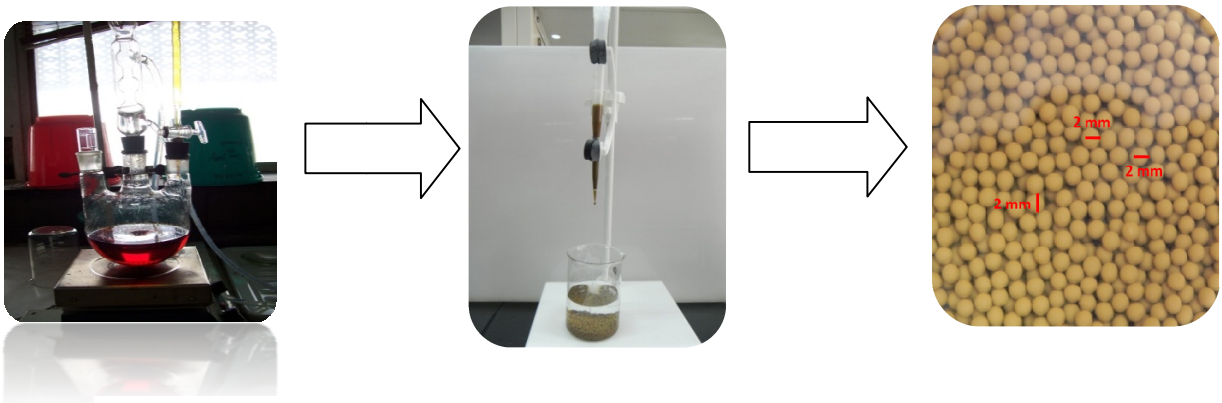

Fig. 2.6 Stepwise synthesis of Cal-Alg-Goe beads

2.1.6 Optimization of loading in the impregnated beads

In order to study the effect of chitosan/goethite/alumina loading on calcium alginate for the sorption, loading of these materials was varied from 1 to 50 wt.%. It was observed that certain percentage loading is optimum as permissible limit of contaminants in drinking water was achieved. Moreover when the loading exceeded a certain value, integrity of the beads was affected and showed a tendency to be brittle. This threshold loading value was 9%, 20%

and 24% respectively for chitosan, goethite and alumina respectively. Hence the optimum compositions of these three types of the beads were worked out and are given in Table 2.1.

Table 2.1: Optimum composition of the hybrid alginate beads

Hybrid beads	**Optimum composition**
Cal-Alg-Chi	7% chitosan loading in 4% calcium alginate
Cal-Alg-Alu	22% alumina loading in 2% calcium alginate
Cal-Alg-Goe	18% goethite loading in 4% calcium alginate

2.2 Synthesis of Silica microspheres (SM) based hybrid materials

An interesting expansion of the hybrid materials is that the hollow inorganic spheres can be

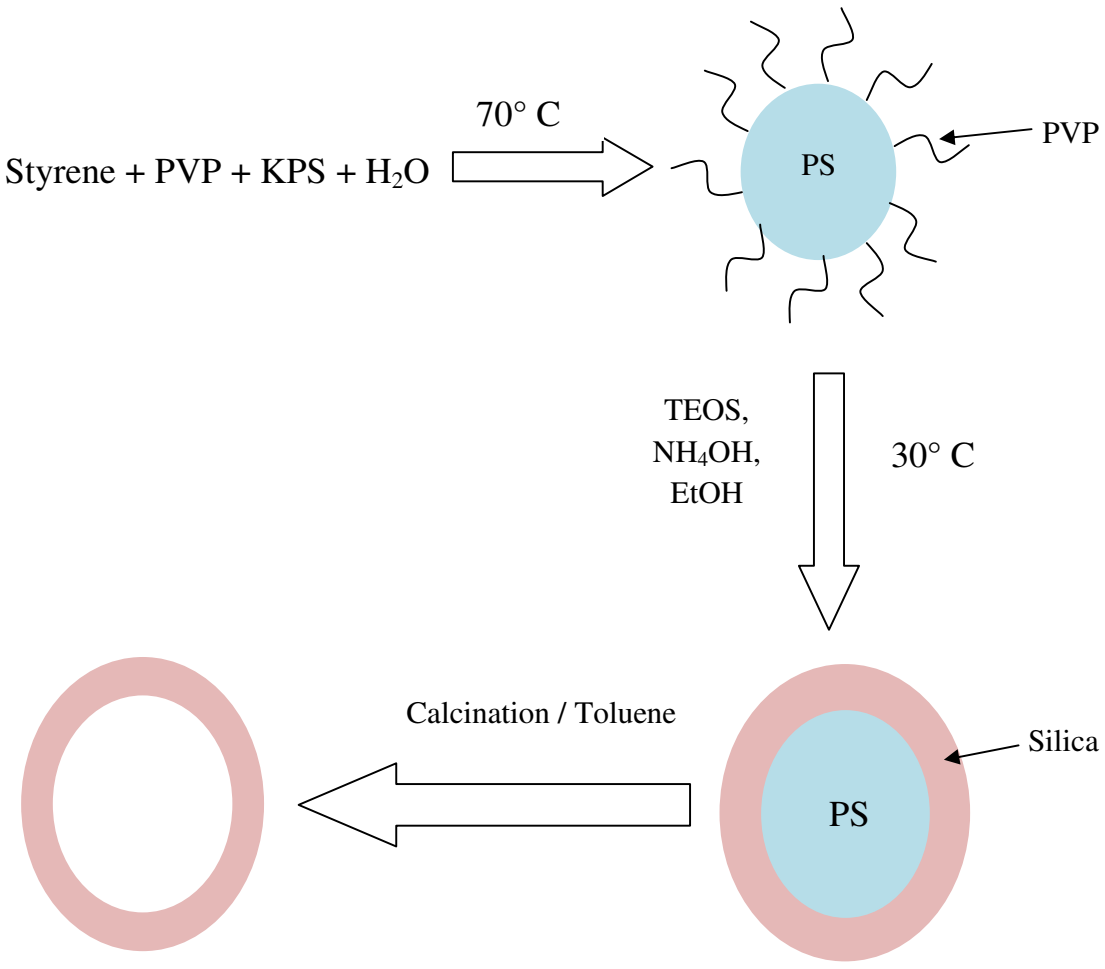

Silica microsphere

Fig. 2.7 Schematic presentation of SM synthesis

obtained followed the synthesis of the core-shell particles. Hollow inorganic particles are a special class of core-shell particles in which the core consists of air or solvent, and such hollow spheres can find applications in many fields. Most methods of fabrication of hollow silica spheres involve removing the core by calcinations [23,162-166] or dissolution into solvents [167,168] Recently, Wu et al [169] reported a method for the fabrication of monodisperse hollow silica microspheres via a one-step process, which meant that the formation of the inorganic shells and the dissolution of core particles occurred in the same medium. Synthesis of SM as discussed in this thesis was carried out in two steps (Fig. 2.7). In the first step, monodispersed polystyrene (PS) particles were prepared by emulsion polymerization through sol-gel route. In the second step, the PVP functionalized PS latexes were reacted with tetraethyl orthosilicate (TEOS) in a solution of ammonia in ethanol to yield silica coated latex particles in a seeded growth process.

2.2.1 Preparation of polyvinylpyrrolidone (PVP) functionalized polystyrene (PS) latexes

The monodispersed PS particles were prepared by emulsion polymerization. Measured quantity of styrene 10 g, PVP (1.5 g) and water (90 mL) were charged into a 250 mL Teflon

Fig. 2.8 Autoclave used for the SM synthesis

autoclave. The solution was stirred and deoxygenated by bubbling nitrogen at room temperature for 30 min. Then, the mixture was slowly heated to 70 ºC, followed by addition of 10 mL of aqueous solution containing potassium peroxodisulfate (KPS) (0.1 %), and the reaction was carried out at 70 ºC for 24 h in an autoclave (100 mL capacity teflon lined stainless steel autoclave; maximum operating pressure upto 100 bar; make: Amar equipments; Fig. 2.8) [170-172].

2.2.2 Formation of silica-coated PS particles and silica microspheres (SM)

The polyvinylpyrrolidone (PVP) functionalized polystyrene latexes were reacted with tetraethyl orthosilicate (TEOS) in a solution of ammonia in ethanol to yield silica coated latex particles in a seeded growth process. In a typical procedure, NH_4OH solution and PS emulsion were added into ethanol under stirring, and the mixture was kept at 30 ºC. Then, 10 mL solution of the TEOS in ethanol was added slowly to the suspension under stirring at 30ºC at a rate of 1 mL h^{-1} using a peristaltic pump. The reaction mixture was stirred at 30 ºC for an additional 5 h. After cooling to room temperature, the suspended particles were separated using ultracentrifuge (Ultra 5.0, Hanil Scientific) at 35000 rpm for 2 h. Then the dried particles were treated with toluene to dissolve the PS and to make it porous and hollow and again washed and dried before use [171].

In the formation of SM, PVP first participated in the polymerization reaction as a stabilizer or surfactant and then played a coupling agent role in the latter process. The polystyrene particles were dissolved subsequently or simultaneously during the sol-gel coating process followed by treatment with toluene to form silica microspheres. Silica was formed from the hydrolysis of the TEOS followed by condensation reaction as shown in Fig. 2.9.

Hydrolysis

$$Si(OCH_2CH_3)_4 + 2\,H_2O \longrightarrow Si(OH)_4 + 4\,CH_3CH_2OH$$

Condensation

$$Si(OH)_4 \longrightarrow SiO_2 + 2\,H_2O$$

Fig 2.9: Formation of silica from TEOS

2.2.3 Preparation of silica microspheres (SM) impregnated calcium alginate (Cal-Alg-SM) beads

The prepared SM in two steps could directly be used as sorbent for suitable materials. In order to ease the separation of SM from the aquatic medium after use, the SM was impregnated in alginate matrix. A 0.4 M solution of sodium alginate (Na-Alginate) in 100 mL of water was prepared. Weighed SM [10% (wt./vol.)] was mixed thoroughly in the solution to make it homogeneous. Then the mixture was stirred (600 rpm) for 5 h taken in polypropylene bottles and was added drop wise into 250 mL 4% calcium chloride ($CaCl_2$) solution using a peristaltic pump. The uniformity of the beads in shape and size were maintained by controlling the flow rate of the homogenised mixture of SM and Na-alginate into the solution of calcium chloride by using peristaltic pump and a tube of 1.5 mm diameter. The size and shape of the beads as observed in digital image is shown in Fig. 2.9.

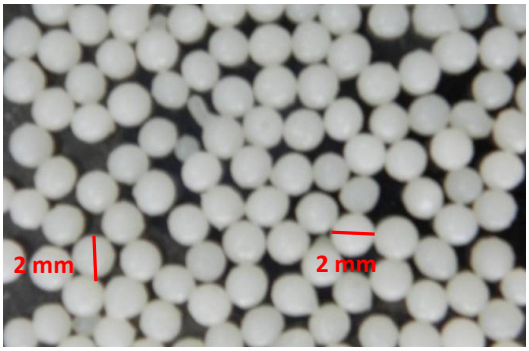

Fig. 2.10: Digital image of Cal-Alg-SM bead

The average diameter of the beads was 2 ± 0.2 mm and optimum composition of 10% SM loading in 4% Ca-alginate and 86% water content making it permeable. Na alginate reacted with $CaCl_2$ to form beads of Ca alginate, entrapping the SM within it. The beads were stable, homogenous and permeable to water. Chemical analysis carried out after digestion of the pure beads showed that the presence of Ca, Si along with low molecular weight elements C, O, N, H which suggests proper impregnation of SM into the calcium alginate matrix. C/N, C/H ratios were obtained as 256 and 6.6 respectively.

2.3 Techniques used for characterization

Various instrumental techniques were involved starting from the separation and characterizations of the hybrid materials, analysis of the trace and heavy elements upto the quantification of the contaminants. In this section the techniques used for the characterization of the synthesized hybrid materials are discussed.

2.3.1 Measurement of size distribution (mean hydrodynamic diameter) and zeta potential

Size distribution and zeta potential of the silica microspheres and TiO_2 NP in water samples were studied by using Malvern Zetasizer Nano ZS with an autotitrator (MPT-2) for zeta potential measurement. Measurements were taken by dynamic light scattering using He–Ne laser with a power of 4.0 mW and wavelength of 633 nm. The intensity of the scattered light was measured using an avalanche photodiode detector (@173º) at room temperature (25 ºC) having a quantum efficiency of 50 % at 633 nm. The size range it can measure is 0.6nm to 6 micron.

2.3.2 Spectroscopic investigation (Attenuated total reflectance-Fourier transform infrared)

The Attenuated total reflectance-Fourier transform infrared (ATR-FTIR) spectra of the hybrid materials under different conditions were recorded between 500 and 4,000 cm^{-1} with a spectrum resolution of 4 cm^{-1} by using Fourier transform spectrometer [Spectrum One (Bruker) Model α-ALPHA-P] equipped with the universal ATR as an internal reflection accessory (diamond crystal) which have composite zinc selenide optics. It has a source of silicon carbide rod and DTGS as detector. Raman spectrometry of the samples was carried out using Horiba Lab RAM Raman spectrometer having a 633 nm laser as excitation source.

2.3.3 Scanning electron microscope with energy dispersive X-ray spectrometry (SEM-EDS)

The surface morphology of the sorbents and nano materials used in this thesis were studied using scanning electron microscopy coupled with energy dispersive X-ray fluorescence spectrometry (EDS) (Instrument Model No. TESCAN VEGA MV 2300T). SEM produces images of a sample when a focused beam of electrons is scanned across its surface. The electrons interact with atoms in the sample, producing various signals such as secondary electrons and characteristics x-rays, which are then detected to obtain information about the sample's surface topography and composition, respectively. SEM can achieve resolution of ~10 nm. Both secondary electron and back scattered detectors were used for imaging. Before recording the surface morphology, gold coating of the samples were carried out using mini sputter coater.

The compositional analysis has been carried out using energy dispersive x-ray analysis system (OXFORD INCA) equipped with SEM. The minimum detection limit (MDL) of the EDX is about ~1 wt%. X-rays are produced as a result of ionization of an atom by high-energy radiation wherein an inner shell electron is removed. To return the

ionized atom to its ground state, an electron from a higher energy outer shell fills the vacant inner shell and, in the process, releases an amount of energy equal to the potential energy difference between the two shells. This excess energy, which is unique for every atomic transition, will be emitted by the atom either as an X-ray photon or will be self-absorbed and emitted as an Auger electron.

2.3.4 X-ray diffraction (XRD)

For determination of the structure of the Cal-Alg-Alu beads and TiO_2 NP, x-ray diffraction measurements were carried out. Powder X-ray diffractometer (Proto XRD) in θ-2θ scan mode was used to characterize the orientation and structure of the samples. The X-ray source used was Cu K_α having wavelength of 1.54Å. Scanning range was 10-90º.

2.3.5 Surface area measurement

The surface area of the few sorbents as required was measured by evaluating sorption and desortion isotherm and using BET isotherm (Instrument used: model: Surfer; Thermo Scientific). Physical adsorption of gas molecules on a solid surface serves as the basis for analysis of the specific surface area of a material. The BET theory refers to multi layer adsorption, and non-corrosive gas nitrogen was used as adsorbate to determine the surface area. Bead samples were cryo-dried before BET measurement.

2.4 Characterization of hybrid materials

The synthesized hybrid materials were characterized using various techniques as mentioned in the above section.

2.4.1 Characterization of alginate based beads

From the digital images of the beads shown in Fig. 2.3 (Cal-Alg beads), 2.4 (Cal-Alg-Chi beads), 2.5 (Cal-Alg-Alu beads), 2.6 (Cal-Alg-Goe beads), 2.10 (Cal-Alg-SM beads) the

uniformity in shape and size of the beads could be confirmed. The optimum composition of the beads as given in table 2.1 was verified by suitable chemical analysis. High water content of the beads makes them permeable to contaminants. Elemental characterisation of the beads was carried out by using CHNS analyser, whereas the concentration of Ca was determined after digestion of the beads using ICP-OES.

(a) Cal-Alg-Chi beads:

The ATR-FTIR of Cal-Alg-Chi beads is shown in Fig. 2.11. ATR-FTIR analysis carried

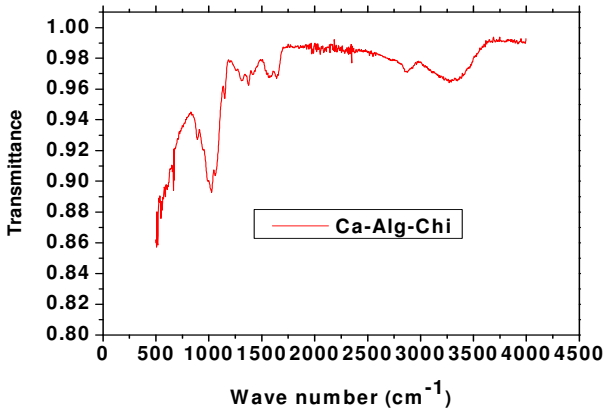

Fig. 2.11: FTIR spectrum of Cal-Alg-Chi beads

out at different portion of the beads confirms the uniform distribution of chitosan in the Ca-alginate matrix. The major bands appearing in the spectrum were due to the vibration modes of different functional groups present in the chitosan. In the spectrum of pure Cal-Alg-Chi beads, bands appearing from 3700 cm^{-1} to 3000 cm^{-1} were due to stretching vibrations of OH groups. Stretching vibration of C–H and N-H bonds (2870-2920 cm^{-1}), NH_2 stretching and -OH stretching (3450 cm^{-1}) overlap in this region [178]. Vibration in the range of 1640-1700 cm^{-1} is due to vibrations of carbonyl bonds (C=O) and amide groups (-CONH-). Two bands near 1250-1300 cm^{-1} are due to –OH and –C-O-C vibration. Absorption band near 1080–

1030cm^{-1} are because of CO present in COH, COC and CH_2OH [179]. SEM images taken of the beads before and after the uptake show the surface morphology of the Cal-Alg-Chi beads (Fig. 2.12). In Fig. 2.12A image of the full beads were shown after cryo-drying and gold coating to make it conducting. Fig. 2.12B gives the SEM image of the cross section of a particular bead. The average size of the beads was 2 ± 0.2 mm as shown in Fig. 2.4.

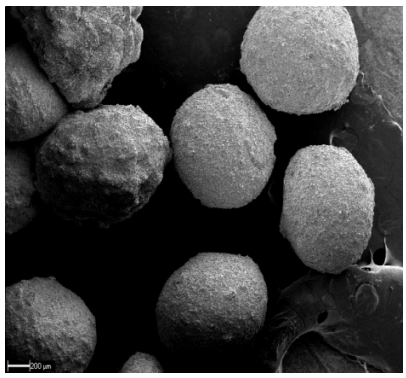

Fig.2.12A: SEM image of Cal-Alg-Chi beads (cryo dried)

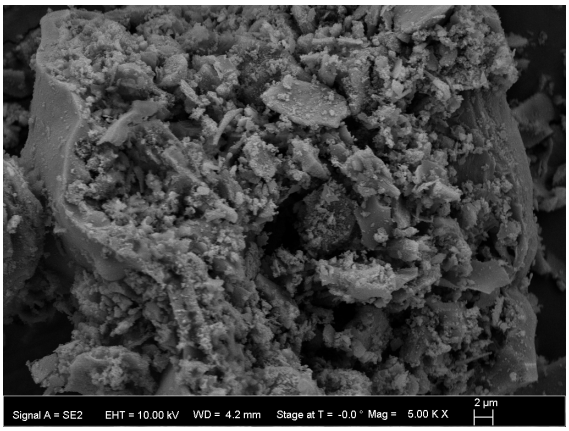

Fig.2.12B: SEM image of cross-section of Cal-Alg-Chi beads

(b) Cal-Alg-Alu beads:

The SEM image of Cal-Alg-Alu beads is shown in Fig. 2.13. As can be seen from Fig. 2.13, the sorbent does not possess any well-defined porous structure. EDS analyses were performed to determine the elemental constituents (Fig. 2.14). It shows that the presence of principal elements Ca, Na, Al and O as constituents. The FTIR spectra of pure beads is shown in Fig. 2.15. In FTIR spectra of Cal-Alg-Alu beads (before adsorption) the peaks at 1040 cm^{-1} and 510 cm^{-1} corresponds to the Al–O stretching vibration [180-182]. The average size of the beads was 2 ± 0.2 mm as shown in Fig. 2.5.

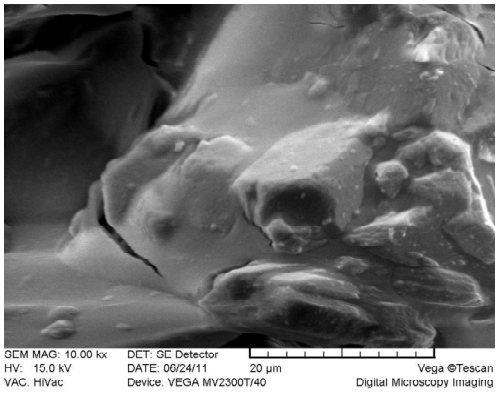

Fig.2.13: SEM image of Cal-Alg-Alu beads

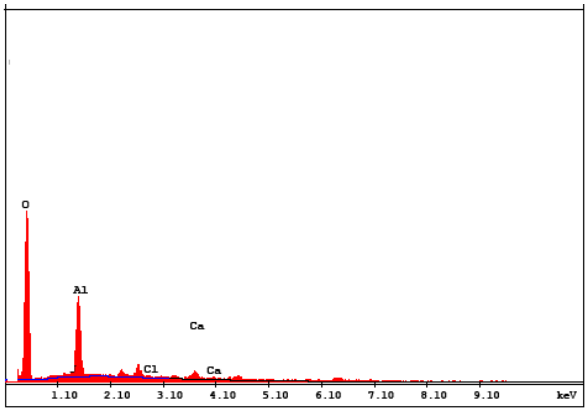

Fig.2.14: EDS spectrum of Cal-Alg-Alu beads

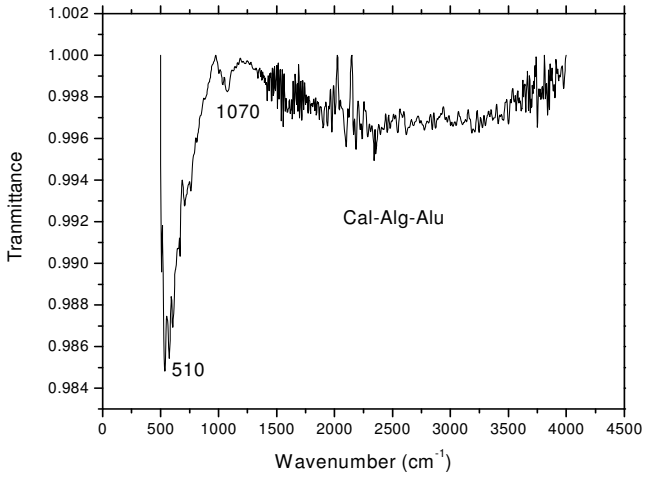

Fig. 2.15: FTIR spectrum of Cal-Alg-Chi beads

(c) Cal-Alg-Goe beads:

Prior to the synthesis and charecterisation of the Cal-Alg-Goe beads, the synthesized goethite was first charecterised. Goethite (α FeO(OH) was confirmed as the main product by PXRD (Powder X-Ray Diffraction) and by recording its ATR-FTIR spectrum between 500 -1400 cm^{-1}.

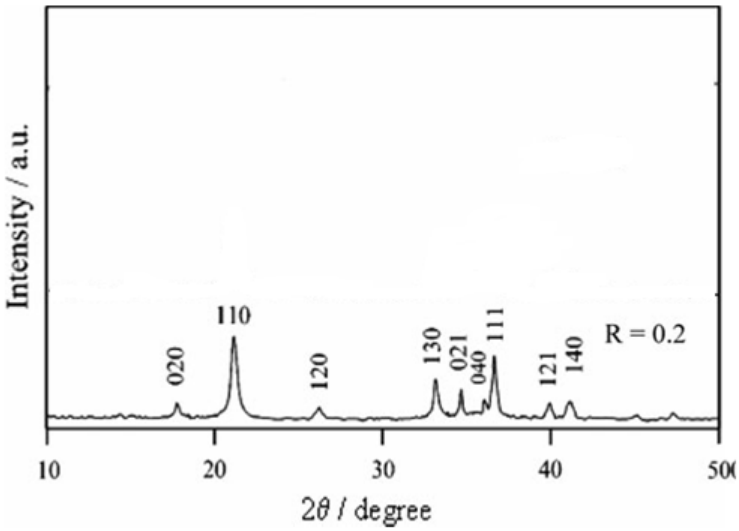

Fig.2.16: XRD pattern of goethite

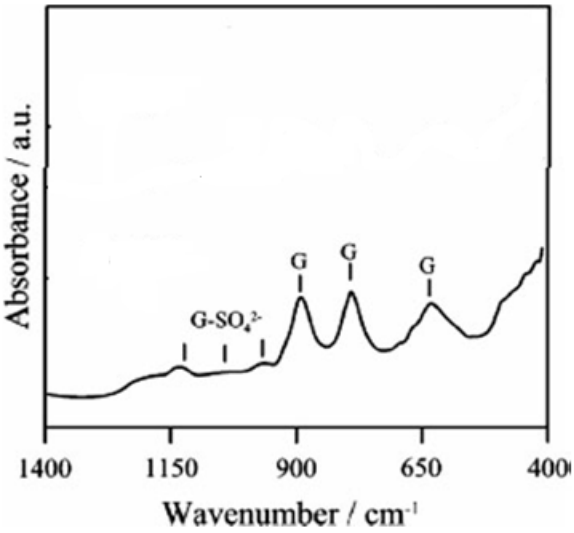

Fig. 2.17: FTIR spectrum of goethite

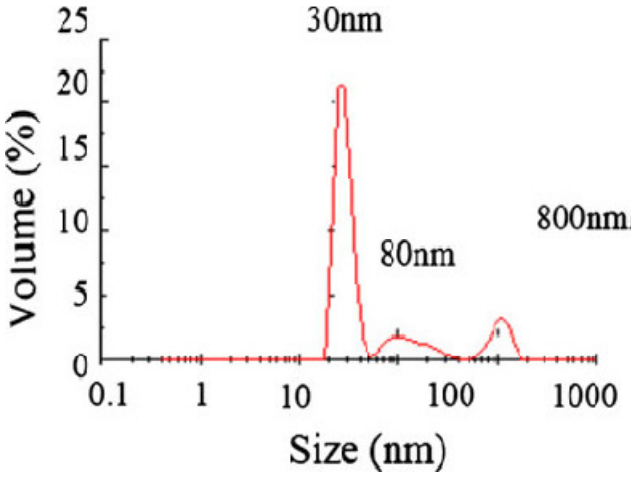

Fig. 2.18: Size distribution of goethite

XRD as given in Fig. 2.16, shows that goethite was the main product obtained. The main vibration bands generally attributed to goethite [183-184] are found at 630, 795 and 890 cm^{-1} which are also observed in case of synthesised goethite (Fig. 2.17). Additional bands at 975, 1,055 and 1,130 cm^{-1} may be attributed to sulphate ions adsorbed on the surface of the goethite crystals [184]. Hydrodynamic size distribution of goethite powder was recorded in a

water medium using dynamic light scattering (DLS) technique and observed that goethite formed was a polydispersed suspension having particle sizes in the range of 60-900nm (Fig. 2.18). From this Fig. it is clear that suspension of goethite was dominated by 30 nm particles followed by 80 and 800 nm particles. From the plot of zeta potential with pH (Fig. 2.19), isoelectric point (or PZC) of goethite was obtained around pH 6.0 which suggests positive surface charge on the particles below pH 6.0 and negative charge above pH 6.0. The surface charge of goethite originates mainly from ionization of surface groups or surface chemical reactions. Surface charge on these groups is strongly dependent upon pH, being positive at lower pH and negative at higher pH.

Coming to the Cal-Alg-Goe beads, the uniformity of the beads in shape and size were maintained by controlling the flow rate of the homogenised mixture of goethite and calcium alginate in the solution of calcium chloride. Photographic image of Cal-Alg-Goe beads are shown in Fig. 2.6. The average size of the beads was 2 ± 0.2 mm.

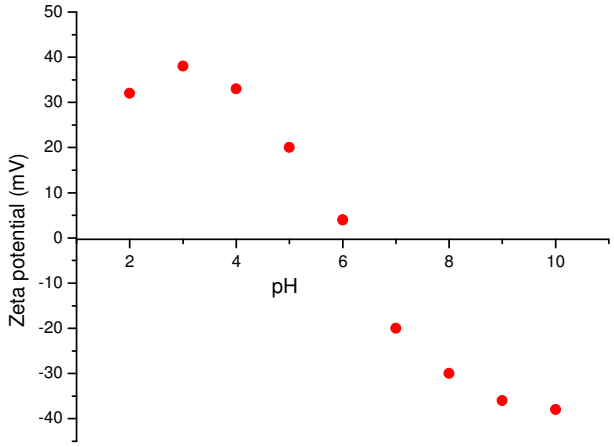

Fig.2.19: Plot of zeta potential of goethite at different pH

The SEM image of a Cal-Alg-Goe bead is shown in Fig. 2.20. XRF analyses were performed to determine the elemental constituents of Cal-Alg-Goe beads, the principal elements Ca, Fe were observed in case of Cal-Alg-Goe beads (Fig. 2.21). Chemical analysis carried out after digestion of the beads showed that the presence of Fe, Ca along with low molecular weight elements C, O, N, H which suggests proper impregnation of goethite into the calcium alginate matrix. The composition of the bead (18% goethite loaded in 4% alginate) as given in table 2.1 was verified.

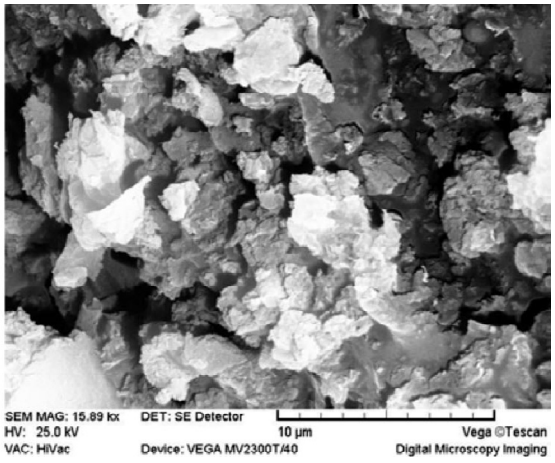

Fig. 2.20: SEM image of Cal-Alg-Goe beads

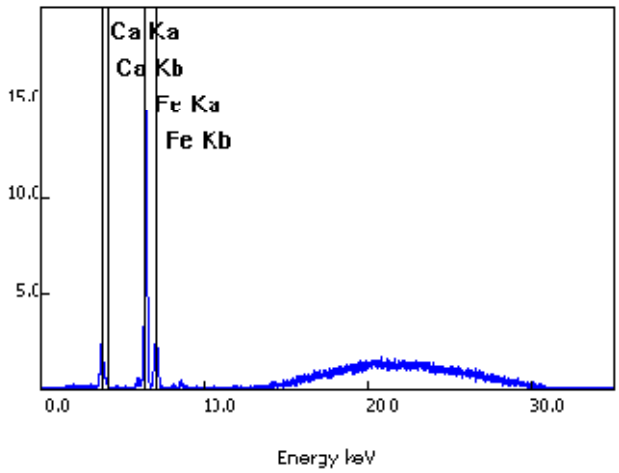

Fig. 2.21: XRF spectrum of Cal-Alg-Goe beads

2.4.2 Characterization of silica microsphere based hybrid materials

Silica microsphere was used as sorbent both as powder as well as calcium alginate impregnated beads.

(a) Silica microspheres (SM)

The size distribution of the SM as determined by the zeta sizer nano (ZS) showed mean value of 220±20 nm. The zeta potential values evaluated at various pH, showed an isoelectric point or PZC at around pH 2 (Fig. 2.22). It was therefore positively charged below pH 2 and negatively charged above pH 2.

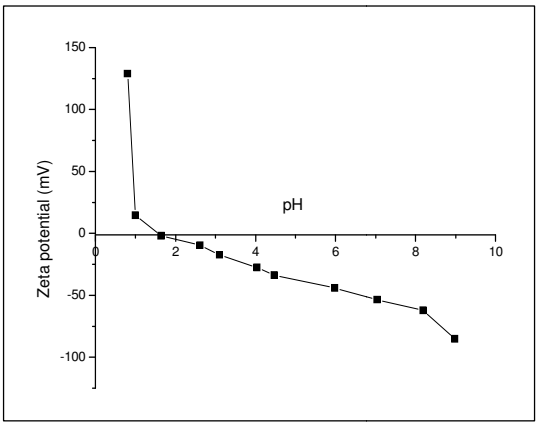

Fig. 2.22: Plot of zeta potentials of SM at various pH

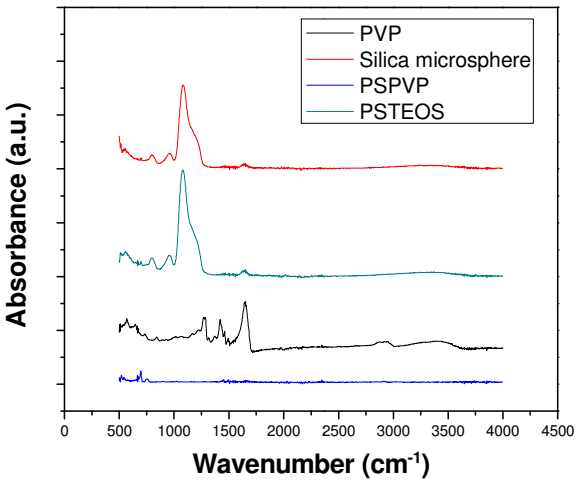

Fig. 2.23: ATR-FTIR spectra at different stages of SM formation

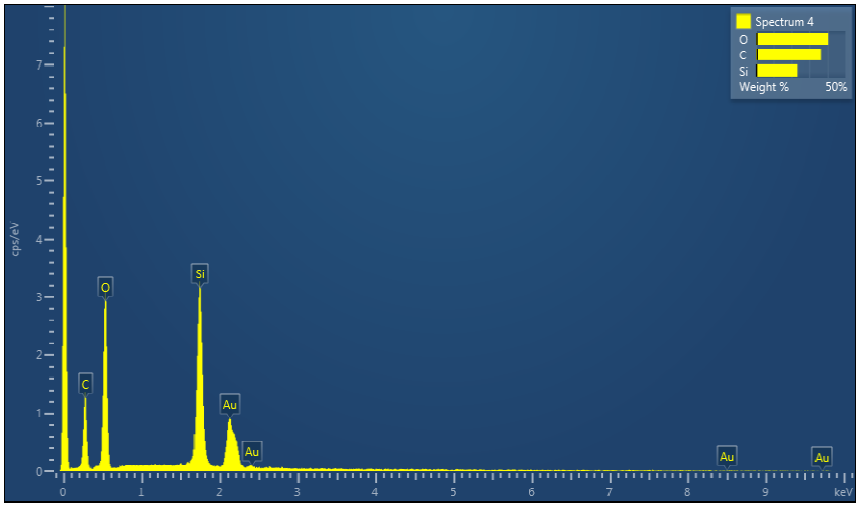

Fig. 2.24: EDS spectrum of SM

The surface charge of SM originates mainly from ionization which is strongly dependent upon pH as clear from Fig. 2.22. Fig. 2.23 shows the ATR-FTIR spectrum of the microspheres taken at different stages. Band at 1100 cm^{-1} in Fig. 2.27 indicates the presence of Si-O-Si bending vibration and band at 806 cm^{-1} is due to symmetric stretching. No trace of unreacted PVP was observed in the final product which is clear from Fig. 2.23. The

chemical composition of the developed SM was verified by EDS spectra as well as by chemical analysis. Presence of peaks of silicon and oxygen in the EDS (Fig. 2.24) suggest the SM formation which was confirmed through chemical analysis.

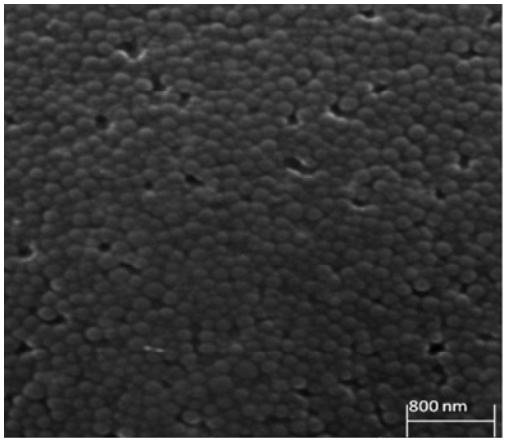

Fig. 2.25: SEM image of SM

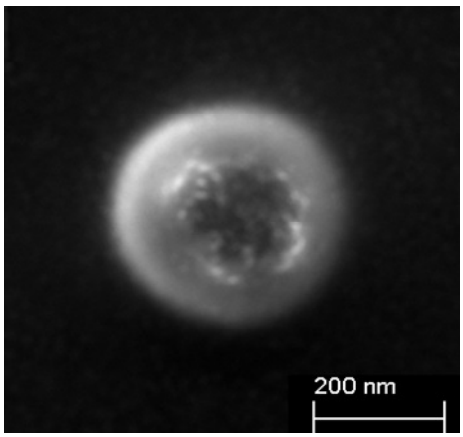

Fig. 2.26: SEM image of a single SM

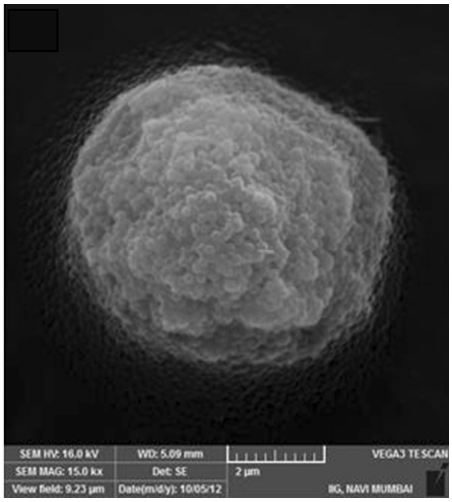

Fig. 2.27: SEM image of agglomerated SM

The SEM images show the surface morphology and spherical shape of the SM (Fig. 2.25 and 2.26). Fig. 2.26 shows a single microsphere and the hollowness within it. These silica microspheres once kept tends to coagulate and one needs to ultrasonicate it before further

processing to get enhanced effectiveness. One such agglomeration is visible in the SEM image taken before ultrasonication (Fig. 2.27).

The BET measurement showed a high specific surface area (32.6 m^2 g^{-1}) of the SM making it suitable to be used as sorbent. BET isotherm for both adsorption and desorption is given in Fig. 2.28. Average pore diameter was found to be 1.35 nm and the pore size distribution is given in Fig. 2.29. Chemical analysis conducted confirmed that the particles are comprised of pure SiO_2, with no indication of impurity elements.

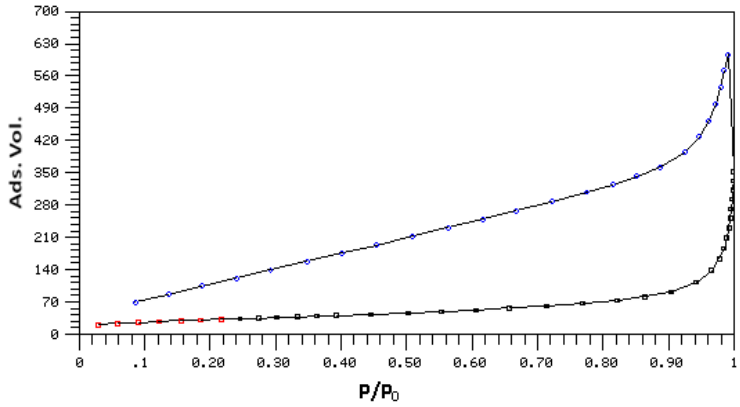

Fig. 2.28: BET isotherm of SM

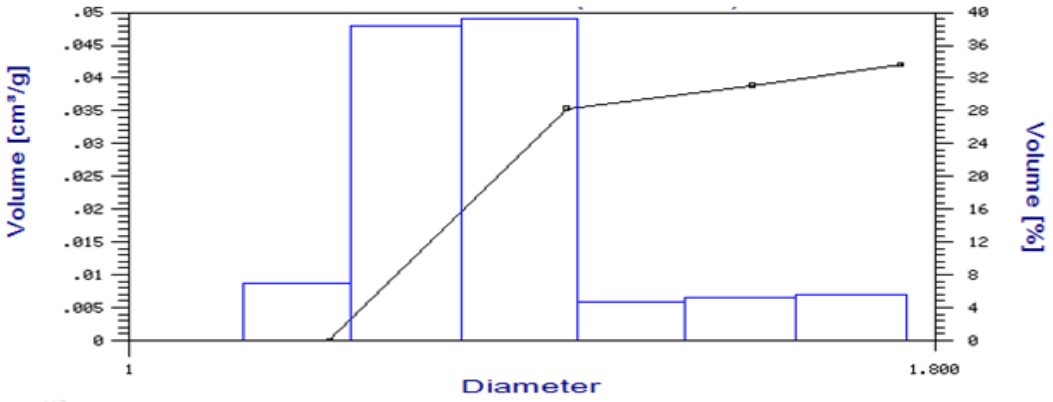

Fig 2.29: Pore size distribution of silica microsphere (SM)

(b) Silica microspheres impregnated calcium alginate beads

Calcium alginate immobilization of SM involved displacement reaction like other alginate impregnated beads. The average diameter of the beads was 2 ± 0.3 mm as can be seen in the

digital image (Fig. 2.10) of the beads. The BET measurement showed a specific surface area of 28.3 m^2 g^{-1} for Cal-Alg-SM beads. The beads were cryo dried before proceeding for BET measurement. BET isotherm is given in Fig. 2.30. Average pore diameter was found to be 1.36 nm and the pore size distribution is given in Fig. 2.31. SEM and FTIR analysis of the beads were also carried out which will be discussed in details in the subsequent chapters along with the contaminants sorbed beads.

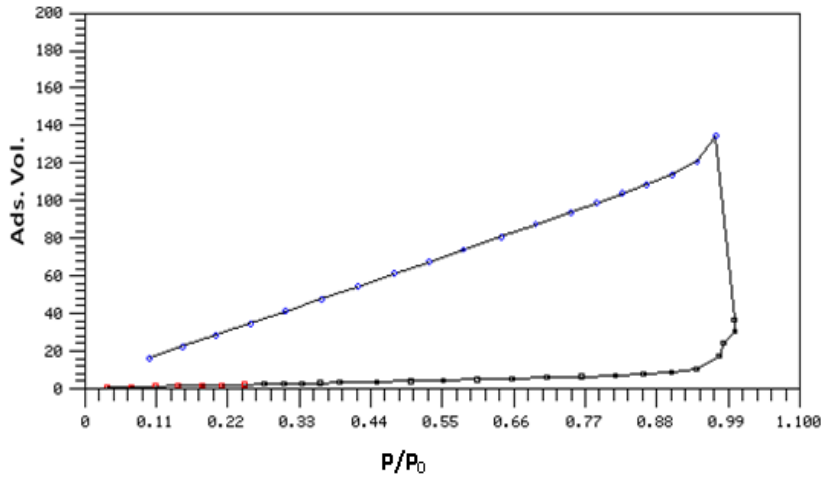

Fig. 2.30: BET isotherm of Cal-Alg-SM beads

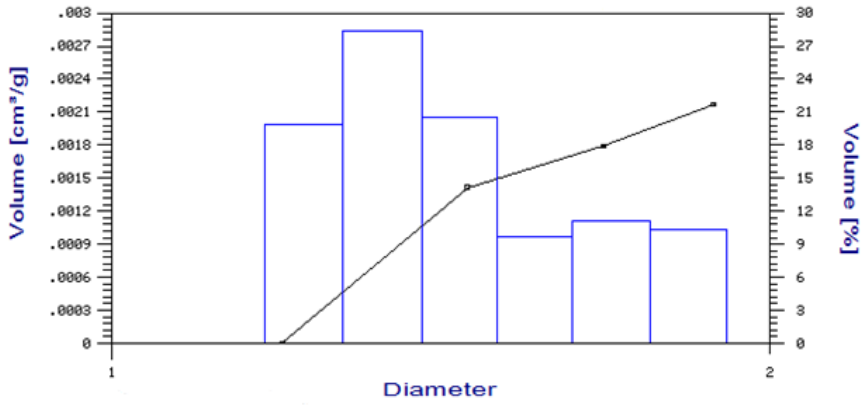

Fig. 2.31: Pore size distribution of Cal-Alg-SM beads

2.4.3 Stability of the beads

The stability of the alginate beads is an important factor. We have used four different types of impregnated alginate (Cal-Alg-Chi, Cal-Alg-Alu, Cal-Alg-Goe, Cal-Alg-SM) and one pure calcium alginate beads as hybrid materials. All these beads were found to be extremely stable for months when stored in demineralised water. Stability of the beads was however checked without storing them in water. Under this condition beads were found to slowly lose the water content in it but its integrity was not affected. Beads were completely dried keeping

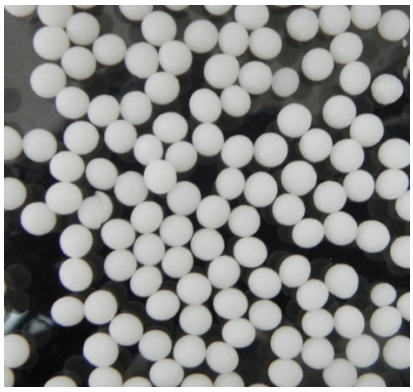

Fig. 2.32A: 6 months old Cal-Alg-Chi beads

Fig. 2.32B: Dried and 6 months old Cal-Alg-Chi

under IR lamp as well as cryo-dried and then its effectiveness for contaminant removal was checked. The uptake capacity of the beads was not reduced when completely dried and old beads (four months) were used indicating the functional integrity of the prepared hybrid materials. No change in the physical properties was observed due to storing them for a prolonged period. Digital images of the Cal-Alg-Chi beads (Fig. 2.32 A & B) and Cal-Alg-SM beads (Fig. 2.33 A & B) taken after 6 months both wet as well as in the dried condition are given here.

Fig. 2.33A: 6 months old Cal-Alg-SM beads

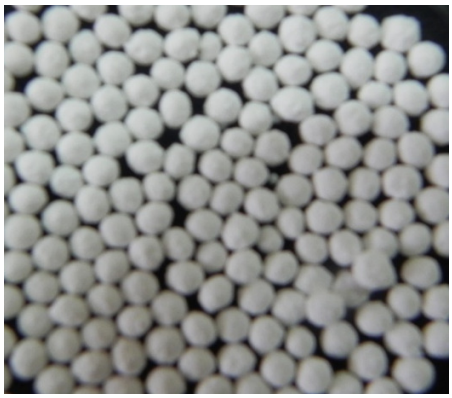

Fig. 2.33B: Dried and 6 months old Cal-Alg-SM

2.5 Techniques used for isolation

To separate out the silica microsphere from the solution phase both ultracentrifuge and ultrafiltration was used. Low temperature vacuum ultracentrifuge used had maximum rotation speed of 55000 rpm (Ultra 5.0, Hanil Scientific). Most of the separation were carried out by centrifugation at 30000 rpm for 30 minutes. For the separation of suspended nanoparticle ultra-filtration was performed with an Amicon Stirred Cell (Model M2000) (Fig.

Fig 2.34: Ultrafiltration system

Fig.2.35: ICP-OES system with autosampler

2.34). To concentrate the solution with a particles of a particular size range, the solution was passed through the ultra-filtration membrane of cellulose acetate. Ultra-filtration cell is used in concentration operation modes. In this mode, N_2 gas is applied with pressure (0.5 kg cm^{-2}) directly to the ultra-filtration cell. Nanoparticles (solute) above the membrane molecular weight cut-off were retained in the cell while water and solute below the cut-off passed into the filtrate. Constant stirring above the membrane surface was employed to avoid the accumulation of solute molecules at the membrane surface. Before using, the membranes were soaked in 0.1 M nitric acid for one day and then in distilled de-mineralized water for 3 days. Before putting the sample, 500 mL of deionised water was passed through these membranes and this solution was used for blank sample preparation.

2.6 Techniques used for quantification

The contaminants studied in this thesis varied from conventional pollutants, radioactive pollutants to nanoparticles, different types of techniques were therefore involved in the analysis and quantification of these contaminants. The techniques used for quantification can

Table 2.2 Emission lines used in ICP-OES

Element	Emission wavelengths (nm)
U	263.553
	385.958
Th	401.913
	283.232
As	193.759
	197.262
Ti	308.802
	334.904
Eu	381.965
	318.967

be broadly categorized into two parts i.e. emission spectrometric techniques for metals and α spectrometry for radioactive content.

2.6.1 Emission spectrometric technique

The concentrations of the contaminants like U, Th, As, Ti (in TiO_2 NP) and Eu (as chemical analogue of Am) at various stages of the experiments were measured by Inductively Coupled Plasma Optical Emission Spectrometer (ICP-OES, model ACTIVA S, from Horiba 128 Jobin–Yvon SAS, France) with simultaneous solid state detector (Fig. 2.35). ACTIVA utilizes a large no. of pixels, ultra-low noise, and high quantum efficiency charge-coupled device (CCD) solid-state detector. ACTIVA includes a unique optical design featuring a 0.64m Czerny-Turner optical system and holographic gratings of 4,343 grooves per mm and 2,400 grooves per mm. Covering the full 6 mm height of the plasma, ‘‘Normal Analytical Zone Multi-WAV’’ acquisition mode provides complete sample fingerprinting of 75 elements in less than 30 s. It gives resolution up to 10 pm. Temperature of the plasma ranges between 8000 -10,000^{O}C whereas the analysis zone have a temperature of 8000^{O}C. The calibration of instrument was carried by using Aldrich/ Fluka ICP-OES standard solutions. Intensity of emission was measured at two different wavelengths for each element analyzed and the average concentrations from two wavelengths were used in the wotk. The energies of the highly sensitive lines selected for quantification are given in table 2.2. For the quantification of samples with high organic content, organic part was destroyed by microwave ashing in case of solid and by addition of hydrogen peroxide and nitric acid in case of solution before digesting the metal ion making a 2% HNO_3 solution. All the interferences were taken care and the relative standard deviations were within ± 2.0%. For

determination of arsenic in the ppb range (less than 1 mg L^{-1}) Inductive Coupled Plasma-Mass Spectrometer (ICP-MS, model VG PQ ExCell, VG Elemental, UK) was used.

2.6.2 α- spectrometric technique

Alpha activity measurement was required for the quantification of amrecium, pluotonium and uranium. Quantitative estimation of radionuclides concentration was carried out by pre-concentrating it with $Fe(OH)_3$. This separates them from Ca, Mg and amphoteric elements. In case of sample with high value of DOC, the samples were refluxed with 8 N HNO_3 and H_2O_2 to destroy the DOC before pre-concentrating with $Fe(OH)_3$. In general iron, associated with matrix have a lot of interference due to its preferential electro deposition on stainless steel planchet. Separation of Fe from radionuclides was therefore necessary. Standard protocols were adopted for the radiochemical separation in various fractions [173-177]. The analysis carried out after quantitative electroplating of radiaonuclides on a stainless steel (SS) planchet. The electrolyte solution used was $(NH_4)_2SO_4$ and H_2SO_4 mixture at pH 2.2. Set up is shown in Fig. 2.36. The electroplating was done at an applied voltage of 6 V and 0.3 A current for 3 h. Electroplating was stopped by slightly raising the pH by addition of few drops of ammonia. The deposited radionuclide on SS planchet was converted to oxide by heating the planchet on a bunsen burner flame until red hot. The planchet was counted overnight (60,000s) in a alpha spectrometer having PIPS (passivated implanted planner silicon) detector coupled with a 1K MCA (multi channel analyser). The resolution of the detector was 18 keV for ^{239}Pu and efficiency was 21.3%. The calibration of the system was carried out by using a mixed alpha point source of ^{239}Pu (5155 keV), ^{244}Cm (5806 keV) and ^{241}Am (5486 keV). A typical α spectrum of the mixed source is shown in Fig. 2.37. The efficiency of the system was evaluated by using ^{241}Am standard having an activity of 83.33

Bq. This electrodeposited source was prepared by using standard solution of ^{241}Am received from IAEA. For the purpose of quality assurance, a control sample from a reference soil material (IAEA-376) having $^{239+240}$Pu concentration 0.3 Bq kg^{-1} was digested and analysed in a similar manner as an unknown. The results obtained (0.28–0.31 Bq kg^{-1}, n=4) and the recommended values were in close agreement.

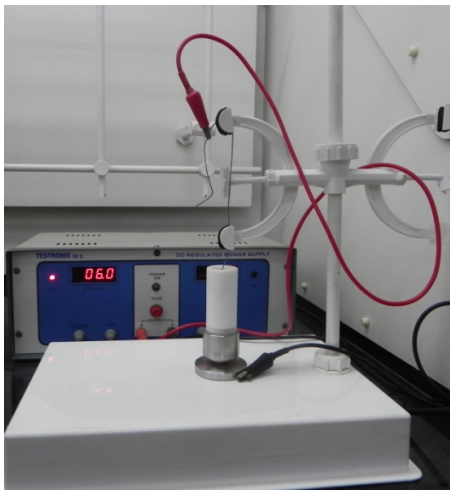

Fig. 2.36: Electro deposition set up

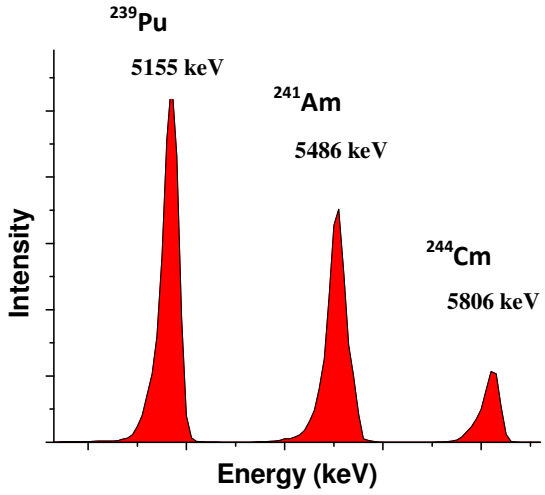

Fig. 2.37: Typical α spectrum of mixed source

2.6.3 Determination of TiO_2 NP concentration

Concentration of TiO_2 NP was determined in terms of total elemental concentration of titanium and was converted to equivalent amount of TiO_2. TiO_2 NP suspension could not be directly introduced into the nebuliser of ICP-OES, so before determination of concentration by ICP-OES, it was digested with the help of hydrofluoric acid and nitric acid at a ratio of 1:5 in a teflon beaker and subsequently heating on a hot plate at 70-80 $^{\circ}$C for 30 min, then evaporated to dryness by heating at 100-120 ºC. The residue was finally dissolved in 2% HNO_3 solution and made upto 25 mL for analysis using ICP-OES. The emission lines of 381.965 nm and 318.967 nm were used for titanium determination.

2.6.4 Measurement of fluoride

Two different methods were involved for determination of fluoride concentration.

(i) Ion selective electrode

Ion selective electrode determination of F^- was done by using an ion selective electrode (Metrohm make Model 692) sensitive to the concentration of the fluoride ion. Before measurement pH was adjusted to 5.5 adding TISAB (Total Ionic Strength Adjustment Buffer) to each set. CDTA (cyclohexane diaminotetra acetic acid) was used as chelating agent to release the bound fluoride in the solution. Method detection limit is 0.1µg mL^{-1}.

(ii) Ion chromatography

The concentration of fluoride in the solutions was also determined by using ion chromatography (Dionex, RFICS-2000, Ion Chromatography system,). KOH cartridge having a strength of 30 mM was used as a mobile phase and delivered at the flow rate of 1.0 mL min^{-1} with injection loop of 25µL. A separation column, IonPac® AS 23-HC, 4.0 mm×250 mm (Dionex), a guard column, IonPac® AG23-HC, 4.0mm×50mm (Dionex, USA), and membrane suppressor, ASRS 3000 were used. The data acquisition was performed using Chromeleon 6.5 (Dionex). Method detection limit was 1 ng mL^{-1}.

2.3.5 Measurement of physicochemical characteristics

Various physiochemical characteristics like pH, conductivity, and redox potential was measured by using pH meter (Model $PICO^+$, Lab India) and conductivity meter (Model $PICO^+$, Lab India). In case of redox potential measurement single pin platinum electrode was used instead of single pin glass electrode (used in case of pH measurement). For measuring the organic carbon content, the samples were treated with 8 N HCl to destroy the inorganic

carbon and washed with ultrapure water and carbon content was measured by using elemental (C, H, N, S, O) analyser (Model Flash EA 1112, Make Thermo Finnigen).

2.3.6 Elemental profile

For quick screening of the elemental profile potable XRF (Innovex) was used. It uses X-ray tube of W target (40 KV) and Si PIN detector. It has a resolution of 200eV at 5.95 KeV Mn K_{α} line. For the C, H, O, N determination elemental analysis was carried out by using Elemental analyzer. The concentrations of various metal ions were either measured by Atomic Absorption Spectrometry (AAS, Model: SavantAA Σ from GBC scientific) or Inductive Coupled Plasma-Optical Emission Spectroscopy (ICP-OES, model Activa S; Horiba Jobin Yvon). Dionex Ion Chromatrography (RFICS 2000) was used for determination of the anions. The calibrations for all the elements were carried out by using Fluka standards in HNO_3 medium.

Chapter 3

Decontamination of groundwater from radionuclides (U, Th, Pu, Am) using hybrid materials

---

3.1 Introduction

Wide spread drinking water resources contamination by radioactive constituents can result either from catastrophic incidents (Chernobyl in 1986 and Fukishima in 2012) or natural geological processes e.g. uranium in groundwater of certain district of Punjab, India. In this chapter, the uptake studies of the radionuclides are described. All three categories of the hybrid materials [alginate based; core-shell type; organic coating on inorganic substrate] were utilised for the removal of radioactive contaminants.

3.1.1 Sample preparation

Glassware and polypropylene bottles used for the experiment were cleaned, rinsed thoroughly with demineralised water and dried under IR lamp before use. All chemicals used in this thesis work were of analytical grade of Merck–Aldrich. Doubly distilled water (Millipore) was used throughout the experiment for the preparation of the reagents. Standard stock solutions of the radionuclides in nitric acid medium were used for spiking the water samples used for the experiment. Standard 1000 μg mL^{-1} stock solution of uranium [$UO_2(NO_3)_2$] and thorium [$Th(NO_3)_4$] were used for spiking the water samples in different concentration range. The stock solution of $^{239+240}Pu$ and ^{241}Am in 0.2 M HNO3 were used to spike the demineralised water or filtered groundwater. The pH of the solutions was adjusted as per the requirement of the experiment using 0.1 M nitric acid and sodium hydroxide solutions. Measured quantity of the sorbent (hybrid materials) were added in the sets and later on separated after uptake. Beads were separated by simple decantation whereas for silica microspheres ultrafiltration or ultracentrifuge was used. Different physico-chemical parameters of the water samples were measured before and after the uptake. The glassware

used were kept in 5% nitric acid overnight and subsequently washed several times with double-distilled deionized water before using.

3.1.2 Sorption experiment

The sorption studies of radionuclides on hybrid materials were carried out in batch process. Desired concentration of radionuclide solutions were prepared into polypropylene bottles from dilution of the stock solution and known weight of sorbent was added into it. The sets were kept for sufficient time with intermittent shaking to attain the equilibrium. The solution was decanted, the concentration of uranium was determined and the amount of contaminants sorbed was calculated from following equation (Eq-1),

$$Q_e = \frac{(C_o - C_e) * V}{W} \qquad (3.1)$$

Where,

C_o is the initial concentration of contaminant (mg L^{-1}) before uptake

C_e is the equilibrium concentration of contaminant (mg L^{-1}) after uptake

Q_e is the sorption capacity (mg g^{-1}) at equilibrium

V is the volume (mL) of solution and

W is the mass (g) of sorbent used.

The effect of contact time was examined by varying the time from 1 min to 30 h with fixed initial concentration of contaminants and fixed dose rate of sorbent. The effect of pH on sorption was investigated by preparing solutions of different pH.

3.1.3 Isotherm study

In order to evaluate the sorption capacity of sorbent for contaminants and to get a better inshight into the mechanism the isotherms were studied. To evaluate the sorption isotherm, the equilibrium sorption of contaminant was studied as a function of contaminant

concentration at 25-30 ^{O}C. The sorption isotherm is given below for Langmuir (Equation 3.2) model.

$$Q_e = Q_o b C_e/(1 + bC_e) \quad (3.2)$$

Where,

Q_e is the amount of sorbate per unit mass of sorbent (mg g^{-1}) at equilibrium,

C_e is the equilibrium concentration of sorbent,

Q_0 is the solid phase concentration corresponding to the complete monolayer coverage of adsorption sites and

b is a constant related to the free energy of adsorption

The Langmuir isotherm as given in equation 3.2 assumes that the free energy of adsorption does not depend on the surface coverage. It also predicts the solid surface saturation with monolayer coverage of adsorbate at high C_e and a linear adsorption at low C_e values [185,186].

Another most popular isotherm i.e. Freundlich isotherm is given in equation 3.3.

$$Q_e = kC_e^{1/n} \quad (3.3)$$

Where, n is a constant related to the strength of the adsorptive bond and

k is related to bond distribution.

Freundlich isotherm model assumes that the ratio of the amount of solute adsorbed onto a given mass of adsorbent to the concentration of the solute in the solutions is not constant at different solution concentrations [185,186].

For the developed hybrid materials the sorption isotherms were evaluated by studying equilibrium concentration of contaminants both in sorbent and in solution phase

for different initial concentrations. Each set resulted a point in the C_e vs Q_e plot. The experimental points were then fitted in both the isotherms (equation 3.2 and 3.3) keeping C_e as x and Q_e as y. Then the points were iterated for both the equation with some initial guess of the constant parameters (Q_0 and b for Langmuir; k and n for Freundlich) using software Origin 8.0. The outcome resulted the actual value of these constants with certain correlation coefficient (R^2) value. Isotherm for a particular sorption was said to follow a particular model based on the closeness of R^2 to 1.

3.1.4 Kinetics study

To study the dynamics of the solute adsorption process, the kinetics of sorption on hybrid materials were analyzed. Both pseudo-first-order and pseudo-second-order kinetic models were tested (Equation 3.5) keeping other parameters constant [187,188] (Concentration of contaminant, pH, dose rate of sorbent). Pseudo-first-order rate law is given in equation 3. 4. The nonlinear form of the equation is given in equation 3. 4.

$$\frac{dq_t}{dt} = k_1(q_e - q_t) \quad (3.4)$$

Where,

q_e is the amount of sorbent sorbed (mg g^{-1}) at equilibrium,

q_t is the amount of sorbent sorbed (mg g^{-1}) at any instant time t,

k_1 (L min^{-1}) is the rate constant of the pseudo-first-order sorption process.

After the application of the initial condition of $q_t = 0$ at $t = 0$, the linear form of the equation 3.4 is given by equation 3.5.

$$\log(q_e - q_t) = \log q_e - k_1 t/2.303 \quad (3.5)$$

The plot of log ($q_e - q_t$) versus t gives a straight line for the pseudo first order kinetics from which the equilibrium sorption capacity (q_e) and rate constant (k_1) can be estimated.

The pseudo-second-order kinetic model is given below (Equation 3.6).

$$t/q_t = 1/k_2 q_e^2 + (1/q_e)t \quad (3.6)$$

where k_2 is the rate constant for the pseudo-second order kinetics.

A plot of t/q_t vs t is made and from the intercept, the rate constant (k_2) can be estimated.

3.2 Uranium uptake by Cal-Alg-Chi beads

In the present section, the works carried out on removal of uranium from potable water using novel sorbent, chitosan impregnated calcium alginate (Cal-Alg-Chi) bead is described. The synthesis and charecterisation of the hybrid material Cal-Alg-Chi has already been discussed in the previous chapter (Chapter 2).

3.2.1 Uptake study

The sorption of uranium on Cal-Alg-Chi beads was investigated for different initial concentrations (0.1-100 μg mL^{-1}), keeping the sorbent concentration as 5 mg mL^{-1} and the pH of the solution was adjusted to pH 4. The variation in percentage uptake of uranium for different initial concentrations is shown in Fig. 3.1 with the uncertainties calculated from five

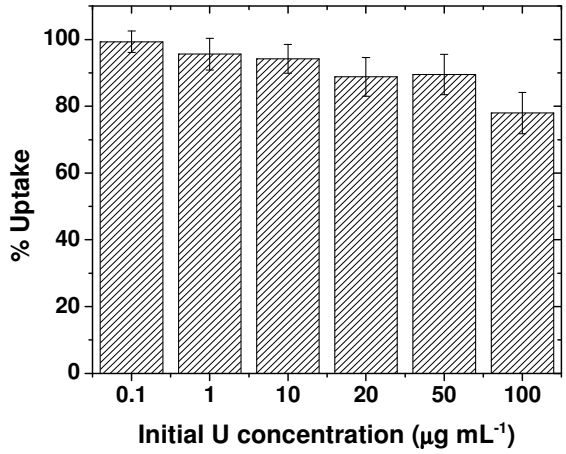

Fig.3.1: Percentage uptake of U as a function of initial U concentration

replicate samples. It's clear from the Fig. that Cal-Alg-Chi beads are capable of more than 90% uranium removal in the concentration range of 0.1-50 μg mL^{-1}.

3.2.2 Comparison with the intrinsic materials

To validate the effectiveness of the hybrid material, sorption experiments were carried out with different constituent of the Cal-Alg-Chi beads individually. A comparison of the uptake by chitosan powder, calcium alginate (Cal-Alg) beads and Cal-Alg-Chi beads is shown in Fig. 3.2. From this Fig. it's clear that the relative uptake is less for pure Cal-Alg beads but high for both pure chitosan powder and Cal-Alg-Chi beads. In case of pure chitosan powder,

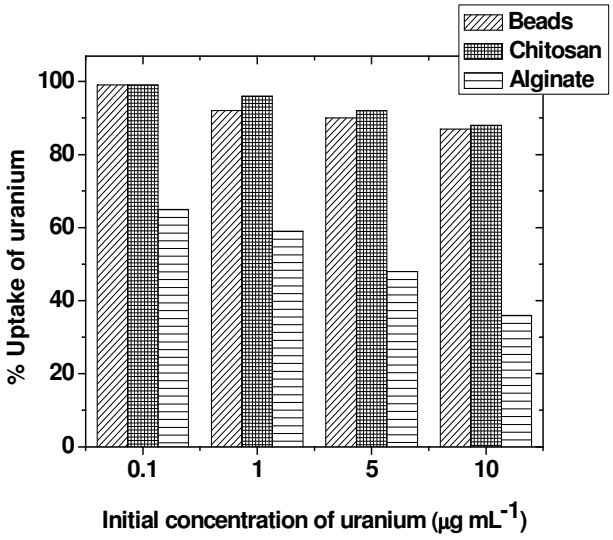

Fig. 3.2: Comparison of % uptake of uranium by chitosan, Cal-Alg and Cal-Alg-Chi beads

it's difficult to isolate after uptake whereas in case of Cal-Alg-Chi beads, solution can simply be decanted or beads can be used in the form of column. The observations suggest that chitosan is mainly responsible for the uranium uptake. The presence of carboxylic acid and hydroxyl groups in the alginate enable it to take up uranyl ions.

3.2.3 Influence of pH

The pH dependence of metal ion strongly influences the sorption phenomenon. The effect of pH on the sorption of uranium on the Cal-Alg-Chi beads was investigated at pH range 1 – 9 keeping initial concentration of uranium as 10 μg mL^{-1} and sorbent as 5 mg mL^{-1}. As shown

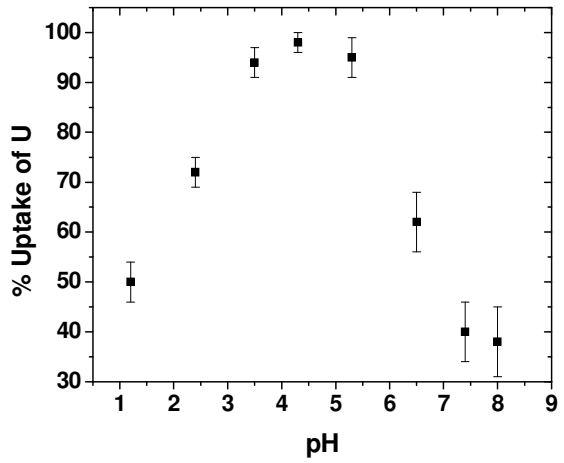

Fig. 3.3: % Uptake of uranium as a function of pH

in Fig. 3.3, the percentage sorption of uranium increases with increasing pH upto 4.5, thereafter decreases with further increase in pH. Maximum sorption of uranium was observed at around pH 3-5, therefore, pH 4 was maintained for the further experiments. The sorption behavior of uranium with pH can be explained by the speciation of uranium as well as by the characteristics of the sorbents. To understand the various uranium species present at different pH, work carried out by Wolery [189] using computer program EQ3/6 was used. At low pH value (pH 3), the uranium is present mainly in the form of free uranyl (UO_2^{2+}) ion in the solution. But as the pH increases, the uranyl ions are hydrolyzed. The hydrolyzed species ($[(UO_2)_2(OH)_2]^{2+}$, $[(UO_2)_3(OH)_5]^{+}$) and their polymerized products which are mostly present at pH 4-5 are positively charged and are exchanged or interact with the functional groups of the chitosan impregnated into Ca-alginate [190]. At pH above 6, the negatively charged

hydrolyzed species starts predominating. As a result the association with the negative functional groups of chitosan decreases at higher pH and subsequently the uptake also decreases. At very low pH value the positively charged uranyl ions compete with the H^+ ion present in the solution, therefore the sorption of uranium decreases.

3.2.4 Optimization of contact time

In order to optimize the time required for the equilibrium to establish, experiments were conducted for uranium uptake at pH 4 keeping the concentration of uranium at 100 μg mL^{-1} with a sorbent dose of 5 mg mL^{-1}. Fig. 3.4 shows that the sorption of uranium increases with contact time upto 2.5 hours and thereafter it becomes almost constant. To ensure maximum uranium uptake, contact time for all the batch experiments were fixed at 3 hours henceforth. The time (2-3 h) taken for the uptake, can be attributed to the slow rate of uranium diffusion into the alginate matrix (Cal-Alg-Chi beads) which hold the chitosan, responsible for uranium removal.

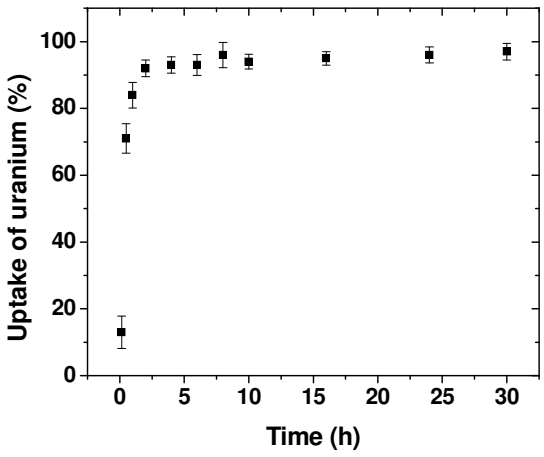

Fig. 3.4: % Uptake of uranium as a function of time

3.2.5 SEM-EDS analysis of the beads before and after the uptake

The SEM images of the cross sections of the Cal-Alg-Chi beads taken before and after uranium uptake (Fig. 3.5A & 3.5C) suggests no well-defined porous structure in the sorbent. Fig. 3.5B and 3.5D give the EDS mapping for uranium scanning a specified cross-sectional area of the pure Cal-Alg-Chi and uranium sorbed Cal-Alg-Chi beads respectively. EDS

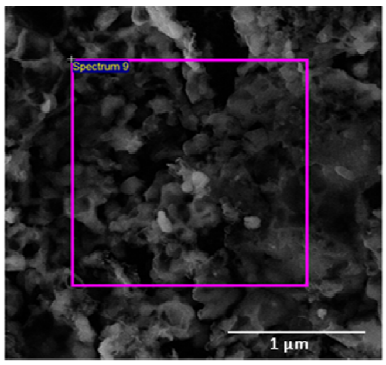

Fig.3.5A: SEM image of Pure Cal-Alg-Chi beads

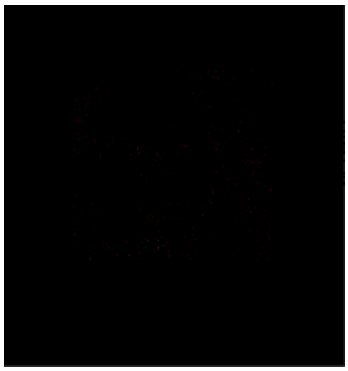

Fig.3.5B: EDS mapping of Pure Cal-Alg-Chi beads

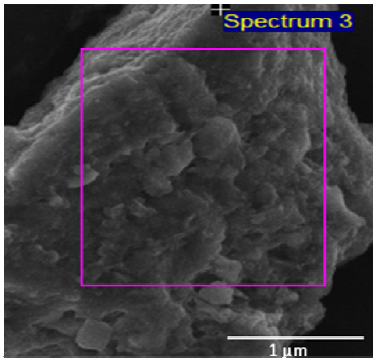

Fig.3.5C: SEM image of Uranium sorbed Cal-Alg-Chi beads

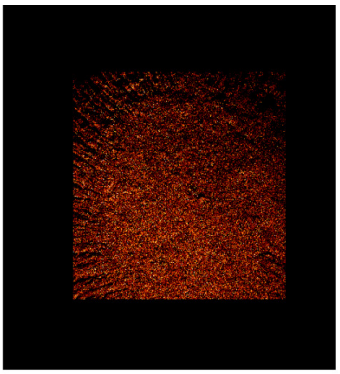

Fig.3.5D: EDS mapping of Uranium sorbed Cal-Alg-Chi beads

mapping was performed to verify the presence and distribution of uranium in the pure and uranium sorbed beads. From the uranium mapping it is clear that no signature of uranium in case of pure Cal-Alg-Chi beads (Fig. 3.4B), whereas uranium was seen to be uniformly distributed in the case of uranium sorbed Cal-Alg-Chi beads (Fig. 3.5D).

3.2.6 FTIR analysis of the beads before and after the uptake

The FTIR spectra of pure and uranium sorbed Cal-Alg-Chi beads are shown in Fig. 3.6. In the spectrum of pure Cal-Alg-Chi beads, bands appearing in different regions are explained in the previous chapter. Stretching vibrations of OH groups gave bands at 3700 cm^{-1} to 3000 cm^{-1}, C–H and N-H bonds at 2870-2920 cm^{-1}. Vibration in the range of 1640-1700 cm^{-1} is due to vibrations of carbonyl bonds (C=O) and amide groups (-CONH-). Two bands near 1250-1300 cm^{-1} are due to –OH and –C-O-C vibration. Absorption band near 1080–1030 cm^{-1} are because of CO present in COH, COC and CH_2OH.

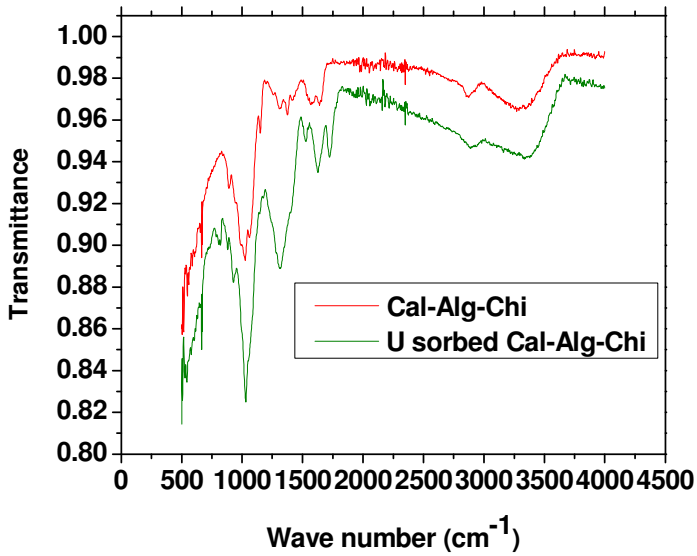

Fig. 3.6: FTIR spectra of pure and uranium sorbed Cal-Alg-Chi beads

In FTIR spectrum of Cal-Alg-Chi beads taken after uranium sorption (Fig. 3.6), vibration bands in the range of 1500-1700 cm^{-1} were seen to be shifted and separated. The reason may be attributed to the interaction of uranyl ions with carbonyl groups of the amide group. The band near 1250-1300 cm^{-1} became more defused and broadened and two bands got merged together in case of uranium sorbed Cal-Alg-Chi beads which may be because of the interaction of uranyl ions with oxygen atoms of –C-O-C bond and –OH bond. These

above observations indicate probable interaction between Cal-Alg-Chi beads (carbonyl and hydroxyl groups in chitosan) and uranyl ions present in the solution.

3.2.7 Sorption isotherm

Isotherm for the uranium sorption on Cal-Alg-Chi beads is plotted and fitted in both the above discussed isotherms. As seen from the isotherm plots that experimental data fits Langmuir model (Fig. 3.7) well with a R^2 value of 0.99 while in case of Freundlich model (Fig. 3.7) R^2 was 0.95. Observation indicates that the sorption of uranium on Cal-Alg-Chi beads is a monolayer adsorption. Langmuir constant Q_0 which is the measure of the monolayer adsorption capacity was obtained as 36.04 mg g^{-1}. It is in close agreement with the experimentally determined sorption capacity (34.7 mg g^{-1}).

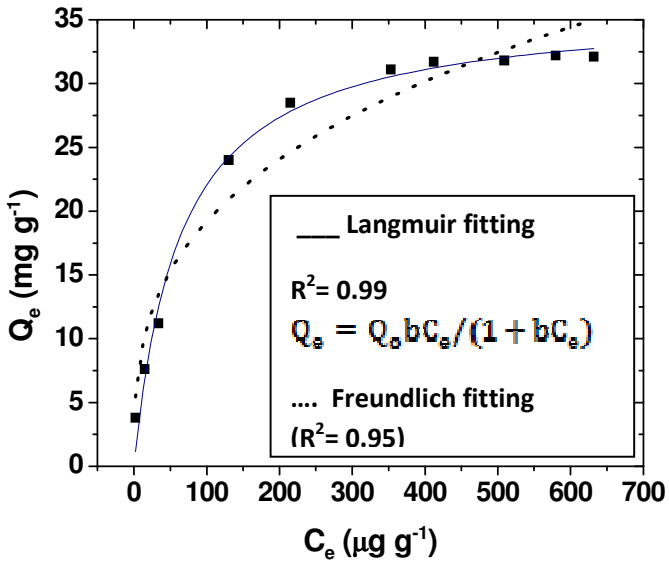

Fig. 3.7: % Sorption isotherm plot of uranium on Cal-Alg-Chi beads

3.2.8 Sorption kinetic modeling of uranium sorption on Cal-Alg-Chi beads

Kinetics data was plotted and fitted in both pseudo-first-order and pseudo-second-order kinetic models. From the linear correlation coefficient (R^2) values it was clear that the

pseudo-second-order rate law was fitted well (R^2=0.99) as given in Fig. 3.9 compared to the pseudo-first-order model (R^2=0.85) (Fig.3.8). The rate constant value was obtained as 0.153 g $mg^{-1}h^{-1}$ using the slope (for q_e) and intercept of the fitted line.

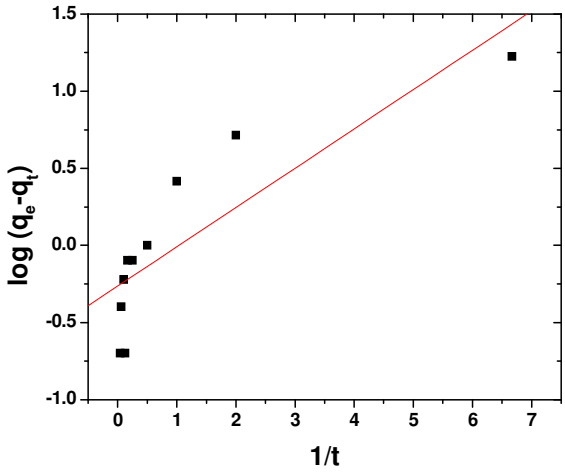

Fig. 3.8: Pseudo-first-order kinetic fitting of uranium sorption on Cal-Alg-Chi beads

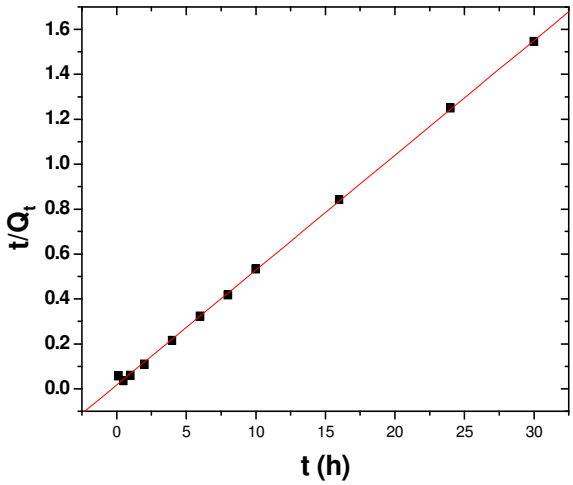

Fig. 3.9: Pseudo-second-order kinetic fitting of uranium sorption on Cal-Alg-Chi beads

3.2.9 Recovery of uranium from saturated Cal-Alg-Chi beads

Beads were highly efficient for more than 100 cycles and in each cycle 500 litre of water having 300 ng mL^{-1} of uranium was decontaminated. Uranium recovery from the saturated Cal-Alg-Chi beads, was carried out with 0.1 M HNO_3. More than 99% of the sorbed uranium was recovered. No other major element was found in the eluted solution as experimentally evaluated by recording the emission spectra by using ICP-OES.

3.3 Uranium and thorium uptake by silica microspheres

The core shell type hybrid material silica microspheres have good potential to be used as removing agent for radionuclides. They were synthesized and characterized as discussed in the previous chapter (Chapter 2). In the section, we look into its applicability for the removal of two most important radionuclides for nuclear industry namely uranium and thorium.

3.3.1 Sorption of U and Th

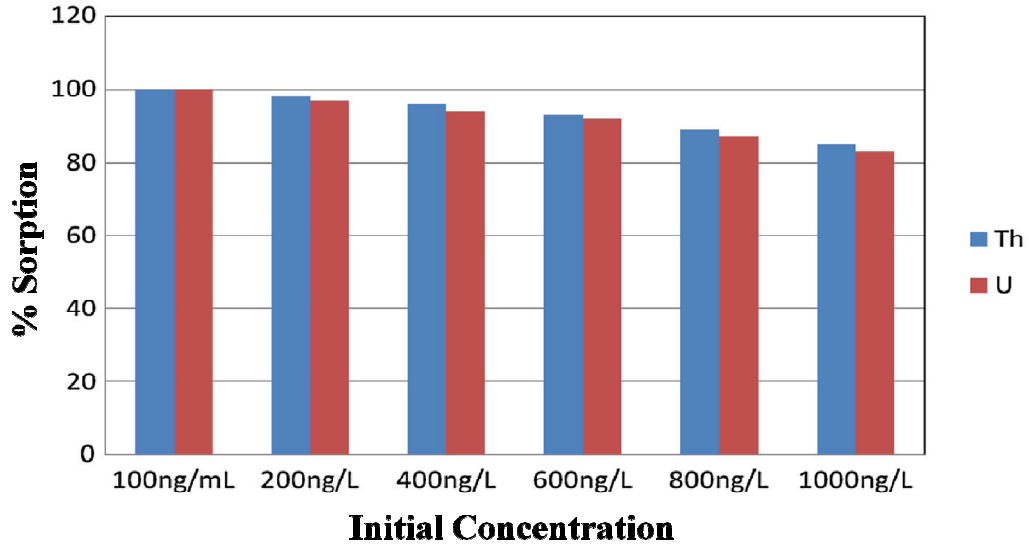

Fig. 3.10: % Sorption of U and Th on silica microspheres for different initial concentrations

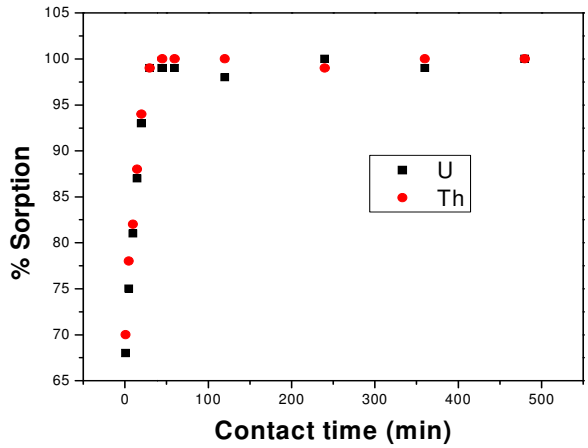

Fig. 3.11: % Sorption of U and Th on silica microspheres with time

Fig. 3.10 gives the sorption profile of uranium and thorium at pH 3 at six different concentrations (100–1,000 ng mL^{-1}) of U and Th. All the experiment was carried out either with U or Th separately. From Fig. 3.10, it is evident that more than 99 % of U and Th got sorbed on the silica microspheres. The contact time of the sorbent with radionuclides was varied from 1 minutes to 10 hours keeping other parameters constant and it was observed that

the equilibrium reaches after 30 minutes (Fig. 3.11), so the optimum contact time was decided as 30 minutes.

3.3.2 pH optimization for sorption of U and Th by silica microsphere

In order to have effective sorption of U and Th by the silica microsphere, pH was optimized. The sorption profile of U and Th at concentration of 100 Bq L^{-1} was observed at different pH. Experimental evidence clearly indicates that at pH 3-4 more than 99 % sorption of U and Th took place. In order to understand the various species of uranium present at pH 3, 5 and 6, work carried out by Wolery using computer program EQ3/6 was used [189,191]. As per this uranium speciation model, initial uranium solutions showed that the uncomplexed uranyl ion $[UO_2]^{2+}$ dominates the U(VI) speciation at pH 3 and with the increase in pH, fraction of $[UO_2]^{2+}$ decreases sharply [192-196]. There is little change in sorption was observed with a change in pH. This is because chemical properties of Th are relatively simple. Th has only one stable oxidation state, IV, under all redox conditions in natural waters, and Th(IV) ions are extremely particle reactive. The reactions and equilibrium equations for sorption of Th on silica are very similar to the proton exchange [197-199].

3.3.3 Evaluation of the sorption capacity of the silica microsphere

Sorption capacity of the microsphere was evaluated by carrying out the U and Th sorption experiments in the batch mode at pH 3, and each time the level of uranium and thorium was increased with an increment of 5 mg L^{-1} of the sample was processed after initial equilibration time of 30 min. After reaching the equilibrium concentrations of U and Th as 30 mg g^{-1} and 36 mg g^{-1} respectively in the SM, elevated levels of U and Th were observed in the equilibrium solutions.

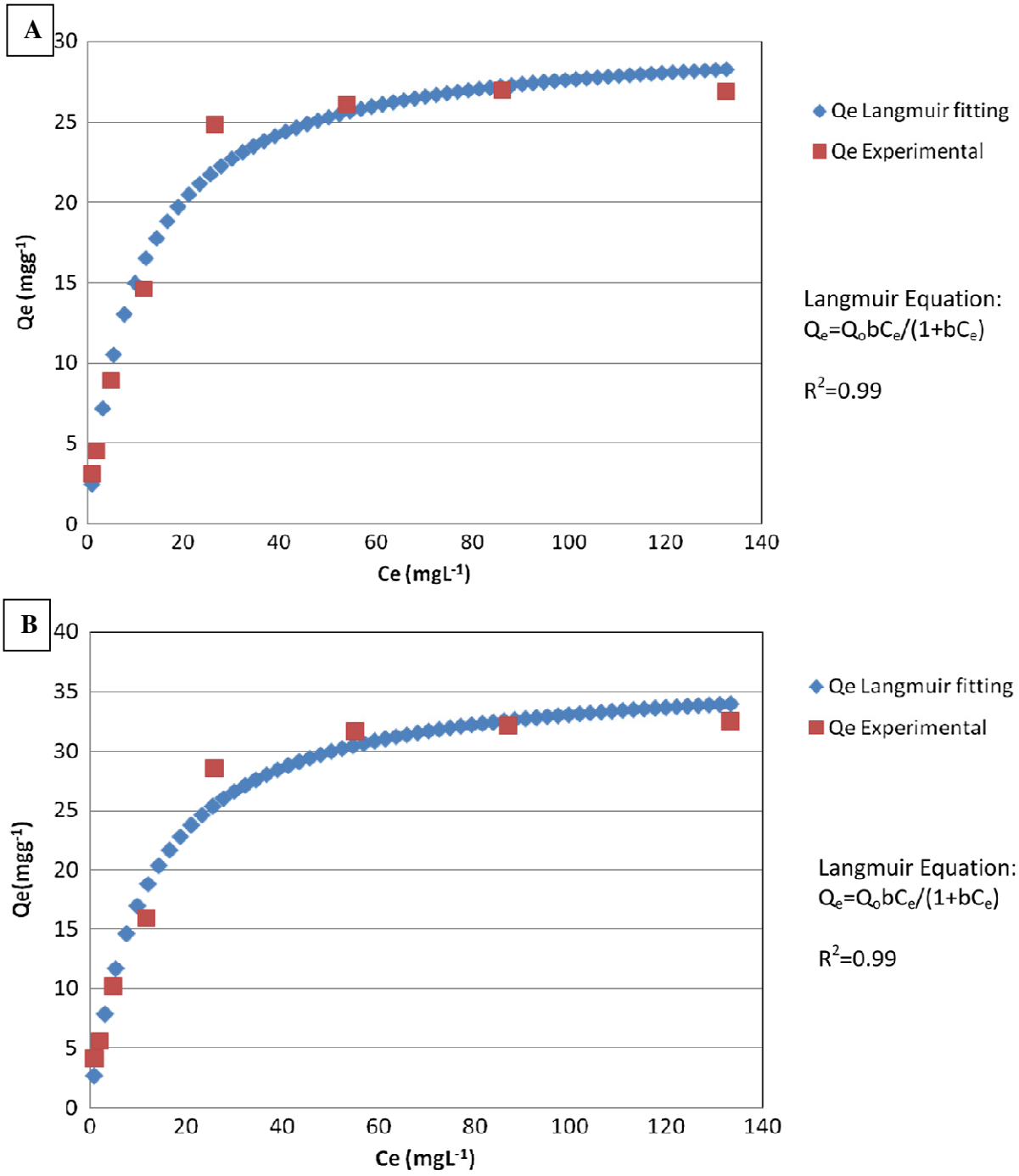

Fig. 3.12: A: Model (Langmuir fitting) of the experimental data for sorption of uranium.

B: Model (Langmuir fitting) of the experimental data for sorption of thorium.

The sorption capacity was therefore evaluated as 0.12 and 0.16 mmol g^{-1} (on wet basis) in case of uranium and thorium respectively. Experimentally observed sorption capacity of uranium and thorium are very close to the Langumir constant Q_0 (Fig. 3.12), which is measure of the monolayer adsorption capacity, as obtained, 30 and 36 mg g^{-1} respectively for U and Th. It is also clear from the Fig. 3.12 and R^2 values, experimental data are very close to the Langmuir type adsorption model.

3.3.4 Probable mechanism for thorium sorption on silica microsphere surface

2 ≡SiOH denotes a combination of two surface sites on the silica surface which are close enough to simultaneously chemically bind a sorbing Th^{4+} ion. However, at pH 8 and above, the prevailing inorganic species of Th in groundwater are hydroxo and carbonato complexes, in approximately equal proportions. In fact, in organic-free solutions, thorium, an A-type metal ion, will strongly hydrolyze to form polyhydroxy colloidal complexes [200-201].

$$2 \equiv SiOH + Th^{4+} + H_2O = (\equiv SiO)_2 Th^{2+} + 2H^+$$

3.3.5 Desorption of U and Th from silica microsphere

Desorption of U and Th from the silica microsphere was done by 30 mL of 3 M HNO_3. Fig. 3.13 shows the elution curve. From this elution curve, it is clear that only 95 % sorbed U and 70 % sorbed Th ions will be extracted back from the silica microsphere. Lower desorption of Th is due to highly particle reactive nature of Th^{4+}, because of it Th is tightly bound within the silicate structure. After elution, the microsphere can be reused for the subsequent sorption of U and Th. Microsphere was found suitable for 30 cycles for U and 20 cycles in case of Th. Thereafter, 25% degradation in the sorption capacity of silica microsphere was observed.

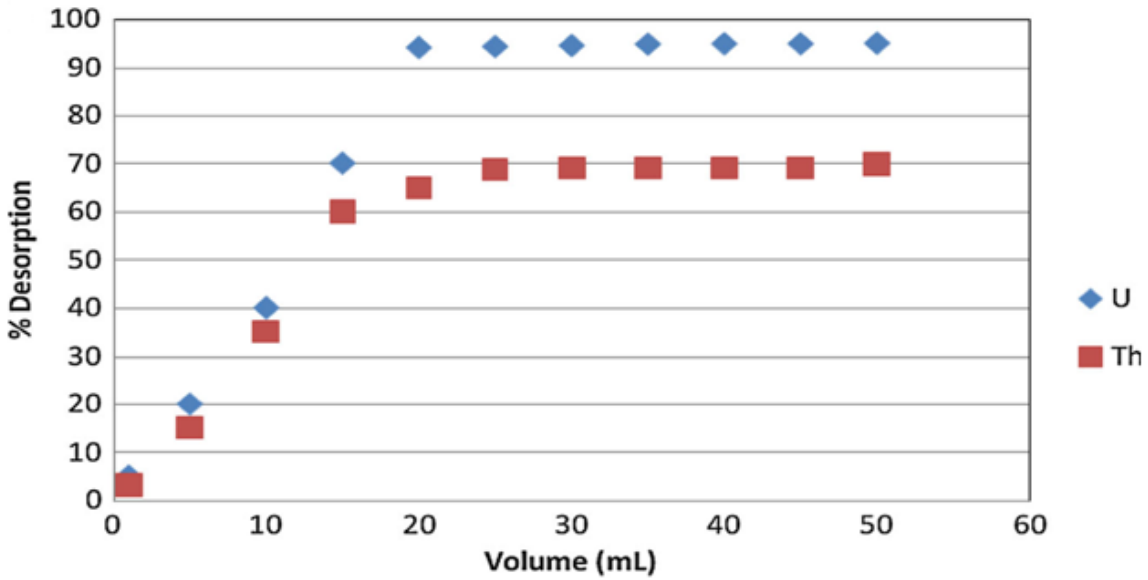

Fig. 3.13: Variation in percentage desorption of uranium and thorium from silica microsphere with different amount of 3M HNO_3

3.4 Americium removal by Cal-Alg beads

Till now the alginate beads discussed were impregnated with certain material, the pure form of the calcium alginate beads were in fact very effective for removal of low activity level of radionuclides. In this particular section, effort was made to utilize the calcium alginate as such for removal of low level ^{241}Am from potable water originated from different geochemical environments.

3.4.1 Variation of sorption of ^{241}Am on calcium alginate column with time at different concentration of ^{241}Am

Fig. 3.14 gives the sorption profile of ^{241}Am at pH 4 at three different concentrations of ^{241}Am i.e. 10 Bq L^{-1}, 50 Bq L^{-1} and 100 Bq L^{-1}. From this Fig., it is evident that within 200 minutes, more that 99% Am^{3+} gets sorbed on the column. In view of this, elution of the spiked samples in all the experiment was done after 200 minutes, maintaining the elution rate of 2 mL min^{-1}.

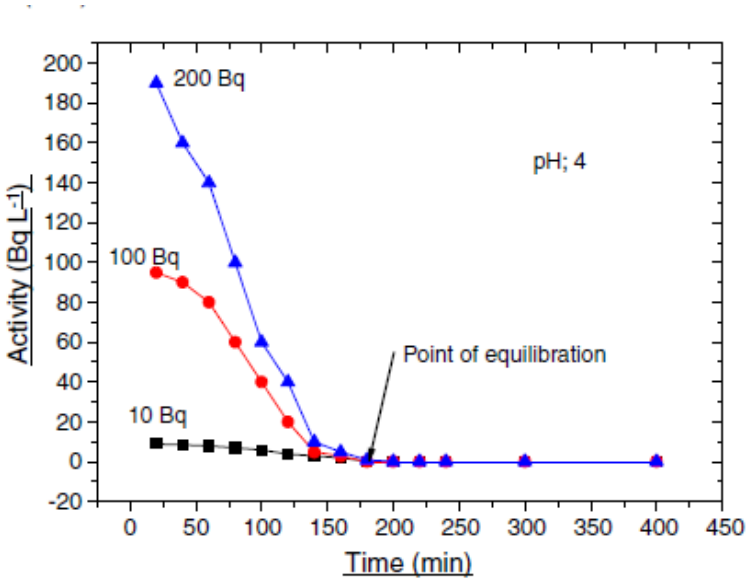

Fig. 3.14: Time of sorption optimization by calcium alginate beads column at different concentrations of ^{241}Am.

3.4.2 pH optimization for sorption of ^{241}Am by calcium alginate beads column

In order to have effective sorption of ^{241}Am by the Ca-Alg beads column, pH is optimized. Fig. 3.15 shows the sorption profile of ^{241}Am having a concentration of 500 Bq L^{-1} at different pH values. From this Fig. it is clear that at pH 4 more than 99% sorption of ^{241}Am is

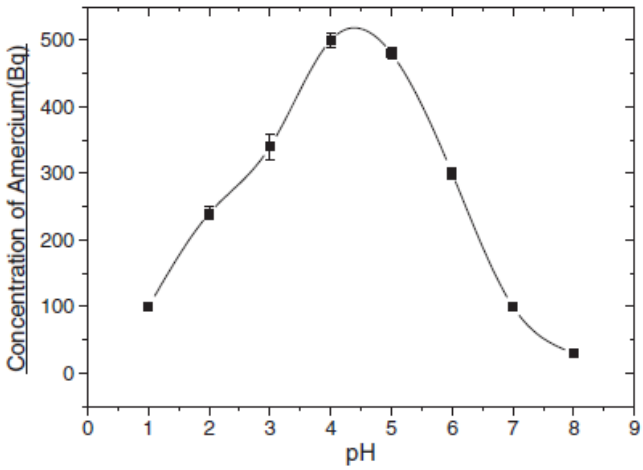

Fig. 3.15: Sorption profile of ^{241}Am on calcium alginate beads at different pH

there. This is attributed to the ionization of COOH group of the alginate biopolymers [202]. At this pH maximum ionization is achieved and these ionized sites are available for binding with Am^{3+}. At pH greater than 4, due to higher concentration of OH^- ions the Am is present as neutral species $Am(OH)_3$ and not available to bind with COO^-.

3.4.3 Evaluation of the sorption capacity of the column for ^{241}Am

Sorption capacity of the column was evaluated by carrying out the Am^{3+} elution in the batch mode and each time 500 Bq L^{-1} of the sample was passed through the column after giving initial equilibration time of 200 minutes, elution was done at 2 mL m^{-1}. After passing 19.9 L of water column showed a value between 0.08 and 5 Bq L^{-1}. Therefore the sorption capacity

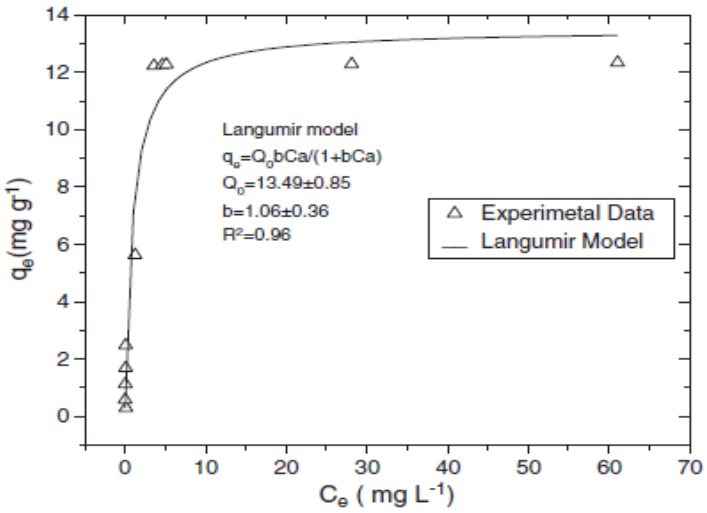

Fig. 3.16: Langumir isotherm for Eu^{3+} on calcium alginate column

evaluated is 10,000 Bq g^{-1} (on wet basis) which is equivalent to 0.33 nmolg^{-1}. To meet the regulatory requirements in the lab experiments with ^{241}Am were carried out in dilute solutions, which probably is the reason for lower sorption capacity. Therefore to evaluate the sorption capacity, sorption isotherms of Eu^{3+} for alginate gels were obtained in awide range

of initial concentration of Eu^{3+} (Chemical analogue of Am^{3+}) from 1.3×10^{-4} to 6.6×10^{-2} M. Europium is the heavy homolog of americium. The stability of the higher oxidation states of the transuranium elements typically decreases with increasing atomic number [118,203,204]. In agreement with this, the trivalent state of americium is the most stable oxidation state, and it is the homolog of americium, (Am^{3+} radius=0.99 A) [205]. The equilibrium amount of

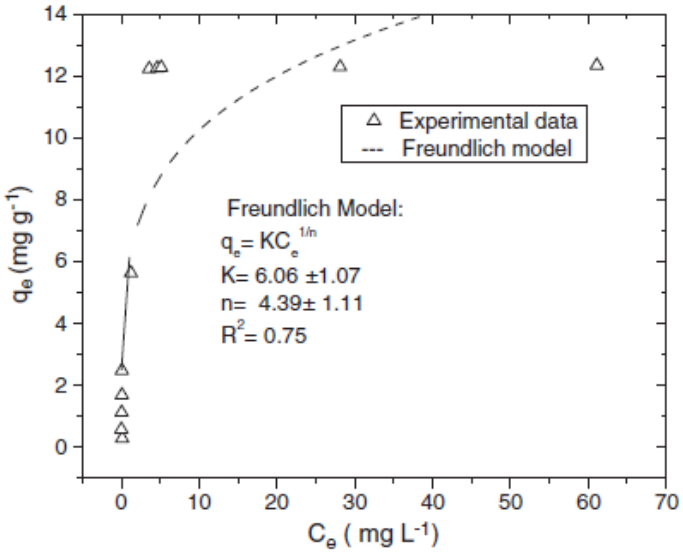

Fig. 3.17: Freundlich isotherm for Eu^{3+} on calcium alginate column

Eu^{3+} adsorbed on alginate gel increased with equilibrium concentration of Eu^{3+}, and then approached a constant value. Experimentally observed sorption capacity is 12.16 mg g^{-1} which is very close to the Langmuir constant Q_0 (Fig. 3.16), which is the measure of the monolayer adsorption capacity, as obtained, 13.49±0.85 mg g^{-1}. Fig. 3.17 gives the experimental fit of Freundlich isotherm model. As is clear from Fig. 3.16 and 3.17, experimental data and R^2 values that sorption follows Langmuir-type adsorption model.

3.4.4 ATR-FTIR study of Eu–calcium alginate interaction

The incorporation of Eu^{3+} ions into the gel matrices was confirmed by studying the ATR-FTIR spectrum of dry powdered beads of Eu^{3+} loaded calcium alginate beads. Fig. 3.18

shows the comparative ATR-FTIR spectrum of dry sodium alginate and Eu^{3+} loaded calcium alginate spectrum. The powder sodium alginate FTIR spectrum showed the characteristic peaks at 3242 cm^{-1} (OH stretching), 1607 and 1407 cm^{-1} (–COO asymmetric and symmetric stretching), 1024–1004 cm^{-1} (C–OC antisymmetricstretching) and carboxyl and carboxylate at about 1000 to 1400 cm^{-1}. Whereas it is clear from ATR-FTIR spectrum of Eu loaded

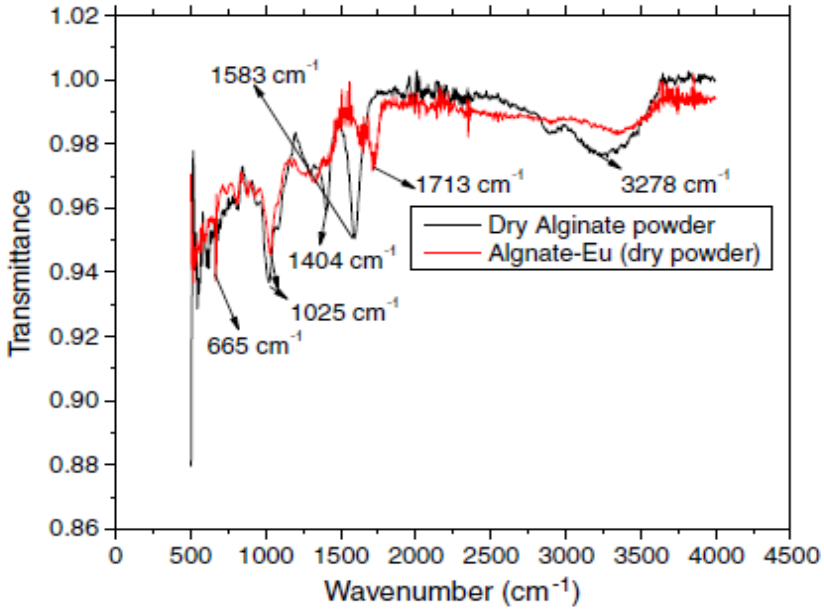

Fig. 3.18: ATR-FTIR spectra of dry powder of calcium alginate and Eu^{3+} loaded Ca-Alg powder

alginate that there is decrease in transmittance intensity and shift in the peaks at 1025 cm^{-1}, 1404 cm^{-1}, 1583^{-1} and 1713 cm^{-1} (COO asymmetric and symmetric stretching and C–OC antisymmetric stretching). This is attributed due to binding of Am^{3+}/Eu^{3+} with –COOH and to some extent with O=C and OH groups.

3.4.5 Probable mechanism of entrapment of Am^{3+} from aquatic medium to Cal-Alg beads

Americium in aqueous solutions is well known to exist in the III, IV, V and VI oxidation states. The hydrated ions Am^{3+}(aq), AmO^{2+}(aq) and AmO_2^{2+}(aq) occur in the absence of

complexing agents [202,203]. Am(III) ion is precipitated by hydroxide, fluoride, phosphate, and oxalate ions. Bio-sorption in algae has been attributed mainly to the cell wall, where both electrostatic attraction and complexation can play a role. Bio-accumulation of lanthanum, uranium and thorium has been investigated by Yong et al [206] and it has been suggested that the uptake of these metal ions by bio-mass mostly depends upon physiochemical adsorption at the cell surface and not on its biological activity. Adsorption properties of alginate were also investigated for Cu^{2+}, Co^{2+}, Zn^{2+}, Cd^{2+}, and La^{3+} ions by Konishi et al. and Jang et al. [121,123,207]. All these studies indicated that the biosorption largely depends upon the chemical speciation of the metal ion in solution. The marine algal matrix of alginate consists of complex hetero-polysaccharides containing both OH and COOH binding sites; therefore the major binding groups are OH, O=C–OH, C=O. Carboxylic group exists in ionized form at pH 4. As pH reaches lower values, the competition between H^+ and cationic species in the solution affects the process, decreasing the uptake [208]. This statement corroborates the results obtained in this work where the pH value around 4 was found to be the ideal to the ^{241}Am removal from aqueous solution using alginate beads. These carboxylic groups are capable of forming complexes with cationic metal. The interaction of Am^{3+} with alginate is mostly ionic species of Am [Am^{3+}(aq), AmO^{2+}(aq) and AmO_2^{2+}(aq)] complexing with –OH, –COOH and O=C groups. In addition to this there is a definite probability that neutral species i.e. [$Am(OH)_3$] may get adsorbed on the algal cell. The charge of the bio-sorbent does depend exclusively on the pH value. Covalent bonding of metals may consume negatively charged groups. Groups become large neutral that would otherwise have been negatively charged in metal free solution of the same pH.

3.4.6 Desorption of ^{241}Am from Cal-Alg column

The desorption of ^{241}Am from the alginate beads was done by 100 mL of 0.6 M HNO_3. Fig. 3.19 shows the elution curve. From this elution curve, it is clear that the Am^{3+} ions adsorbed on the column were readily eluted by flowing 0.6M HNO_3 solution and the elution percentage was estimated to be 99.5. After elution, the alginate column can be reused for the subsequent sorption of Am^{3+}. Column was found suitable for 20 cycles as observed experimentally. Thereafter 20% degradation in the sorption capacity of Ca-Alg was

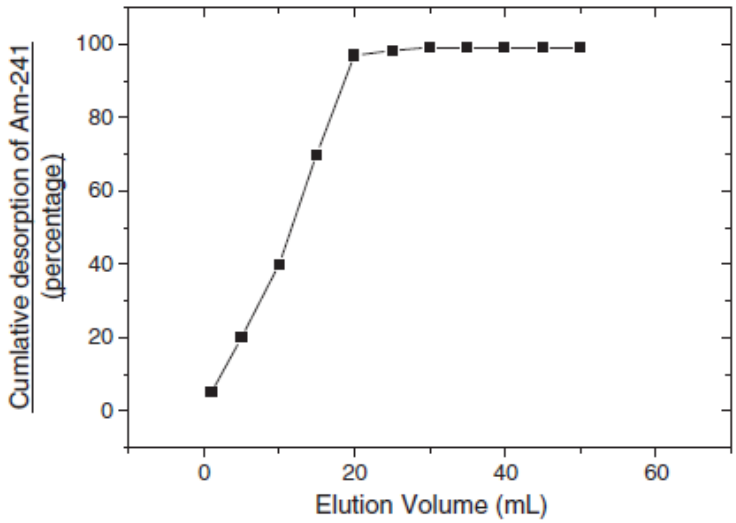

Fig. 3.19: Desorption of ^{241}Am from the calcium alginate column with 0.6 M HNO_3 observed.

3.5 $^{239+240}Pu$ and ^{241}Am removal by using humic coated colloidal suspension of goethite (α-FeO(OH))

In this section a different type of hybrid material is introduced. This is typically an organic coating on an inorganic substance. In this case goethite nano suspension was used as the inorganic phase and humic acid was the organic phase over it. Because of the mixing of both biogenic and geogenic matrixes, it develops unique property to be used as a sorbent for the radionuclides (Am and Pu in this case) removal.

3.5.1 Coating of humic acid (HA) over goethite

Coating of goethite suspensions with humic acid stock solution having a strength of 1 g $L^{-1}$of humic acid was prepared by using commercially available humic acid (Sigma- Aldrich catalogue no. 53680) where the total proton exchange capacity (PEC) was 7.06 ± 0.67 $molg^{-1}$ out of which carboxylic group was 4.80 ± 0.21 mol g^{-1} and the phenolic group was 2.26 ± 0.72 mol g^{-1}. Humic substances which are ubiquitous in groundwater and are generally hydrophilic particles are stabilized by salvation forces. They can be powerful substrates for

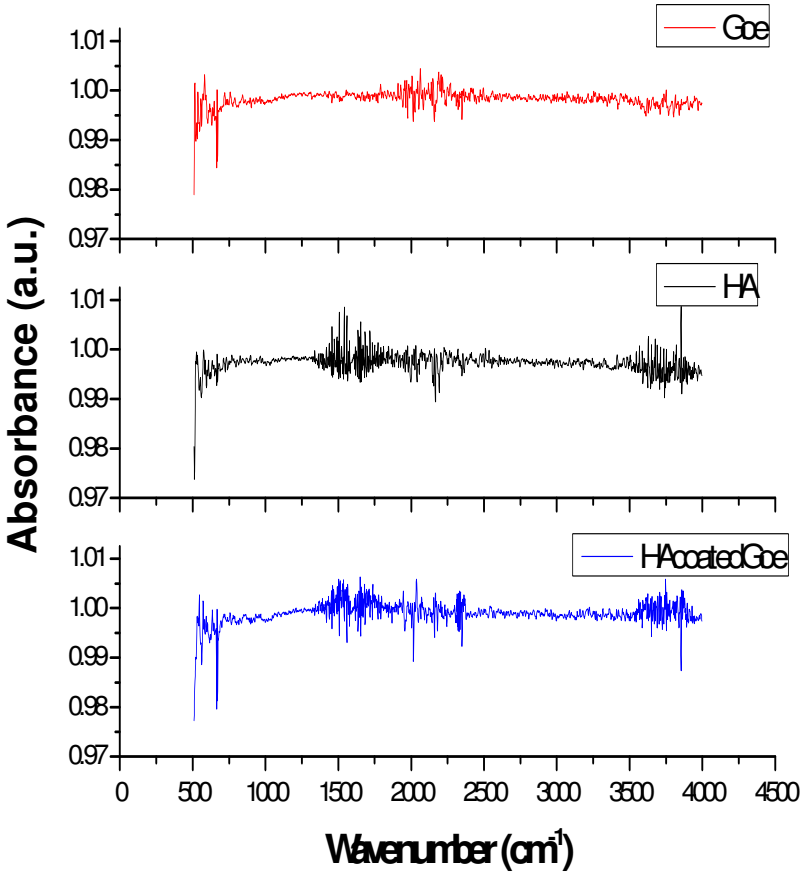

Fig. 3.20: FTIR spectra of goethite (Goe), humic acid (HA) and humic acid coated goethite

uptake of metal cations and are present in variable size ranges. Coating of humic acids was done by soaking the goethite suspensions in HA overnight. Goethite suspension having a mean hydrodynamic diameter of 30 nm was mainly used for this purpose. The qualitative validation of the coating was done by recording their ATRFTIR spectrum (Fig. 3.20) and whereas the quantitative determination was done by measuring the organic carbon content on the particles by using elemental analyzer. It is observed from the ATR-FTIR spectra recorded for goethite, humic acid and humic acid coated goethite that the signature of both goethite (vibration bands at 500-750 cm^{-1}) and humic acid (vibration bands at 1450-1800 cm^{-1} and 3500-4000 cm^{-1}) are present in the spectrum of humic acid coated goethite.

3.5.2 Distribution in different size fractions

Fig. 3.21 gives the distribution of Pu and Am with different size fractions of goethite. From this Fig. it is clear that the 60 % of Pu and Am is associated with 30 nm fraction followed by 80 nm (30 %) and 10 % is associated with fraction concentrated with 800 nm. Poly

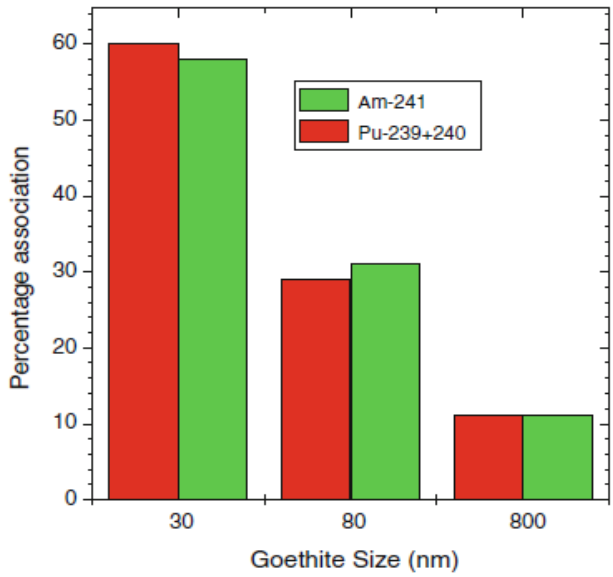

Fig. 3.21: Distribution of $^{239+240}Pu$ and ^{241}Am with different size fractions of goethite

dispersive colloidal suspension was subjected to ultra filtration where suspension is dominated (95 %) with particle of size 30 nm.

3.5.3 Enhancement of selectivity for $^{239+240}$Pu and ^{241}Am by HA coating of colloidal suspension dominated with 30 nm fraction

Fig. 3.22 shows that there is a linear increase in the association of $^{239+240}$Pu and ^{241}Am with the increase in humic acid concentration in the range of 10–60 μg mL^{-1} and thereafter it remains constant with the increase in humic acid concentration. Zeta potential of the HA coated goethite particles is also plotted at each concentration. As evident from the zeta potential measurement of goethite suspension at different concentrations of humic acid (10–100 μg mL^{-1}), stability of the colloidal suspension increases with the increase in concentration of humic acid up to 60 μg mL^{-1} thereafter it shows only minor fluctuation (Fig. 3.22).

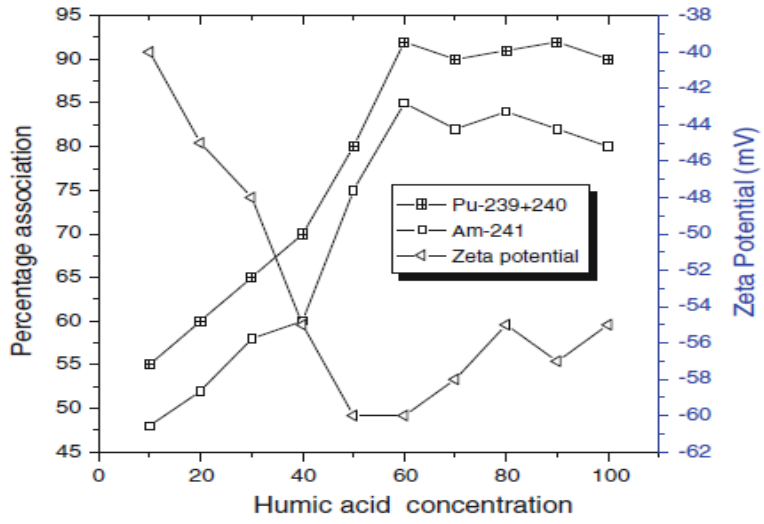

Fig. 3.22: % Association of $^{239+240}$Pu and ^{241}Am with different humic acid concentration along with zeta potential values

3.5.4 Optimization of concentration of goethite suspension

Water contaminated with 100 Bq $L^{-1}$of $^{239+240}Pu$ and ^{241}Am was treated with goethite suspension having Fe concentration in the range of 1–10 mg L^{-1}. It is observed from the Fig. 3.23 that there is a decrease in the concentration of $^{239+240}Pu$ and ^{241}Am with increase in the concentration of Fe up to 8 mg L^{-1} of the solution. Therefore, it can be concluded that the optimum value of goethite suspension is 8 mg L^{-1} for the water sample having a concentration 100 Bq L^{-1} each of $^{239+240}Pu$ and ^{241}Am.

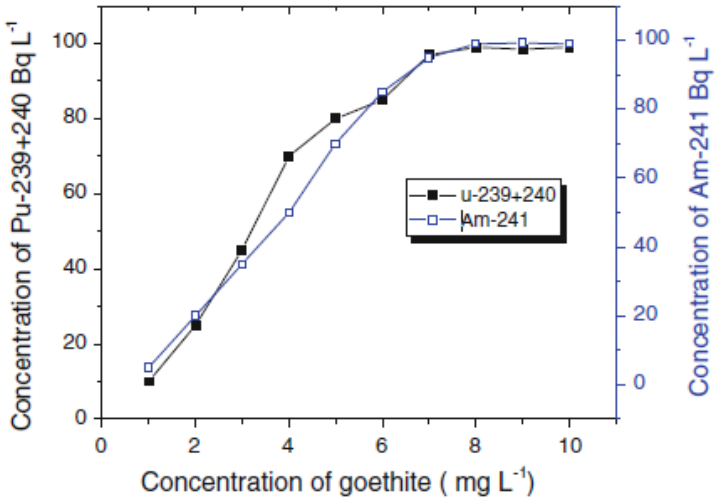

Fig. 3.23: Optimization of goethite concentration for the removal of $^{239+240}Pu$ and ^{241}Am from potable water

3.5.5 Separation of goethite suspension from potable water

Water samples after treatment with the goethite or humic acid coated goethite were subjected to pass through ultrafiltration cell in filtration mode (allow all the solution to pass through the membrane) having a membrane of 500 NMWL (Nominal Molecular Weight Limit) to remove the humic coated goethite suspension.

3.5.6 Probable mechanism of Pu and Am interaction with humic coated goethite suspension

Humic acid binding model V is used to explain the interaction between humic acid coated goethite with $^{239+240}$Pu and ^{241}Am [208]. As per this model, the organic substances possess variable charge, and this influences their ion exchange properties. The charge depends not only on the acidity of the heterogeneous functional groups of humic acid, but also on the specific binding of metals and on electrostatic effect which result from the relatively large size of humic acid molecules. The association of $^{239+240}$Pu and ^{241}Am with humic acid associated goethite under aquatic conditions may be the consequence of complexation or chelation of Pu and Am at the adjacent anionic sites of humic acid. In general, radionuclides in higher oxidation states and with smaller ionic radii form stable complexes with organic acids, Pu (oxidation state +4, ionic radius 0.90 A^o) seems to form more stable chelating complexes with natural humic acid [204,208].

To verify the impact of humic acid on the goethite colloids, the goethite suspension was filtered through ultra filtration membrane and examined using scanning electron microscopy (SEM-EDS). Fig.s 3.24 and 3.25 show the elemental analysis for the residue collected on ultra-filtration membrane in the samples having dissolved organic carbon (DOC) 10 and 60 μgL^{-1} respectively. Both the samples have similar goethite suspension (30nm size). Due to agglomeration of colloids on the membrane, no specific information regarding size could be obtained from SEM. The elemental analysis carried out by EDS clearly indicate the presence of Fe and C in samples having DOC, 60 $\mu g\ L^{-1}$ (Fig. 2.24) whereas in the sample having DOC l0 $\mu g\ L^{-1}$, peaks only due to carbon were observed (Fig. 3.25).

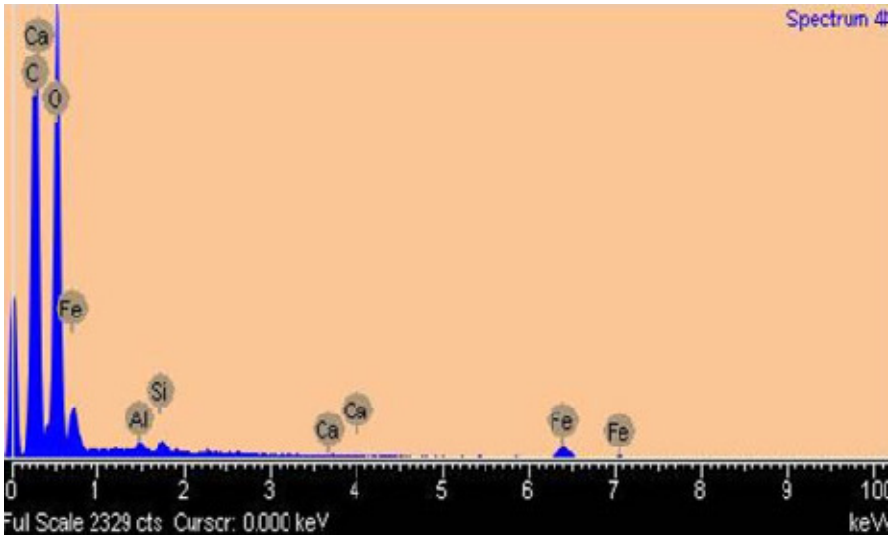

Fig. 3.24: Energy dispersive X-ray spectrum compost of α FeO(OH) and DOC 60 µg mL^{-1}

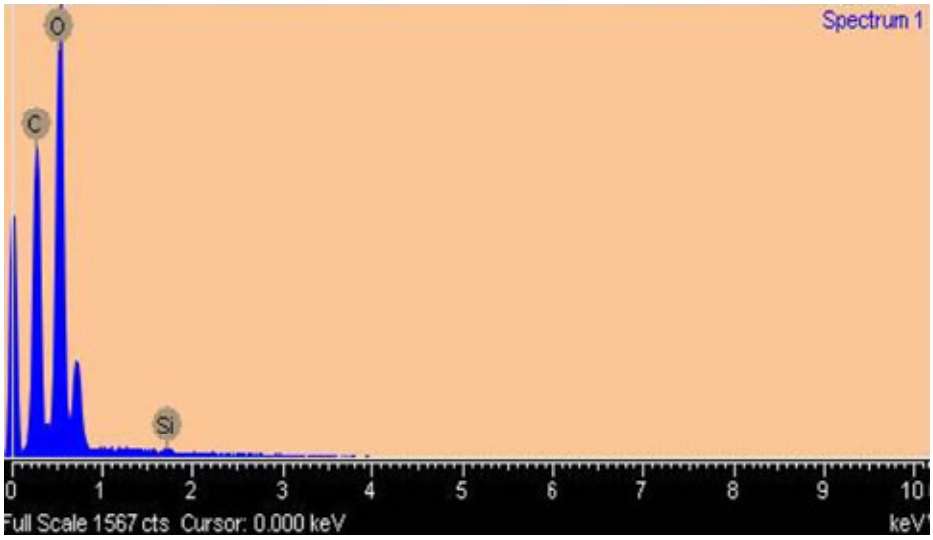

Fig. 3.25: Energy dispersive X-ray spectrum compost of α FeO(OH) and DOC 10 µg mL^{-1}

Residue on the membrane were also analyzed for Fe content in two different samples by using Inductive coupled plasma-optical emission spectroscopy and showed higher presence of Fe in samples having 60 µg L^{-1} DOC compared to sample with 10 µg L^{-1} of

DOC. These observations also clearly demonstrate the stability of goethite suspension at elevated level of DOC.

Chapter 4

Removal of TiO_2 nanoparticles from aquatic medium using hybrid material

---

4.1 Introduction

With the growth of industry and development of nanotechnology, there has been a tremendous growth in the application of nanoparticles (NPs) for various uses like antibacterial materials, drug delivery systems, cosmetics, sunscreens and electronics. Concerns have been raised in recent times that TiO_2 NP may throw challenges to human health because of its unique bioactivity as many in vitro and in vivo toxicological studies showed adverse effect of TiO_2 NPs on living organisms. To address this issue, highly efficient hybrid material was synthesized and used for TiO_2 NP removal from aquatic environment.

4.2 Sample preparation and characterization of TiO_2 nanoparticles

Water samples were contaminated with TiO_2 NP powder procured from Nanoshel having stock no. NS6130-03-350. Working TiO_2 NP suspensions in the range of 10 – 10000 µg mL^{-1} were prepared by accurately weighing the TiO_2 NP powder and mixing it in water followed by ultrasonication (Retsch UR1, 35 kHz) for 6h. As TiO_2 NP was procured from outside, a detailed characterization was indeed necessary before its use in the laboratory. TiO_2 NP was therefore characterized by XRD, Raman spectroscopy and DLS prior to its use.

4.2.1 Phase confirmation by XRD and Raman spectroscopy

The XRD analysis and Raman spectra confirms the identity of TiO_2 NP as anatase form. The recorded XRD matches (Fig. 4.1) with the standard PCPDF card no. 78-2486 (red lines) which is for the anatase TiO_2 [209,210]. Three major Raman shifts at 399 cm^{-1}, 516 cm^{-1} and 640 cm^{-1} (as shown in Fig. 4.2) also confirms the anatase phase of TiO_2 NP.

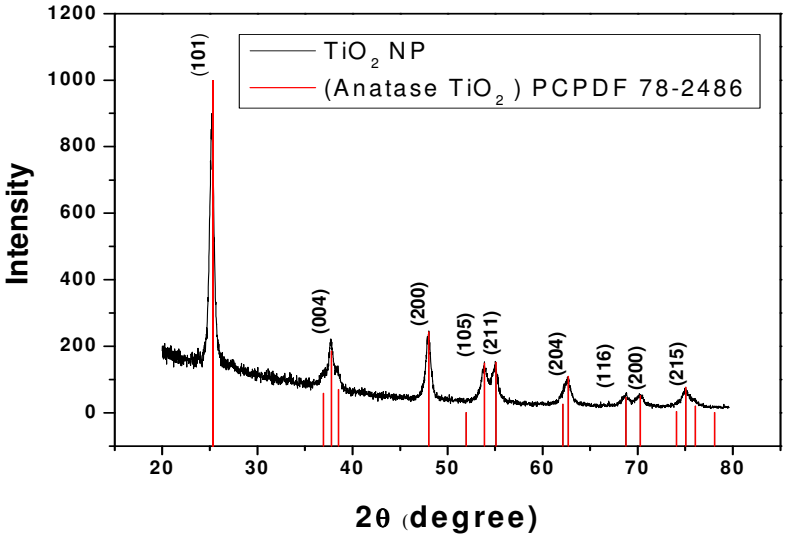

Fig. 4.1: XRD pattern of TiO_2 NP (Anatase)

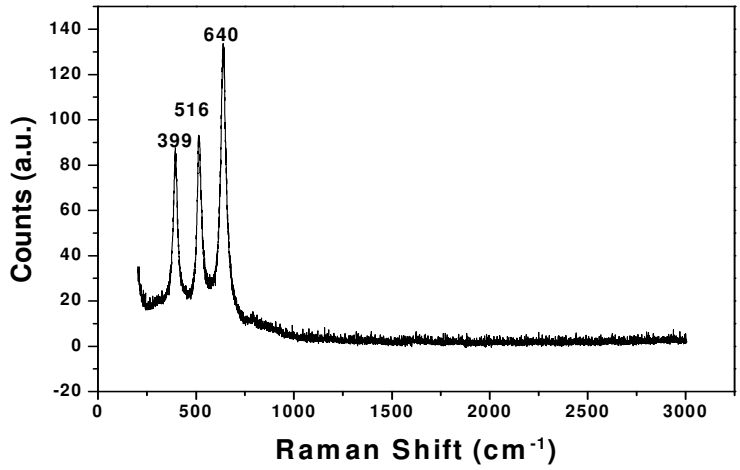

Fig. 4.2: Raman spectrum of TiO_2 NP (Anatase)

4.2.2 Size and morphology analysis

Broadening of the peaks in XRD (Fig.4.1) suggests the smaller size of the particles, however the size was calculated using Sherrer formula (Equ 4.1) considering the FWHM of the most intense peak. The detailed calculation is given below:

$$D_p=\frac{0.94*\lambda}{FWHM*Cos\theta}$$ Equ 4.1

Where, D_p= Average crystallite size, λ is the wavelength of the X-ray used i.e. Cu K_α in this case (1.54 Å), and θ is the Bragg angle. From the most intense peak at the XRD of TiO_2 NP, the required parameters (FWHM, θ) were obtained and D_p was calculated. From the fig 4.1, 2θ was obtained as 25.5946 for the most intense peak and FWHM for the same was 0.293. Using these data the size calculated was 29 nm. This was verified by measuring size by zeta sizer nano ZS which gave a mean diameter of 28.2 nm. The isoelectric point (or PZC) of TiO_2 NP was found at around pH 5 which suggests positive surface charge on the particles below pH 5 and negative surface charge above pH 5. SEM image as given in Fig. 4.3 shows the surface morphology and size of the TiO_2 NP.

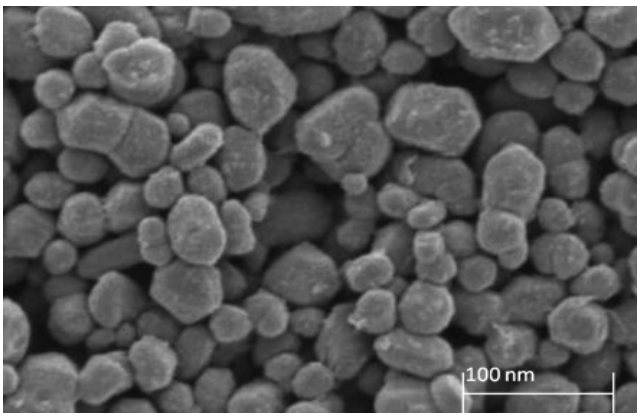

Fig. 4.3: SEM image of the TiO_2 NP

4.3 Removal of TiO_2 NP using Cal-Alg-SM beads

A novel material "calcium–alginate–silica microsphere" (Cal-Alg-SM) bead was developed by impregnating silica microsphere in calcium alginate which has already been discussed in chapter-2. These beads were highly efficient in the removal of TiO_2 nanoparticles from aquatic bodies without disturbing its physicochemical characteristics. In the present section,

we discuss the works carried out on removal of TiO_2 NP from aquatic medium using Cal-Alg-SM beads.

4.3.1 Uptake for different concentrations of TiO_2 NP

The sorption of TiO_2 NP on Cal-Alg-SM beads was investigated in concentration range of 10-1000 μg mL^{-1}, keeping the concentration of sorbent as 10 mg mL^{-1} in a poly-propylene container. Fig. 4.4 shows the variation in percentage uptake for TiO_2 NP at different initial

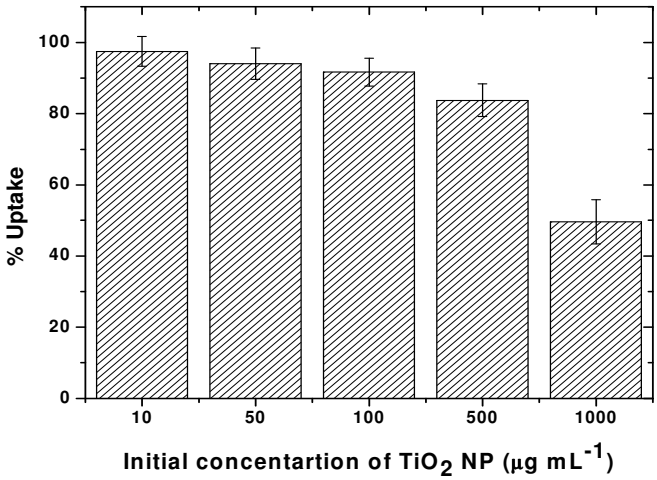

Fig. 4.4: Uptake of TiO_2 NP at different initial concentrations

concentrations with error bars calculated from five replicate samples. From this Fig. it's clear that Cal-Alg-SM beads are capable of sorbing more than 90% TiO_2 NP in concentration range of 10-500 μg mL^{-1}. Similar experiments were also been conducted to quantify the impact of Ca-alginate. It was observed that Ca-alginate could take up only 5-10% of TiO_2 NP, moreover it came out by simply washing the beads with demineralised water. In order to streamline various conditions for sorption of TiO_2 NP by Cal-Alg-SM beads, pH and time of contact were optimized.

4.3.2 Effect of pH and zeta potential

Percentage uptake of the TiO_2 NP was studied at pH range between 1-10, keeping all the sets for 24 h and having initial 100 µg mL^{-1} TiO_2 NP and sorbent as 5 mg mL^{-1}. Experimental results showed that the removal TiO_2 NP by Cal-Alg-SM beads is highly pH dependent (Fig. 4.5). Maximum sorption was observed at around pH 4.0. This can be explained on the basis of positive zeta potential values of TiO_2 NP below pH 5 and negative surface charge of SM above pH 2. The range of pH 3-5 is favourable for the sorption as in this window of pH the surface charges are opposite on the sorbent (SM) and sorbate (TiO_2 NP) (Fig. 4.5). At low pH values, both are positively charged and at high pH value also both are negatively charged and as a result sorption is not a favorable process.

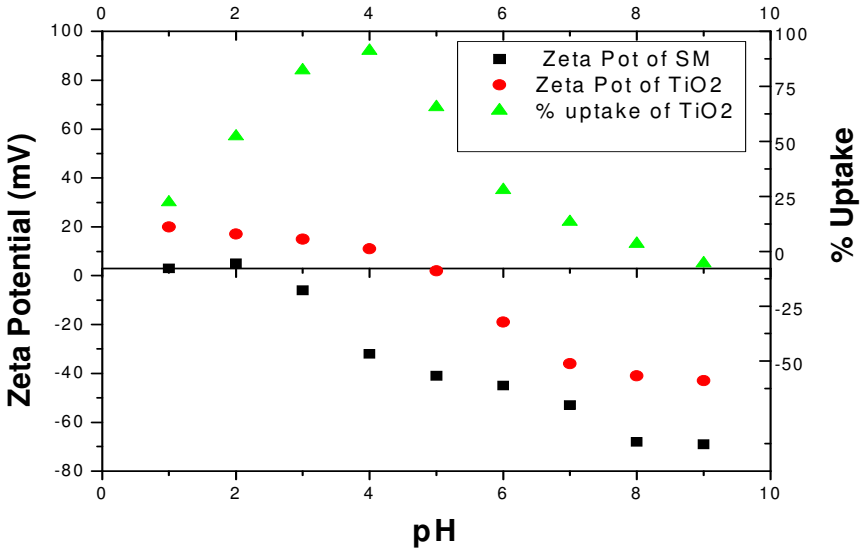

Fig.4.5: % Uptake of TiO_2 NP as a function of pH and zeta potential

4.3.3 Optimization of contact time

In order to optimize the contact time experiments were conducted for TiO_2 NP uptake at pH 4.0 having the concentration of sorbent as 5 mg mL^{-1} for 100 µg mL^{-1} of TiO_2 NP. Fig. 4.6

shows that sorption of TiO_2 NP increases with time up to 8 hours and then it becomes almost constant. The time for all the batch experiments was kept fixed at 8 hours henceforth to ensure maximum uptake of TiO_2 NP. The error bars drawn were calculated based on analysis of five replicate samples The kinetics was seen to be little slow. The reason may be attributed to the slow rate of diffusion of TiO_2 NP into the alginate matrix which held the SM responsible for TiO_2 NP removal.

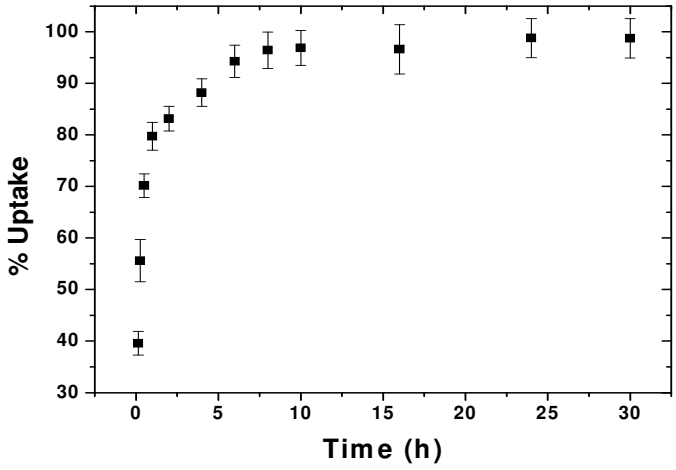

Fig. 4.6: Effect of contact time on the uptake of TiO_2 NP on Cal-Alg-SM beads

4.3.4 Effect of dose rate

The effect of dose of sorbent was studied under the fixed concentration of TiO_2 NP (100 µg mL^{-1}), pH 4-5 keeping the contact time at 8h. The result is given below (Fig. 4.7). It shows that the percentage uptake initially increases up to dose rate of 5 mg g^{-1} thereafter becomes almost constant. So dose rate of 5 mg g^{-1} was used for most of the experiments.

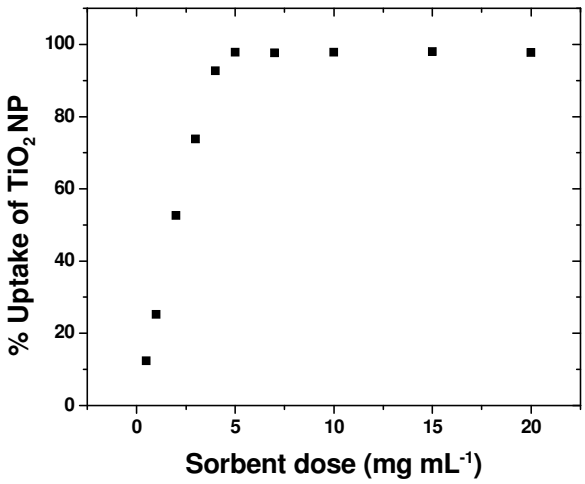

Fig. 4.7: Effect of dose rate of Cal-Alg-SM beads on the uptake of TiO_2 NP

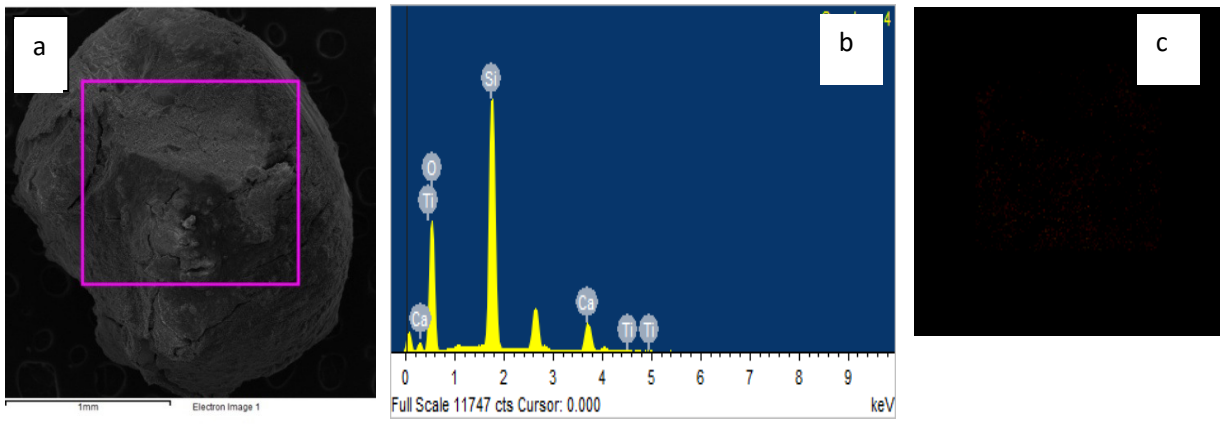

Fig. 4.8: SEM EDS analysis of Pure Cal-Alg-SM beads (A): SEM; (B): EDS spectra; (C): Elemental mapping for Ti

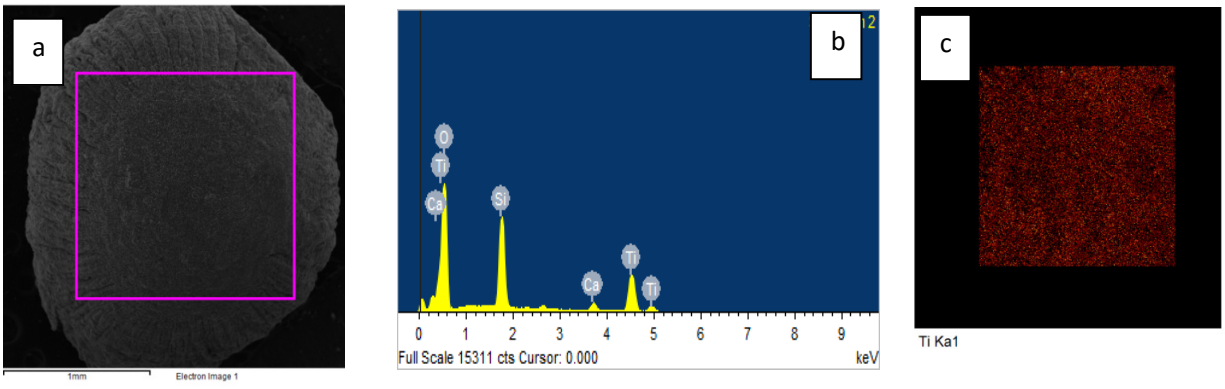

Fig. 4.9: SEM EDS analysis of TiO_2 NP sorbed Cal-Alg-SM beads (A): SEM; (B): EDS spectra (C): Elemental mapping for Ti

4.3.5 SEM-EDS analysis of the beads before and after the uptake

The SEM images of the beads taken before and after uptake of the TiO_2 NP (Fig. 4.8A & 4.9A) suggests that the sorbent does not possess any well-defined porous structure. EDS analysis was performed to determine the elemental constituents of pure and TiO_2 NP sorbed Cal-Alg-SM beads (Fig. 4.8B and 4.8B). In Fig. 4.8B spectrum shows the presence of titanium besides the principal elements Ca, Si in case of TiO_2 NP sorbed Cal-Alg-SM beads whereas no titanium peak was observed in the pure Cal-Alg-SM beads (Fig. 4.8B). The mapping of titanium, scanning a specified cross-sectional area in the beads, showed no signature of Ti in case of pure beads (Fig. 4.8C), whereas in the case of TiO_2 NP sorbed Cal-Alg-SM beads, it was seen to be uniformly distributed (Fig. 4.9C).

4.3.6 FTIR analysis of the beads before and after the uptake

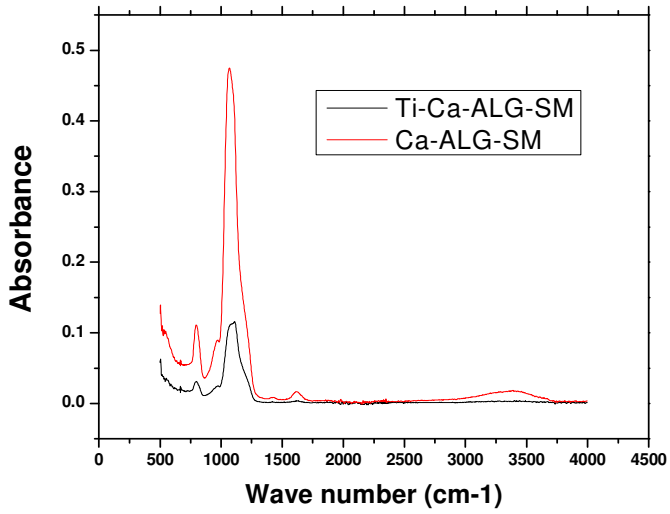

Fig: 4.10: ATR-FTIR spectra of pure and TiO_2 NP sorbed Cal-Alg-SM beads

The FTIR spectra of pure and TiO_2 NP sorbed Cal-Alg-SM beads are shown in figure 4.10. In FTIR spectra of Cal-Alg-SM beads taken before sorption, the peaks at 806 and 1100 cm^{-1} corresponds to the SM vibrations bands. The same peaks are not affected in case of TiO_2 NP

sorbed Cal-Alg-SM beads. These observations suggest that probably no direct bonding takes place between Cal-Alg-SM beads and TiO_2 NP, therefore the interaction may be due to electrostatic attraction or due to adsorption.

4.3.7 Sorption isotherm

In order to evaluate the sorption capacity of Cal-Alg-SM beads for TiO_2 NP, the equilibrium sorption of TiO_2 NP was studied as a function of TiO_2 NP concentration at 25-30 ^{O}C. The

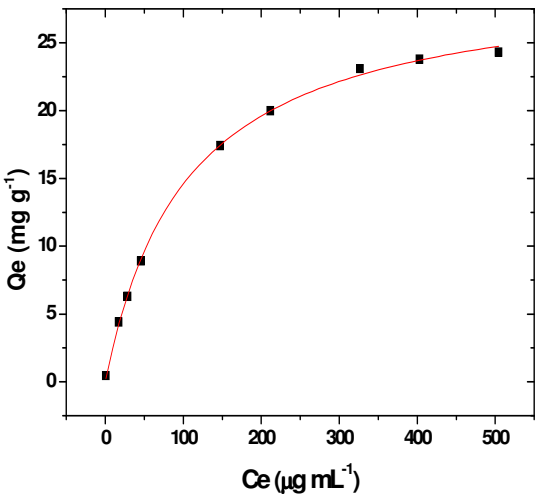

Fig: 4.11: Langmuir isotherm plot for TiO_2 NP sorption on Cal-Alg-SM beads

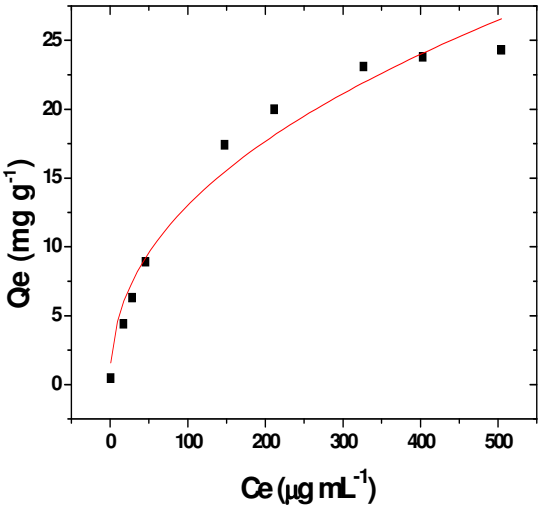

Fig: 4.12: Freundlich isotherm plot for TiO_2 NP sorption on Cal-Alg-SM beads

sorption isotherms are fitted in Langmuir (Fig. 4.11) and Freundlich (Fig. 4.12) isotherms. It is clear from the isotherm plots that Langmuir isotherm (Fig. 4.11) fits the experimental data well with the R^2 value of 0.99 in comparison to the Freundlich model (R^2 = 0.96) (Fig. 4.12). This indicates that the sorption of TiO_2 NP on Cal-Alg-SM beads is a monolayer adsorption. The monolayer adsorption capacity which is measured as the Langmuir constant Q_0, was obtained as 29.9 mg g^{-1} from fitting (Fig. 4.11) and it is very close to the experimentally determined sorption capacity (28.4 mg g^{-1}).

4.3.8 Sorption kinetic modelling of TiO_2 NP on Cal-Alg-SM beads

To study the dynamics of the solute adsorption process, the kinetics of TiO_2 NP sorption on Cal-Alg-SM beads was analyzed using pseudo-first-order and pseudo-second-order kinetic models keeping other parameters constant (Concentration of TiO_2 NP 100 µg mL^{-1}, pH 4,

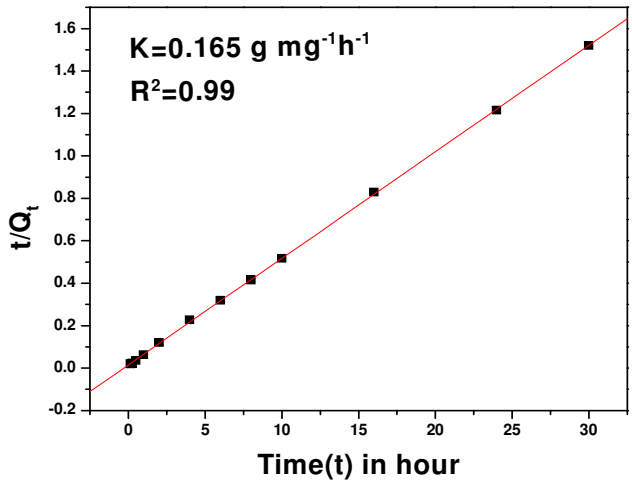

Fig. 4.13: Pseudo-second-order kinetic fitting of TiO_2 NP sorption on Cal-Alg-SM beads

dose rate 5 mg mL^{-1}). From the linear correlation coefficient (R^2) values it was clear that the pseudo-second-order rate law was fitted well (R^2=0.99) as given in figure 4.13 compared to the pseudo-first-order model (R^2=0.75). The rate constant value was obtained as 0.165 g $mg^{-1}h^{-1}$ using the slope (for q_e) and intercept of the fitted line.

4.3.9 Mechanism of sorption

Mechanism of the uptake is governed by the sorption of TiO_2 NP species on silica microspheres. The surface chemistry of both SM and TiO_2 NP varies with pH. It is clear from Fig. 4.5 that the PZC of SM is about pH 2 and for TiO_2 NP is around pH 5. At these pH, the hydroxyl group of both SM and TiO_2 NP is protonated with only one proton and net surface charge becomes zero. At low pH value, the hydroxyl groups at the surface of the SM (SiO_2)

are doubly protonated and thus the surface charge of the SM is positive. But at pH above 2.0; SM is negatively charged which is clear from the zeta potential values. Similarly TiO_2 NP is having positive surface charge below pH 5.0.

Maximum sorption of TiO_2 NP was observed at pH around 3-5 according to our experimental result. At this pH range, the electrostatic attraction between the negative oxoanion of SM and the positive surface charge on TiO_2 NP favours sorption. At lower pH value (pH<2), fully protonated species of both TiO_2 NP and SM are present in solution therefore electrostatic attraction is no longer possible which results in a lower sorption. At pH above 5, both are negatively charged and repel each other and consequently sorption decreases. The sorption of TiO_2 NP having positive surface charge is enhanced by the presence of carboxylic acid and hydroxyl groups in the alginate. But the most important role the alginate serves, is to bind the SM into the matrix and because of the formation of the beads separation of the sorbent becomes easy.

4.3.10 Recovery of TiO_2 NP from Cal-Alg-SM beads

Recovery of the sorbate (TiO_2 NP) from the saturated Cal-Alg-SM beads, was carried out with two different eluents (a) 0.5 M HNO_3 and (b) mixture of 0.5 M HNO_3 and 1% solution of 30% HF. It was observed that the recoveries were in the range of 5-10% only. Therefore, total recovery of TiO_2 NP from Cal-Alg-SM was carried out by complete destruction of beads using HNO_3 (16N) and HF (30%) in the ratio of 3:1. More than 99% recovery of the sorbate was achieved.

Chapter 5

Hybrid materials for decontamination of groundwater from conventional pollutants (As, F)

5.1 Intoduction

Remediation of contaminated groundwater is of highest priority since billions of people all over the world use it for drinking purpose. Depending on local geology, groundwater contains heavy metals (including radioactive elements) in low levels, but sometimes in concentrations which are not acceptable for drinking water. Several areas of the world have relatively high arsenic & fluoride concentrations in their groundwater used for drinking purpose [94,95]. High arsenic concentrations have been reported recently from the USA, China, Chile, Bangladesh, Taiwan, Mexico, Argentina, Poland, Canada, Hungary, Japan and India. Among 21 countries in different parts of the world affected by groundwater arsenic contamination, the largest population at risk is in Bangladesh followed by West Bengal in India [96]. Since arsenic is highly toxic and carcinogenic, the World Health Organization (WHO) has set the guideline for arsenic in drinking water at 10 μg L^{-1} [64,97]. Daily consumption of water with greater than 0.01 mg L^{-1} of arsenic, less than 0.2 % of the fatal dose, can lead to problems with the skin, circulatory and nervous systems.

Fluoride is an essential constituent for humans and animals depending on the total amount ingested or its concentration in drinking water. The presence of fluoride in drinking water, within permissible limits of 0.5 –1.0 mg L^{-1}, is beneficial for the production and maintenance of healthy bones and teeth, while excessive intake of fluoride causes dental or skeletal fluorosis which is a chronic disease [64]. Drinking water is typically the largest single contributor to daily fluoride intake. For a given individual, fluoride exposure (mg kg^{-1} of body weight per day) via drinking water is determined by the fluoride level in the water and the daily water consumption (litres per day). As there is no treatment for fluorosis, prevention is the only means of controlling the disease [98]. Fluorosis is a disease

that causes mottling of the teeth, calcification of ligaments, crippling bone deformities and many other physiological disorders.

Many countries have regions where the water contains more than 1.5 mg l^{-1} of fluoride due to its natural presence in the earth's crust, or discharge by agricultural and industrial activities, such as steel, aluminum, glass, electroplating. Excessive exposure to fluoride in drinking water, or in combination with exposure to fluoride from other sources, can give rise to a number of adverse effects as discussed in chapter 1.

5.2 Removal of arsenic from groundwater by Cal-Alg-Goe beads

In recent years, arsenic contamination of water has become a major concern on a global scale including the Indian scenario. In the present section, the works carried out on removal of arsenic from groundwater using newly developed hybrid material goethite impregnated calcium alginate (Cal-Alg-Goe) bead is described.

5.2.1 XRF analysis of Cal-Alg-Goe beads before and after the arsenic uptake

The synthesis and charecterisation of the Cal-Alg-Goe beads has already been discussed in chapter 2. In this section we present the results of the X-ray fluorescence (XRF) analysis of

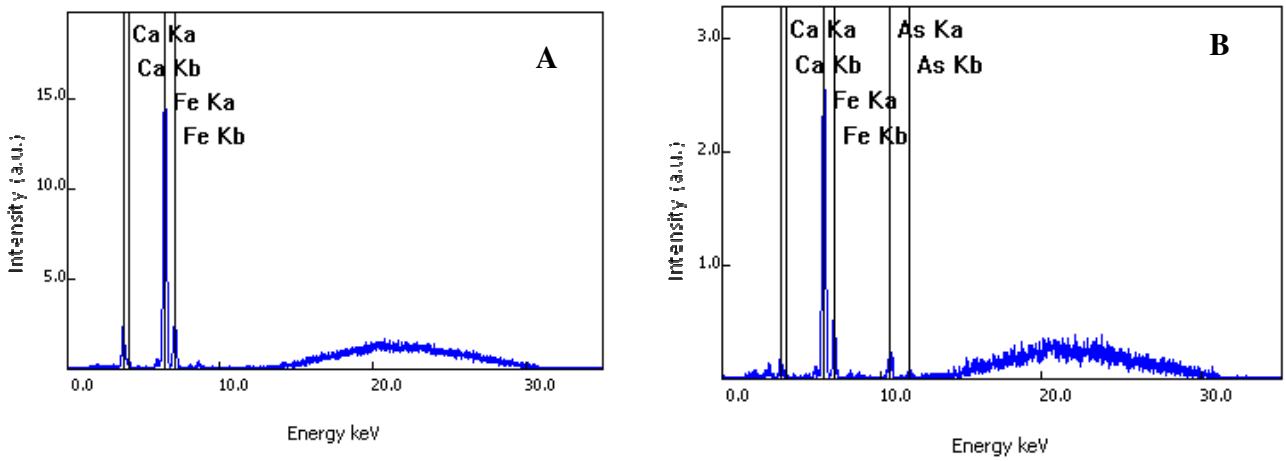

Fig.5.1: XRF spectra of A: Cal-Alg-Goe beads; B: arsenic sorbed Cal-Alg-Goe beads

the pure Cal-Alg-Goe and arsenic sorbed Cal-Alg-Goe beads. XRF analyses were performed to determine the elemental constituents of pure and arsenic-sorbed Cal-Alg-Goe beads, spectrum of the same is shown in figure 5.1 A & B. Presence of arsenic besides the principal elements Ca, Fe was observed in case of arsenic sorbed Cal-Alg-Goe beads (Fig.5.1B) whereas no arsenic peak was observed in the pure Cal-Alg-Goe beads (Fig. 5.1A).

5.2.2 FTIR analysis of Cal-Alg-Goe beads before and after the arsenic uptake

The FTIR spectra of pure and arsenic-sorbed Cal-Alg-Goe beads are shown in figure 5.2. In FTIR spectra of Cal-Alg-Goe beads (before sorption) the peaks at 500-1500 cm^{-1} corresponds to the O-H vibrations band. The same peaks are more diffused and a new peak is observed around 700 cm^{-1} in case of arsenic sorbed Ca-Alg-Goe beads. These observations suggest possible interaction between arsenic and Cal-Alg-Goe beads.

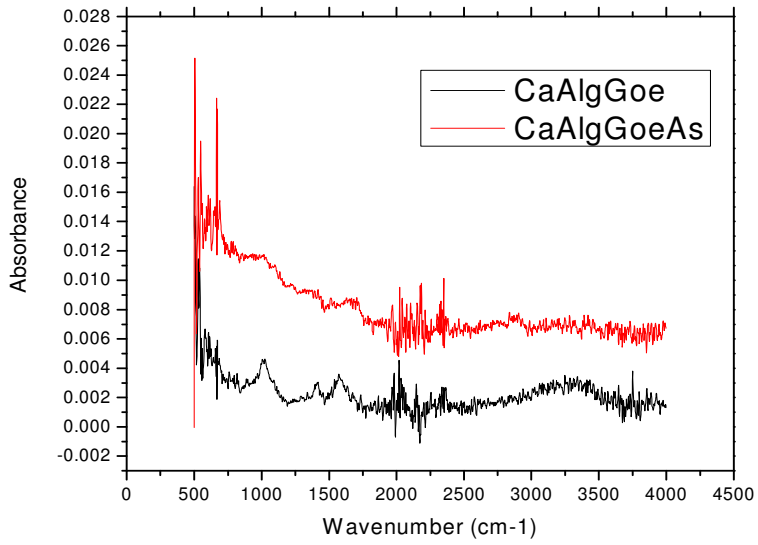

Fig.5.2: FTIR spectra of pure and arsenic sorbed Cal-Alg-Goe beads

5.2.3 Uptake study for different concentrations of arsenic

The sorption of arsenic [As(V)] on Cal-Alg-Goe beads was investigated in concentration range of 10-10000 ng mL^{-1}, keeping the concentration of sorbent as 1.0 mg mL^{-1} in a poly-propylene container having 200 mL capacity. Fig. 5.3 shows the variation in percentage uptake for arsenic at different initial concentrations of arsenic. From this figure it's clear that Cal-Alg-Goe beads are capable of sorbing more than 95% arsenic from the groundwater.

For uptake of arsenic (III) [As(III)], similar experiment was conducted but after oxidising the As (III) into As (V) using nitric acid and hydrogen peroxide as oxidising agents. Thus results of uptake obtained after converting As (III) to As (V) were very close to the results shown in Fig. 5.3.

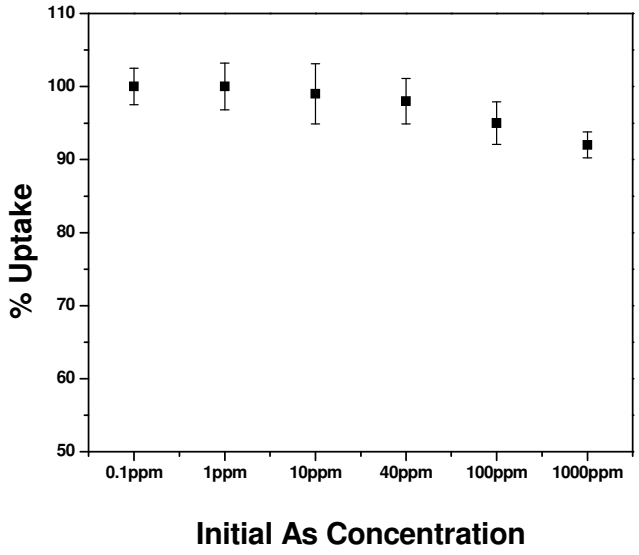

Fig.5.3: Variation in uptake of arsenic by Cal-Alg-Goe beads at different concentrations of arsenic at pH 5

In order to streamline various conditions for sorption of arsenic by Cal-Alg-Goe beads, pH and time of contact were optimized. For all subsequent experiments, As(V) solution was used directly.

5.2.4 Optimization of time

In order to optimize the contact time experiments were conducted for arsenic uptake at different initial concentrations of arsenic (1000, 10000 ng mL^{-1}) at pH 5.0 having the

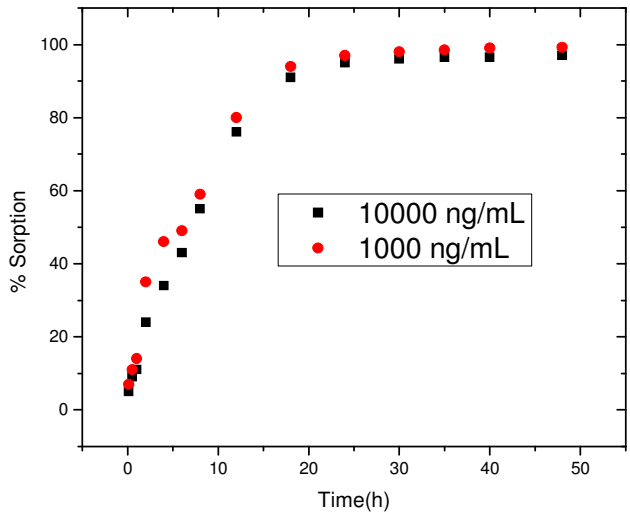

Fig.5.4. Optimization of time for As uptake by Cal-Alg-Goe beads

concentration of sorbent as 0.3 mg mL^{-1} for 10000 ng mL^{-1} and 0.03 mg mL^{-1} for 1000 ng mL^{-1}. Fig. 5.4 shows that arsenic sorption increases with time upto 24 hours and then it becomes almost constant. The time for all the batch experiments were kept fixed at 24 hours to ensure maximum uptake of arsenic. The kinetics was seen to be little slow. The reason may be attributed to the slow rate of diffusion of arsenic into the alginate matrix which held the goethite responsible for arsenic removal.

5.2.5 Effect of pH

Percentage uptake of the arsenic was studied at pH range between 2 - 10, keeping all the sets for 24 h and having initial arsenic solution concentration 1000 ng mL^{-1} and sorbent as 1.0 mg mL^{-1}. From the experimental results (shown in Fig.5.5), it is clear that uptake capacity was

more than 80% for the range of pH 3.0-7.5. These results suggest that the prepared beads can be used for arsenic removal without any pH adjustment in the pH range of 3.0 – 7.5, whereas most of the earlier methods reported for arsenic removal at such low extent, required pH adjustment or some other pre-treatment. Maximum uptake observed at pH 4-6 can be explained by the positive zeta potential values of the goethite at low pH and negative surface charge at higher pH values.

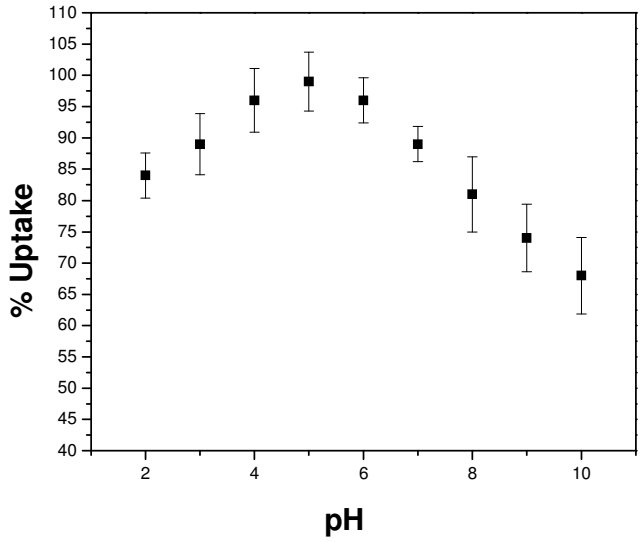

Fig.5.5. Variation of arsenic sorption by Cal-Alg-Goe beads as a function of pH

5.2.6 Sorption Isotherm

The equilibrium sorption of arsenic was studied as a function of concentration at 25-35^{O} C and the sorption isotherms are shown for Langmuir (Fig. 5.6) and for Freundlich (Fig. 5.7) isotherms. As can be seen from Fig. 5.6 and Fig. 5.7, Langmuir model fits the experimental data very well with the R^2 value of 0.98 compared to the Freundlich model (R^2 = 0.83). The Langmuir constant Q_0, which is a measure of the monolayer adsorption capacity, is obtained

as 30.44 mg g^{-1} which is very close to the experimentally determined value (29.3 mg g^{-1}) of sorption capacity.

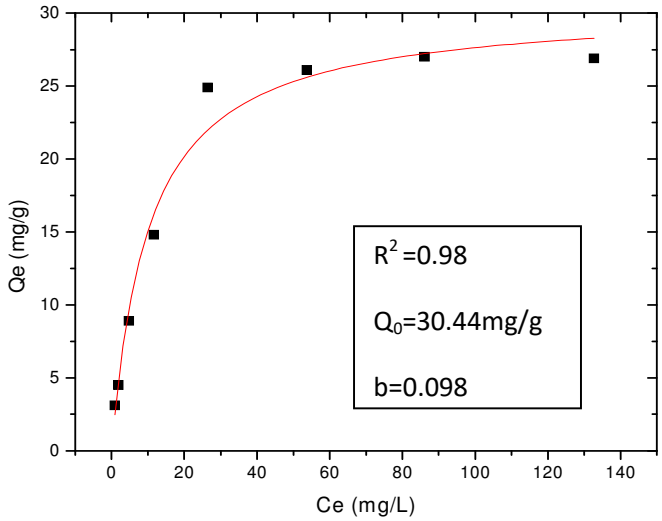

Fig. 5.6: Langmuir isotherm for arsenic on Cal-Alg-Goe beads

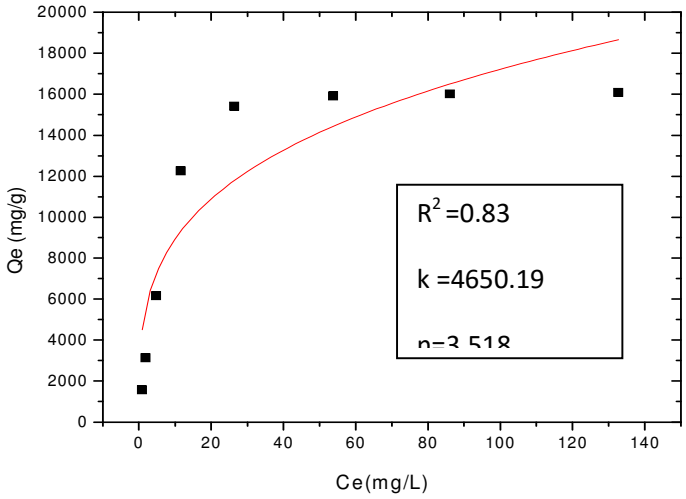

Fig. 5.7: Freundlich isotherm for arsenic on Cal-Alg-Goe beads

5.2.7 Kinetics study

In Fig. 5.8 the pseudo first order kinetics fitting for sorption of arsenic on the Cal-Alg-Goe beads are shown for initial concentration of arsenic as 10 µg mL^{-1} (Fig. 5.8A) and 1 µg mL^{-1} (Fig. 5.8B). The R^2 values for the plots are 0.9923 and 0.9919 respectively suggesting a good fitting of the kinetic data into the pseudo first order rate law. The sorption capacities evaluated from the intercepts were 30.9 mg g^{-1} and 35.9 mg g^{-1} respectively for initial concentration of arsenic as 10 µg mL^{-1} and 1 µg mL^{-1}. Both the values are close to the experimentally determined values which is 29.3 mg g^{-1} for 10 µg mL^{-1} and 33.1 mg g^{-1} for 1 µg mL^{-1} initial concentration of arsenic. As the pseudo-first-order model was sufficient to estimate q_e, pseudo-second-order kinetics was not tested for the estimation of q_e.

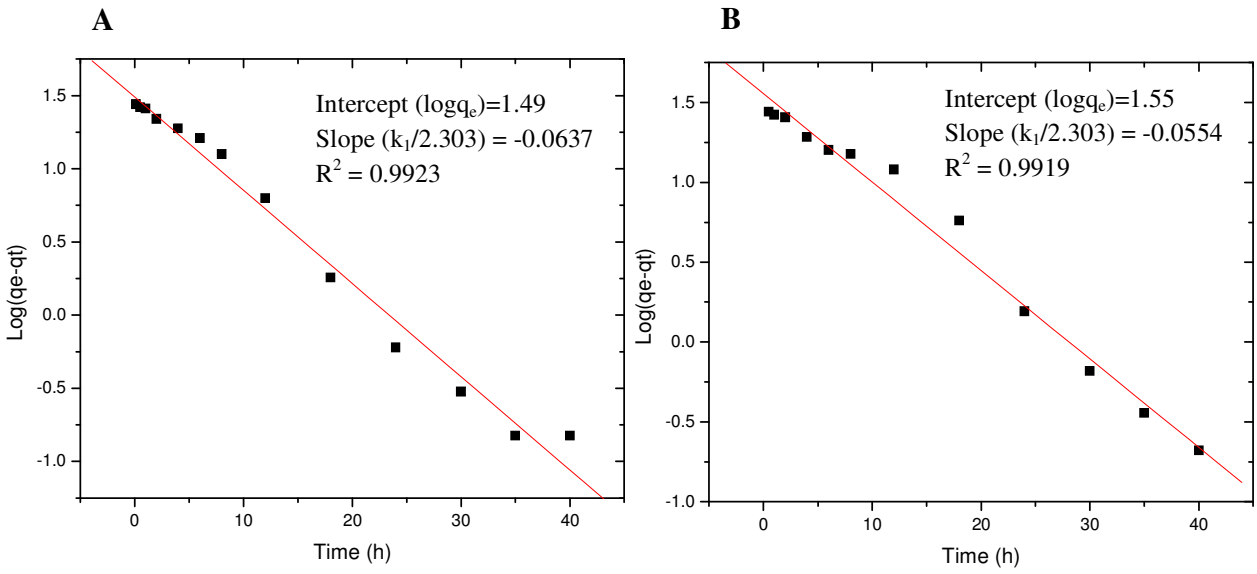

Fig. 5.8: 1st order kinetic fitting for initial concentration of As 10 µg mL^{-1} [A]; 1 µg mL^{-1} [B]

5.2.8 Probable mechanism

Mechanism behind the sorption is governed by both adsorption of different species of arsenic on goethite (H_3AsO_3, $H_3AsO_3^{2-}$, H_3AsO_4, $H_3AsO_4^{-}$,$H_3AsO_4^{2-}$, AsO_4^{3-} etc.) as well as inner

sphere complexes of iron based on the experimental data together with the fraction diagram of arsenic species [211-213] (Fig. 5.9). The sorption of arsenate on beads involves interactions between the sorbate and the hydroxyl group of the goethite [214]. This phenomenon was clearly demonstrated when the sorption of arsenate onto goethite was studied using IR spectroscopy [214]. The surface chemistry of the goethite varies with pH. At low pH, the hydroxyl groups at the surface of the iron oxide are doubly protonated and the surface charge of the iron oxide is thus positive. At a certain pH, the hydroxyl group is

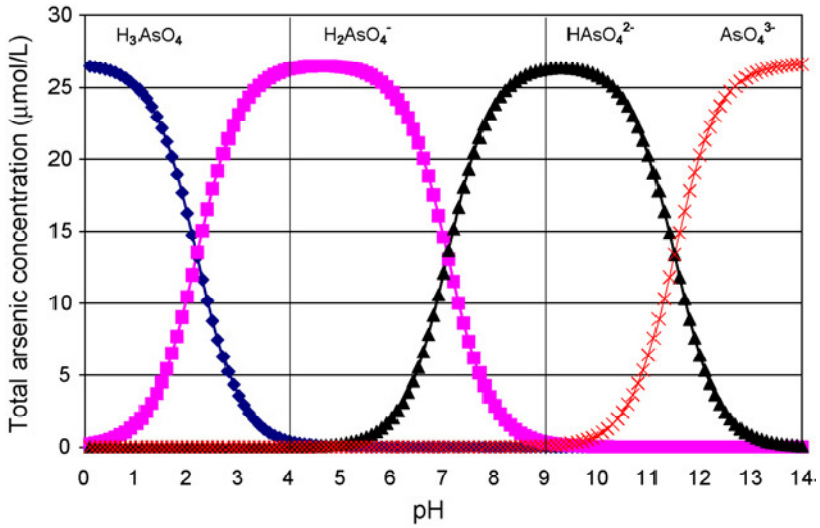

Fig. 5.9 Speciation diagram for As(V): Reproduced with permission from M. Streat, K. Hellgardt, N.L.R. Newton, Hydrous ferric oxide as an adsorbent in water treatment Part 3: Batch and mini-column adsorption of arsenic, phosphorus, fluorine and cadmium ions process safety and environmental protection 86(2008) 21–30, Elsevier License number 3873050870513

protonated with only one proton and thus the (net) surface charge of the iron oxide is neutral (PZC) (Fig. 2.23; Chapter 2). At pH values above the PZC, the hydroxyl group is deprotonated and consequently the goethite surface bears a negative charge. A maximum sorption of arsenate has been observed at pH values around 4-5 according to our

experimental result and also based on some earlier works carried out by other researchers [215]. At these pH values, the electrostatic attraction between the negative oxoanion and the positive charge of goethite favours sorption. At pH lower than 3, fully protonated arsenate (H_3AsO_4) species are present in solution and electrostatic attraction is no longer possible, resulting in a lower sorption. At pH values above the PZC, the iron oxide is negatively charged, and repels the negatively charged arsenate. Consequently sorption is substantially lower at these pH values also. The presence of hydroxyl and carboxylic acid groups in the alginate enhance the sorption of neutral arsenic species at extreme pH values. But the most important role of alginate is to bind the goethite into the matrix and separation of the sorbent became very easy because of the formation of the beads.

5.3 Fluoride removal from groundwater using Ca-Alg-Alu beads

Fluoride contamination in groundwater is the most alarming after arsenic among the so called conventional pollutants. In this part of the thesis, we discuss, the works carried out on removal of fluoride from groundwater using alumina impregnated calcium alginate (Cal-Alg-Alu) bead.

5.3.1 SEM-EDS analysis of fluoride sorbed Cal-Alg-Alu beads

The SEM images of pure and fluoride-sorbed Cal-Alg-Alu beads are shown in Fig. 5.10 (A) and (B). As can be seen from Fig. 5.10 (A), the sorbent does not possess any well-defined porous structure and no significant changes were observed in fluoride-sorbed Cal-Alg-Alu beads (Fig. 5.10 (B)). EDX analyses were performed to determine the elemental constituents of pure and fluoride-sorbed Cal-Alg-Alu beads (Fig. 5.11 (A)and (B)). It shows that the presence of fluoride in small content appears in the spectrum other than the principal

elements Ca, Na Al and O in case of fluoride sorbed Cal-Alg-Alu whereas there is no fluoride peak in the pure Cal-Alg-Alu beads.

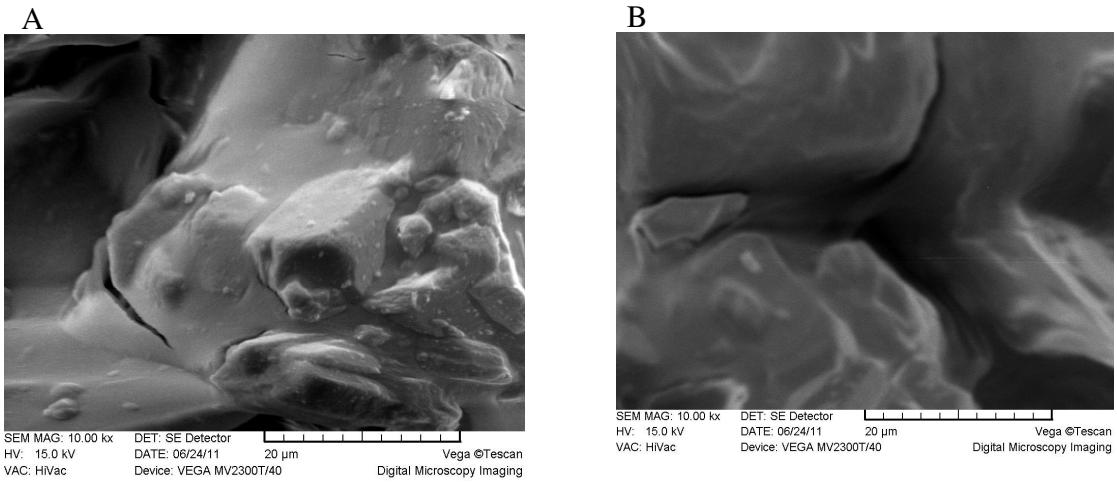

Fig. 5.10: SEM images of (A) Calcium Alginate Aluminum (Cal-Alg-Alu) beads (B) fluoride-sorbed Cal-Alg-Alu beads

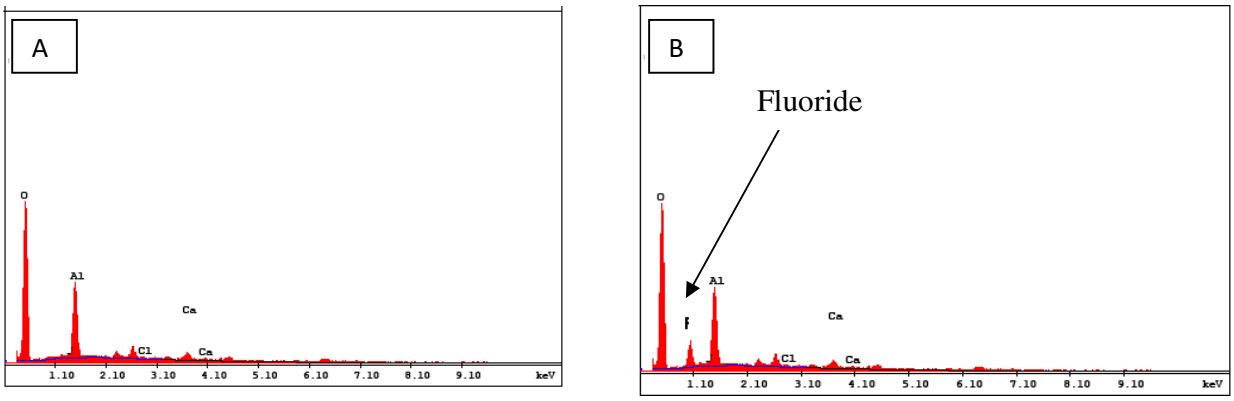

Fig. 5.11: EDS spectra of (A) Calcium Alginate Aluminum (Cal-Alg-Alu) beads (B) fluoride-sorbed Cal-Alg-Alu beads

5.3.2 XRD analysis of fluoride sorbed Cal-Alg-Alu beads

The XRD patterns of Cal-Alg-Alu before and after sorption with fluoride were also recorded. Fig. 5.12 (A) and (B) presents the X-ray diffractograms of original and fluoride-sorbed Cal-

Alg-Alu bead samples. The similarity between the diffractograms of the original and the fluoride-sorbed sample indicates that no significant bulk structural changes occurred at that fluorination level and the fluoride ions do not change the phase of Cal-Alg-Alu compost.

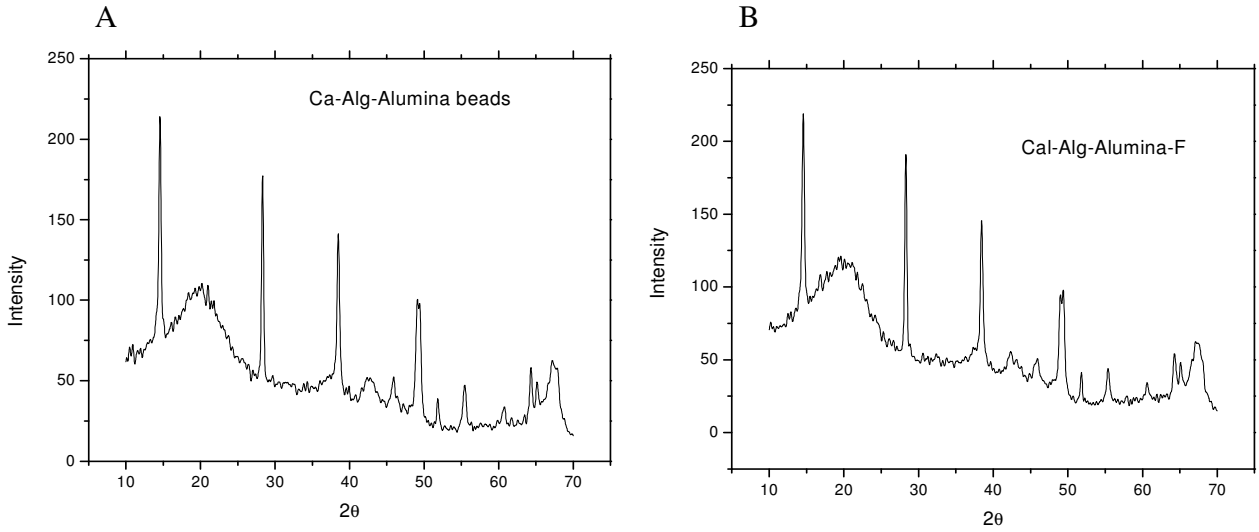

Fig.5.12: XRD pattern of (A) Calcium Alginate Aluminum (Cal-Alg-Alu) beads (B) fluoride-sorbed Cal-Alg-Alu beads

5.3.3 FTIR analysis of fluoride sorbed Cal-Alg-Alu beads

The FTIR spectra of pure and fluoride-sorbed alumina are shown in Fig. 5.13 (A) and (B). In FTIR spectra of Cal-Alg-Alu beads (before sorption) (Fig. 5.13 [A]). The peaks at 1040 cm^{-1} and 510 cm^{-1} corresponds to the Al–O stretching vibration [180-182]. Transmission band at 510 cm^{-1} (extended upto 800 cm^{-1}) and 1070 cm^{-1} and correspond to Al-F and Al-O stretching vibrations respectively. Transmission band at 1400, 1600 and 1840 cm^{-1} are more dominant in case of fluoride sorbed Ca-Alg-Alu beads. The broad band between 3200 – 3500 cm^{-1} is attributed to the atmospheric water vapor. These observations suggest possible interaction between fluoride and Cal-Alg-Alu. Similar observations were reported by Kumar et al [153] in their work on fluoride sorption by nano alumina from potable water.

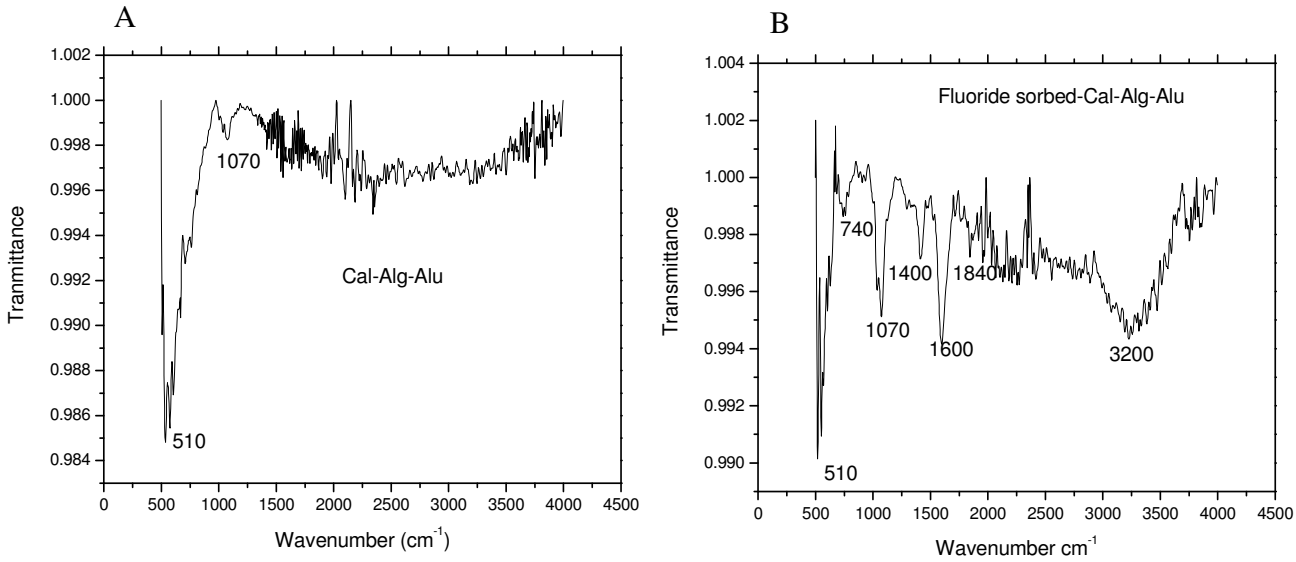

Fig. 5.13. FTIR spectra of (A) Calcium Alginate Aluminum (Cal-Alg-Alu) beads (B) fluoride-sorbed Cal-Alg-Alu beads

5.3.4 Uptake study for different concentrations of fluoride

The sorption of fluoride on Cal-alg-Alu beads was investigated in concentration range of 0.1-1000 μg mL^{-1}, keeping the concentration of sorbent as 20 mg mL^{-1} in a poly-propylene

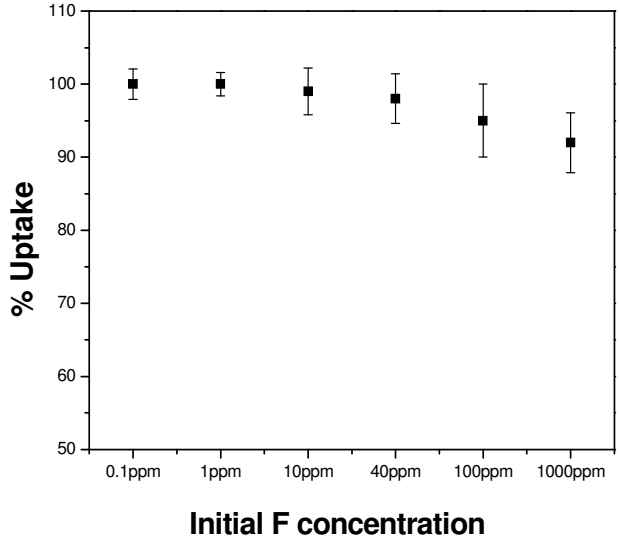

Fig.5.14: Variation in uptake of fluoride by alumina impregnated calcium alginate beads at different concentration of fluoride at pH 7.5

container having 200 mL capacity. Fig. 5.14 shows the variation in percentage uptake for fluoride at different concentrations of fluoride. From this Fig. it's clear that Cal-alg-Alu beads are capable of sorbing more than 98% fluoride from the groundwater. In order to streamline the various conditions for sorption of fluoride by Cal-Alg-Alu beads, pH and time of contact were optimized.

5.3.5 Optimisation of time

In order to optimize the contact time the experiment were conducted for fluoride uptake at different initial concentrations of fluoride [10, 50 and 100 µg mL^{-1}] having the concentration of sorbent as 20 mg mL^{-1}. Fig. 5.15 shows that fluoride sorption increases with time upto 300 minutes, then it becomes almost constant. The time for all the batch experiments were kept fixed at 8 hours to ensure maximum uptake of fluoride. The kinetics was seen to be little slow. The reason may be attributed to the slow rate of diffusion of fluoride into the alginate matrix which held the alumina responsible for fluoride removal.

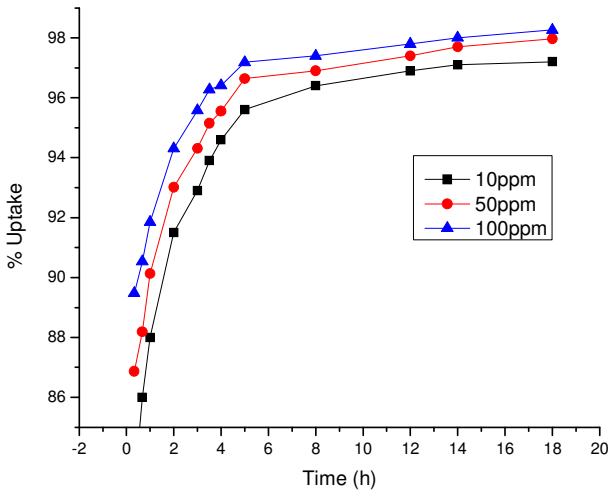

Fig. 5.15: Variation of fluoride sorption by Cal-Alg-Alu beads with time

5.3.6 Effect of pH

Percentage uptake of the fluoride was studied at pH range between 3.5 - 10, keeping all the sets for 300 minutes and having initial fluoride concentration of 100 μg mL^{-1} and adsorbent as 20 mg mL^{-1}. From the experimental results (shown in Fig.5.16) , it is clear that uptake capacity was more than 90% upto pH 9, only above pH 9 it decreases due to competition with OH^- ions. These results suggest that the prepared beads can be used for fluoride removal without any pH adjustment in the pH range of 3.5 – 9.0, whereas most of the earlier methods reported for fluoride removal at such low extent, required pH adjustment or some other pretreatment. This independency of pH makes the Cal-Alg-Alu beads more suitable for fluoride removal from potable water originated from different sources.

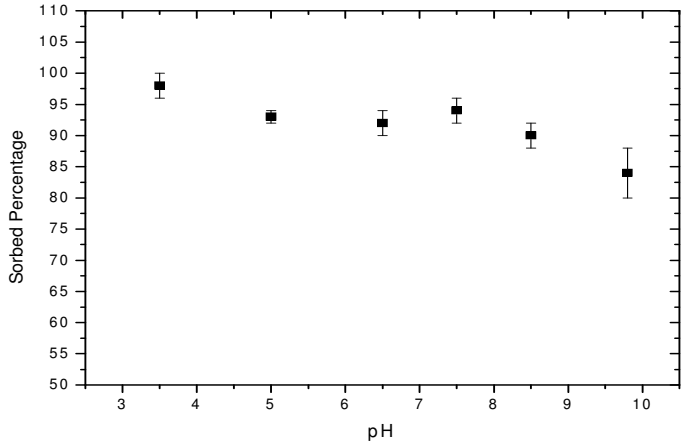

Fig.5.16: Percentage sorption of fluoride by Cal-Alg-Alu at different pH

5.3.7 Effect of other ions on the uptake capacity

Uptake capacity of the alumina impregnated calcium alginate beads were found to be unaffected in the presence of other ions (Na^+, K^+, Ca^{2+}, Mg^{2+}, SO_4^{2-}, Cl^-, I^-, NO_3^-, CO_3^{2-}) upto concentration of 100 mg L^{-1}. Results are given in table 5.1. Presence of any of these tested ions in the drinking water at a concentration higher than 100 mg L^{-1} is never

anticipated. For this study pH was maintained at 7.5 and all the sets were kept for 90 minutes. Under similar condition without addition of any other ions percentage uptake was 96%. Table 5.1: Effect of other ions on the F uptake capacity of the Cal-Alg-Alu beads

Spiked Fluoride concentration (mg L^{-1})	Spiked Ions	Spiked Ion Concentration (mg L^{-1})	% uptake of fluoride (mg L^{-1})
100	Na^{+}	100	96.3
100	K^{+}	100	95.8
100	Ca^{2+}	10 -100	94.7
100	Mg^{2+}	100	94.2
100	Cl^{-}	100	92.1
100	I^{-}	100	94.6
100	SO_4^{2-}	100	95.6
100	NO_3^{-}	100	97.6
100	CO_3^{2-}	100	95.8

5.3.8 Sorption kinetic modeling of fluoride on Cal-Alg-Alu beads

The kinetics of fluoride sorption on Cal-Alg-Alu beads was analyzed using pseudo-first-order and pseudo-second-order kinetic models to identify the dynamics of the solute adsorption process. The best-fit model i.e. pseudo-second-order model (Fig 5.17) was selected based on the match between experimental (qe(exp))and theoretical (qe(cal)) uptake values and linear correlation coefficient (R^2) values at two studied concentrations. The rate equations and the related values are given in table 5.2. The values obtained by pseudo-second-order model were found to be in good agreement with experimental data and can be used to favorably explain the fluoride sorption on Cal-Alg-Alu beads.

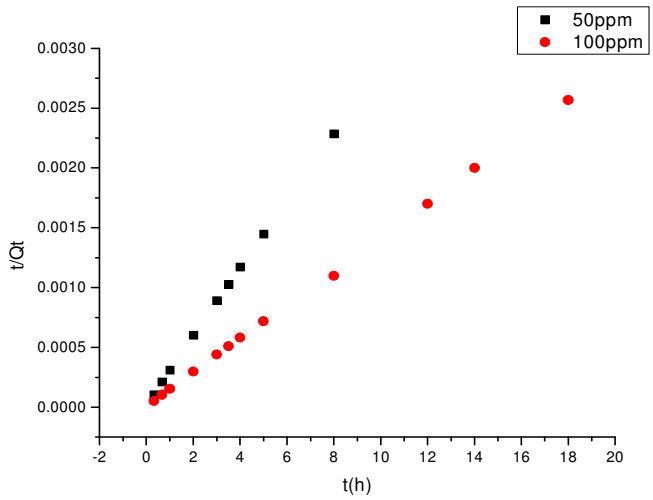

Fig.5.17: Pseudo-second-order kinetic plots of fluoride sorption on Cal-Alg-Alu

Table-5.2: Comparison of pseudo-first-order and pseudo-second-order models parameters, and calculated q_e(cal) and experimental q_e(exp) values for different initial fluoride concentrations

Pseudo first order model: $\log(q_e - q_t) = \log q_e - k_1/2.303\ t$				
C_o (mg L^{-1})	$q_{e(exp)}$ (mg g^{-1})	k_1(min-1)	$q_{e(cal)}$ (mg g^{-1})	R^2
50	3.51	1.09 x 10^{-3}	2.59	0.7037
100	7.09	1.02 x 10^{-3}	5.76	0.6866
Pseudo Second order model: $t/q_t = 1/k^2q_e^2 + (1/q_e)t$				
C_o (mg L^{-1})	$q_{e(exp)}$ (mg g^{-1})	k_2(g $mg^{-1}min^{-1}$)	$q_{e(cal)}$ (mg g^{-1})	R^2
50	3.51	1.69 x 10^{-3}	3.50	0.9998
100	7.09	1.2 x 10^{-3}	7.01	0.9997

q_e: amount of fluoride adsorbed on Cal-Alg-Alu (mg g^{-1}) at equilibrium; q_t: amount of fluoride adsorbed on Cal-Alg-Alu (mg $g^{-1)}$ at time t (min); k_1: rate constant for the pseudo-first-order kinetics; k_2 : rate constant for the pseudo-second order kinetics.

5.3.9 Sorption isotherms

Sorption isotherms are shown in Fig. 5.18 and Fig. 5.19 for Langumir and Frendulich adsorption isotherms respectively. As can be seen, Langmuir model fits the experimental data

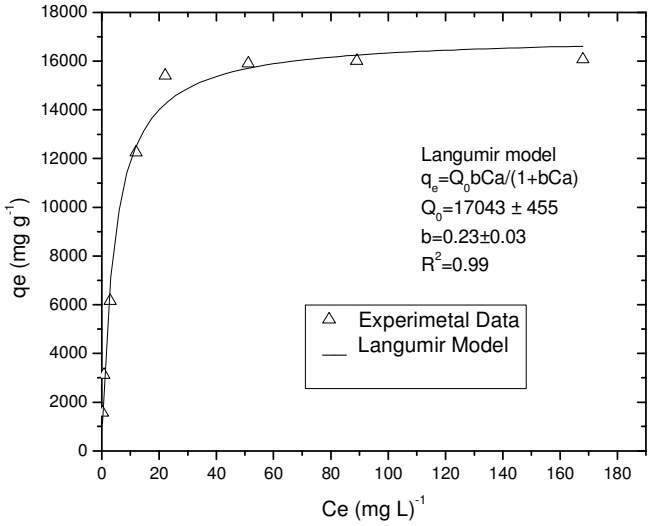

Fig. 5.18: Langumir isotherm for fluoride sorption on Cal-Alg-Alu beads

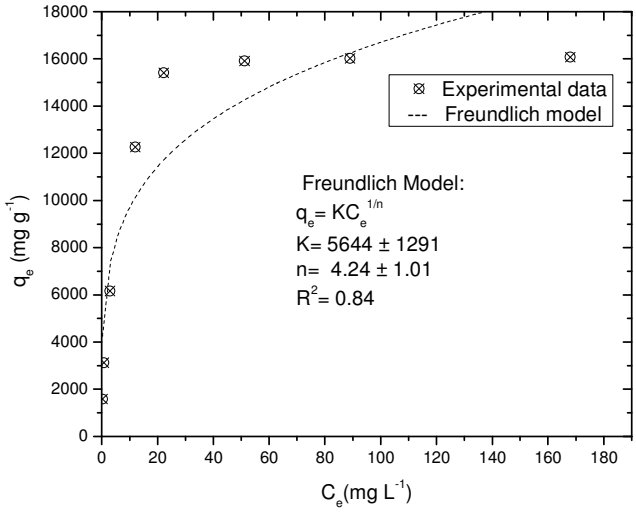

Fig.5.19: Freundlich isotherm for fluoride sorption on Cal-Alg-Alu beads

very well with the R^2 value 0.99 and which is much better than the Freundlich model (R^2 =0.84). It indicates that fluoride is adsorbed on alumina impregnated calcium alginate beads

as a monolayer adsorption. The Langmuir constant Q_0, obtained as 17.0 mg g^{-1} is very close to the experimentally determined adsorption capacity.

5.3.10 Probable mechanism of sorption of fluoride

The mechanism of fluoride removal process has been shown to involve the replacement of OH– with F^- [216]. Fluoride ions an hydroxide ions form complexes with Al(III) ions. Alumina impregnated into the beads gets partly hydrolyzed to form hydroxides, then OH groups are replaced by F^- ion one by one. The schematic is shown below:

$$Al_2O_3 \xrightarrow{H_2O} 2\,Al(OH)_3 \xrightarrow{F^-} 2\,Al(OH)_2F \xrightarrow{F^-} 2\,Al(OH)F_2 \xrightarrow{F^-} 2\,AlF_3$$

The alumina will mostly be present in polymeric species, hence the formed complex with fluoride ion can be generalized as $Al_nF_m(OH)_{3n-m.}$ The spectroscopic analysis indicated that fluoride ions enter the surface of alumina by substituting hydroxyl groups without breaking the bridging Al–O–Al bonds. At higher fluoride loadings, bridging Al–O–Al bonds were found to be broken to sorb more fluoride under the strong electron-withdrawing effect of fluorine. It is expected that similar processes occur on alumina impregnated inside calcium alginate. Zhang et al [217] studied the interaction of fluoride on alumina surface by multinuclear MASNMR (magic angle spinning nuclear magnetic resonance) spectroscopy to identify the fluorine species on the fluorinated-alumina. The spectroscopic analysis indicated that fluorine enters the surface of alumina by substituting hydroxyl groups without breaking the bridging Al–O–Al bonds. At higher fluoride loadings, bridging Al–O–Al bonds were found sorb more fluoride under the strong electron-withdrawing effect of fluorine. In presence of alginate one will have additional –OH groups to enhance the sorption.

In order to verify the individual contribution of alumina and calcium alginate, fluoride sorption experiments were conducted under similar conditions having alumina, calcium alginate beads and Cal-Alg-Alu beads as sorbent. Variation in the percentage uptake by three different sorbents is shown in Fig. 5.20. From this Fig. it's clear that alumina powder and calcium alginate beads are having much poor uptake capacity of the fluoride compared to the alumina impregnated calcium alginate beads. Sorption potential of Cal-Alg-Alu beads in the present study was compared with other adsorbents reported in previous studies for fluoride removal. It is seen that Cal-Alg-Alu used in the present study shows comparable adsorption capacity for fluoride removal compared to some previously developed adsorbents.

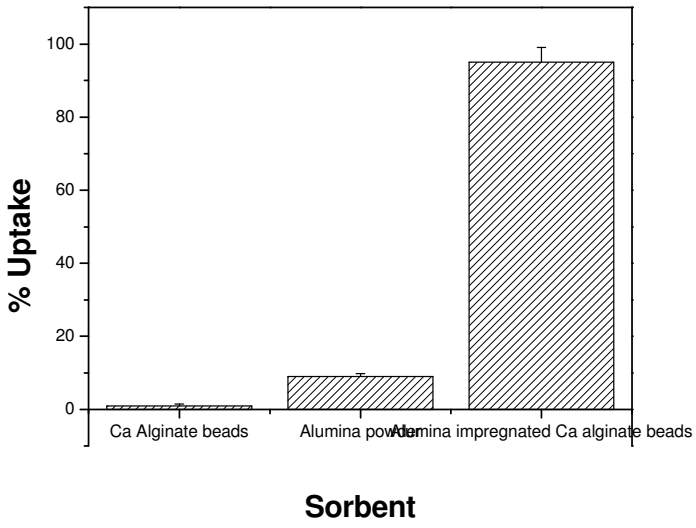

Fig.5.20: Percentage Sorption of fluoride by calcium alginate; Alumina and compost of Calcium Alginate and Alumina (Cal-Alg-Alu)

Chapter 6

Application of the hybrid materials developed under this study for decontamination of Uranium, Fluoride and Arsenic contaminated groundwater under field conditions

---

6.1 Introduction

Basic research, also called pure research or fundamental research, is scientific research aimed to improve scientific theories for improved understanding or prediction of natural or other phenomena. Applied research, in turn, uses scientific theories to develop technology or techniques to intervene and alter natural or other phenomena. Though often driven by curiosity, basic research fuels applied science's innovations. The main aim of applied science is to improve the quality of life by providing basic needs of mankind's.

One of the most pervasive problems afflicting people throughout the world is inadequate access to clean water and sanitation. Problems with water are expected to grow worse in the coming decades, with water scarcity occurring globally, even in regions currently considered water-rich. In many areas of the world the water crisis is not an issue of scarcity, it's an issue of providing access to a clean supply. The lack of access to clean water and sanitation kills thousands of people every year, while countless others struggle to meet their basic needs. As per WHO estimate, 3.575 million people dying each year from water-related disease, our current water crisis is one of epic proportions [64, 97]. At any given time, half of the world's hospital beds are occupied by those suffering from illness brought on by limited access to safe drinking water, poor hygiene and sanitation. Granted these harrowing realities plaguing our society, it's imperative that researchers, engineers and visionaries do what they can to find a solution.

Addressing these problems calls out for a tremendous amount of research to be conducted to identify robust new methods of purifying water at lower cost and with less energy, while at the same time minimizing the use of chemicals and impact on the

environment. In this chapter we discuss, some of the research carried out at lab scale successfully demonstrated in the public domain for decontamination of water.

6.2 Strategies for decontamination of potable water

So the strategies for decontamination may include international, national or regional standards developed from the scientific basis provided in the guidelines. The guidelines describe reasonable minimum requirements of safe practice to protect the health of consumers and derive numerical values for constituents of water or indicators of water quality. It sets the mandatory and maximum permissible limit for each constituent. When defining mandatory limits, it is preferable to consider the guidelines in the context of local or national environmental, geological and socio-economic conditions. The nature and form of drinking-water standards may vary from country to country even region to region. There is no single approach that is universally applicable. The guidelines are applicable to packaged water and ice intended for human consumption.

In the following table (Table 6.1) we give the maximum allowable concentration of constituents as prescribed by WHO and both the desirable limit [62-64,218] and the permissible limit set by Bureau of Indian Standard (BIS) [219,220, 221] for Indian condition.

Table 6.1: The desired, permissible and maximum concentration of constituents as prescribed by WHO and BIS

Sl. No	**Parameter**	**BIS, Indian Standard (IS 10500)**		**World Health Organization (WHO Guidelines)**
		Desirable limit	**Permissible Limit**	**Maximum allowable concentration**
1	Colour	5 Hazen Units	25 Hazen Units	15 True Colour Units
2	Turbidity	5.0 NTU	10 NTU	5.0 NTU
3	pH	6.5-8.5	No relaxation	6.5-8.5
4	Total Hardness (as $CaCO_3$)	300 mg L^{-1}	600 mg L^{-1}	500 mg L^{-1}

5	Chlorides (as Cl)	250 mg L^{-1}	1000 mg L^{-1}	250 mg L^{-1}
6	Residual Free Chlorine (When Protection against viral infection is required it should be Min 0.5 mg L^{-1})	0.2 mg L^{-1}	-	-
7	Dissolved Solids	500 mg L^{-1}	2000 mg L^{-1}	1000 mg L^{-1}
8	Calcium (as Ca)	75 mg L^{-1}	200 mg L^{-1}	-
9	Sulphate (as SO_4^{2-})	200 mg L^{-1}	400 mg L^{-1}	400 mg L^{-1}
10	Nitrate (as NO_3^{+})	45 mg L^{-1}	100 mg L^{-1}	10 mg L^{-1}
11	Flouride (as F^{-})	1.0 mg L^{-1}	1.5 mg L^{-1}	1.5 mg L^{-1}
12	Phenolic Compounds (as C_4H_5OH)	0.001 mg L^{-1}	0.002 mg L^{-1}	-
13	Anionic Detergent	0.2 mg L^{-1}	1.0 mg L^{-1}	-
14	Mineral oil	0.01 mg L^{-1}	0.03 mg L^{-1}	-
15	Alkalinity	200 mg L^{-1}	600 mg L^{-1}	-
16	Boron	1.0 mg L^{-1}	5.0 mg L^{-1}	-
Micro Pollutants (Heavy Metals & Pesticides)				
17	Zinc (as Zn)	5.0 mg L^{-1}	15 mg L^{-1}	5.0 mg L^{-1}
18	Iron (as Fe)	0.3 mg L^{-1}	1.0 mg L^{-1}	0.3 mg L^{-1}
19	Manganese (as Mn)	0.1 mg L^{-1}	0.3 mg L^{-1}	0.1 mg L^{-1}
20	Copper (as Cu)	0.05 mg L^{-1}	1.5 mg L^{-1}	1.0 mg L^{-1}
21	Arsenic (as As)	0.01 mg L^{-1}	0.05 mg L^{-1}	0.01 mg L^{-1}
22	Cyanide (as CN)	0.05 mg L^{-1}	No relaxation	0.1 mg L^{-1}
23	Lead (as Pb)	0.05 mg L^{-1}	No relaxation	0.05 mg L^{-1}
24	Chromium (as Cr^{6+})	0.05 mg L^{-1}	No relaxation	0.05 mg L^{-1}
25	Aluminium (as Al)	0.03 mg L^{-1}	0.2 mg L^{-1}	0.2 mg L^{-1}
26	Cadmium (as Cd)	0.01 mg L^{-1}	No relaxation	0.005 mg L^{-1}
27	Selenium (as Se)	0.01 mg L^{-1}	No relaxation	0.01 mg L^{-1}
28	Mercury (as Hg)	0.001 mg L^{-1}	No relaxation	0.001 mg L^{-1}
29	Sodium (as Na)	-	-	200 µg L^{-1}
30	Uranium	-	-	17 µg L^{-1}
31	Total Pesticides	Absent	0.001 mg L^{-1}	-
32	Aldrin & dieldrin	-	-	0.03 µg L^{-1}
33	DDT	-	-	1.0 µg L^{-1}
34	Benzene	-	-	10.0 µg L^{-1}
35	Hexachlorobenzene	-	-	0.01 µg L^{-1}
36	Pentachlorophenol	-	-	10.0 µg L^{-1}
Radionuclides				
37	Alpha emitters	0.1 Bq L^{-1}	No relaxation	0.1 Bq L^{-1}
38	Beta emitters	1.0 Bq L^{-1}	No relaxation	1.0 Bq L^{-1}

6.3 Ready to use kits for decontamination of groundwater under field condition

Various developed hybrid materials as described in the previous chapters were employed for the decontamination of actual groundwater samples having uranium, fluoride and arsenic contamination. Location of occurrence of various pollutants in India can be known from the data available from Central Pollution Control Board (CPCB) [222,223] in addition to the already published works by various researchers [224-230]. In table 6.2, the locations of occurrence of fluoride and arsenic in India are given. The contaminated water samples were obtained from various parts of India. Uranium containing groundwater samples were obtained from the state of Punjab; fluoride containing samples were obtained from the state of Andhra Pradesh and the arsenic contaminated groundwater samples were collected from the state of West Bengal. In each case, three different samples were collected from three different but adjacent locations within the same district. In the table 6.3 the locations of the places from where the samples originates are given.

Table 6.2: Locations of occurrences of F, As in groundwater in India

Pollutant	**State**	**Places of occurrences**
Fluoride	Andhra Pradesh	Cuddapah, Guntur, Nalgonda, Prakasam, Nellore, Anantapur, Rangareddy, Adilabad
	Bihar	Giridih, Jamui, Dhanbad
	Gujarat	Banskanta, Kachch, Amreli, Surendranagar, Rajkot, Ahmedabad, Mehsana, Sabarkantha
	Karnataka	Tumkur, Kolar, Bangalore, Gulbarga, Bellary, Raichur
	Haryana	Hissar, Kaithal, Gurgaon, Rohtak, Jind, Bhiwani, Mahendragarh, Faridabad
	Kerala	Palaghat, Ananipur, Nellore, Chittoor
	Madhya Pradesh	Bhind, Moerana, Guna, Jhabua, Chhindwara, Seoni, Mandla, Raipur, Vidisha
	Maharashtra	Bhandara, Chandrapur, Nanded, Aurangabad
	Orissa	Bolangir, Bijapur, Bhubaneshwar and Kalahandi
	Punjab	Jalandhar, Amritsar, Bhatinda, Faridkot, Ludhiana & Sangrur
	Rajasthan	Barmer, Ganganagar, Jalore, Nagaur, Pali, Sirohi, Ajmer & Bikaner
	Tamil Nadu	Dharampuri, Salem, North Arcot, Viluppuram, Tiruchirapalli,

		Pudukottai, Chengalput, Madurai
	U.P	Bulandshahar, Unnao, Agra, Aligarh, Mathura, Ghaziabad, Meerut, and Rai Bareilly
	West Bengal	Birbhum
Arsenic	West Bengal	Malda, Murshidabad, Nadia, Malda, North and South-24 Paraganas, Hoogly, Bardhaman, Howrah

Table 6.3: Locations of collection of U, F, As contaminated groundwater

Contaminant in groundwater	**District**	**State**	**Sample identification**
Uranium	Bathinda	Punjab	GW-U-1, GW-U-2, GW-U-3
Fluoride	Nalgonda	Andhra Pradesh	GW-F-1, GW-F-2, GW-F-3
Arsenic	North 24 Parganas	West Bengal	GW-As-1, GW-As-2, GW-As-3

6.3.1 Uranium decontamination kit

Field groundwater samples having elevated levels of uranium received from the state of Punjab, India had been tested with the developed hybrid materials. Both Cal-Alg-Chi beads and silica microspheres (SM) were tested. Table 6.4 shows the level of uranium in those

Table 6.4: Concentrations of U in groundwater samples before and after treatment with the hybrid materials

Sample identification	**Concentration of uranium before treatment (ng mL^{-1})**	**Concentration of uranium after treatment with the Cal-Alg-Chi beads (ng mL^{-1})**	**Concentration of uranium after treatment with the SM (ng mL^{-1})**
GW-U-1	103	11	13
GW-U-2	246	13	12
GW-U-3	450	8	10

samples before and after the treatment with two different hybrid materials. This result clearly indicates the effectiveness of these materials towards removal of uranium from groundwater.

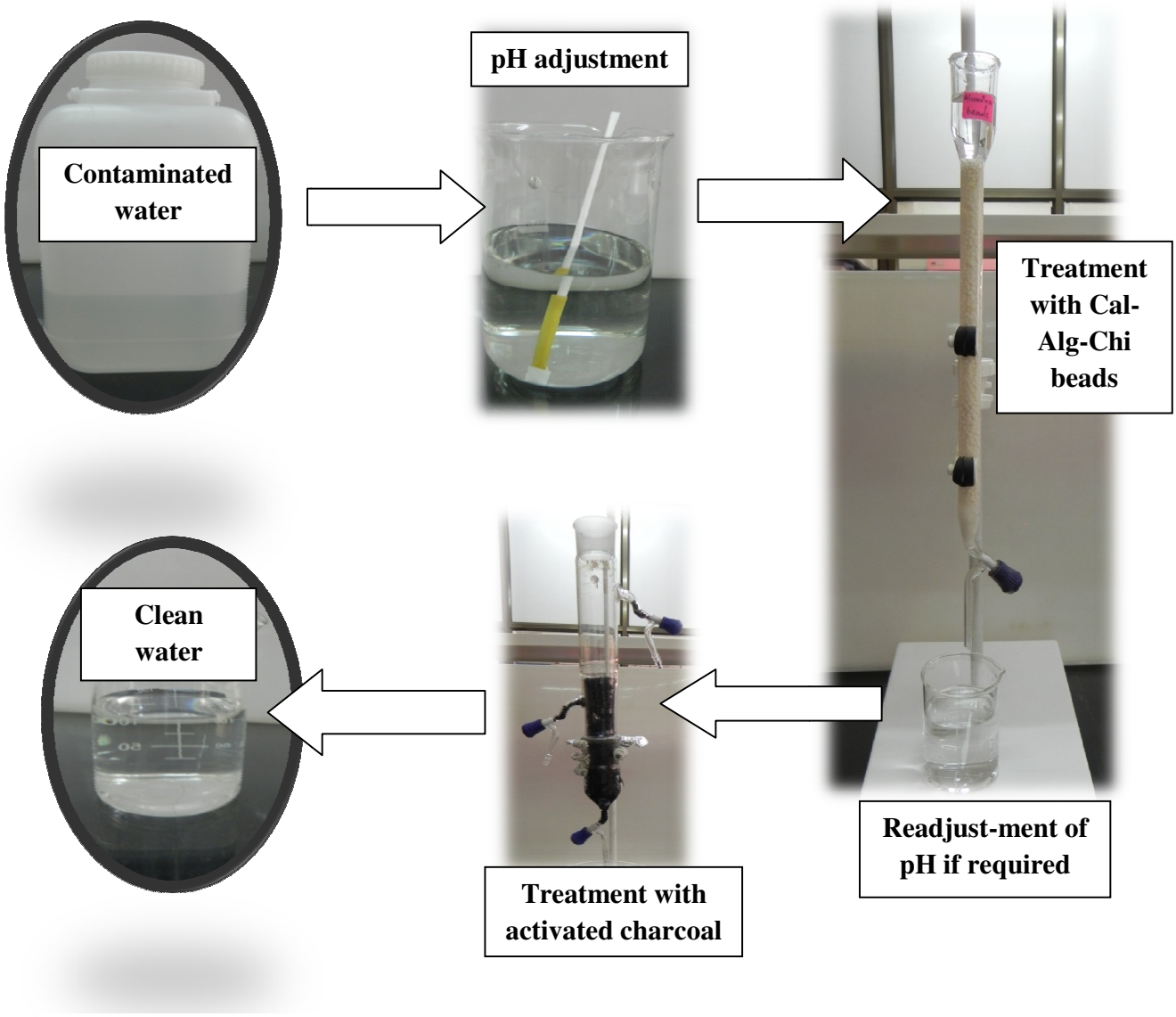

Fig. 6.1: Schematic for the uranium removal with pH adjustment

Both the materials were found to be equally effective, only difference was in terms of kinetics, uptake by SM was faster compared to Cal-Alg-Chi beads. But the Cal-Alg-Chi beads may be favorable if we think to make a kit to be use in the field because of the ease of separation.

For the operation in the plant level, two column can be used sequentially, first after adjustment of the pH to 4-5 (step-I), the contaminated water will be passed through the Cal-Alg-Chi beads filed in a column (step-II), then the pH will be adjusted back according to the groundwater pH at step-III. Now to get the desired concentration of the other ions specially to take care of the ions like NO_3^- or Na^+ added for the adjustment of the pH, the water is passed through the activated charcoal column in the final stage (step-IV) to get the clean uranium free water. The schematic is shown in Fig. 6.1.

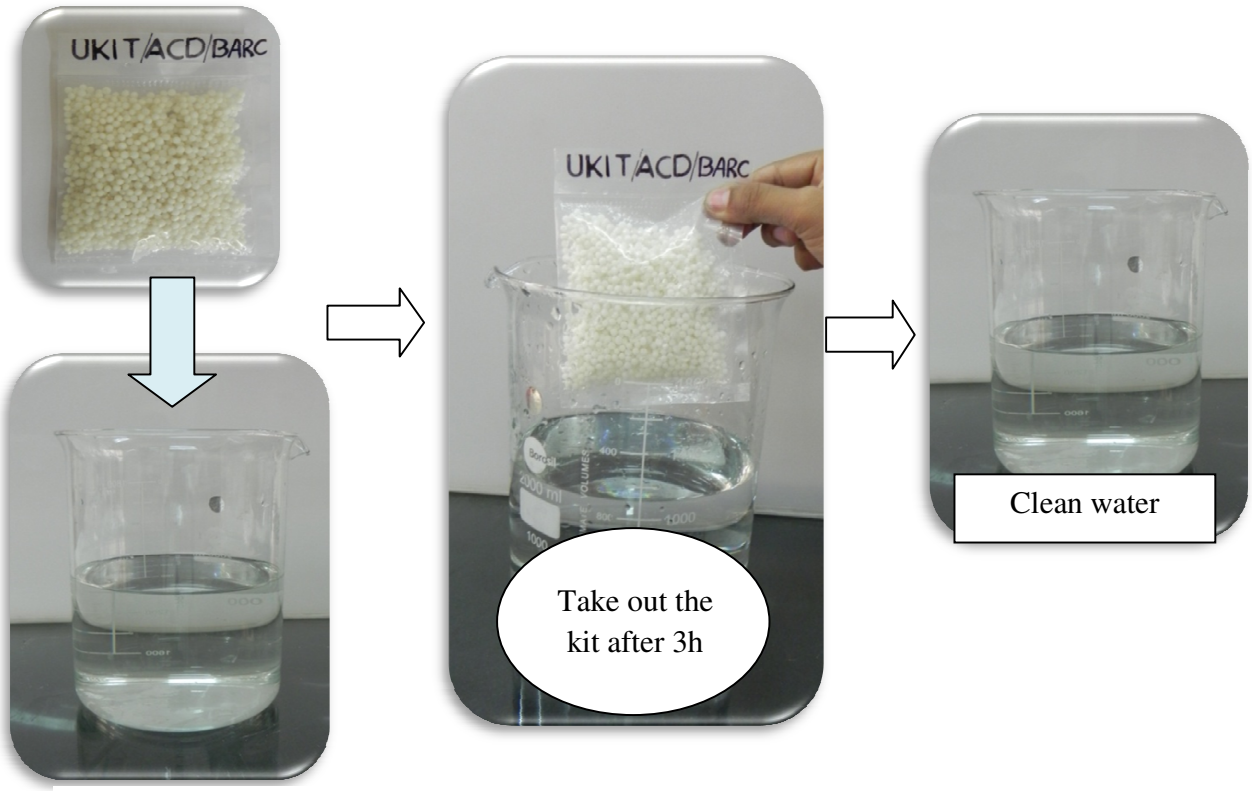

Fig. 6.2: Decontamination of U from groundwater in field condition in batch method

Now to discuss the feasibility of the developed material to be used in field condition for the removal of uranium, we propose both batch and column method. For the batch operation a simple kit containing the Cal-Alg-Chi beads can be dipped into a bucket/beaker of water (20 Litres approximately) and can be taken out after three hours (Fig.6.2). The kit is

basically Cal-Alg-Chi beads contained inside a perforated sealed polythene bag to allow the water to pass through and interact. The dimension of the perforated holes are smaller compared to the size of the beads but sufficient to pass water. The same kit can be used 50 times before requirement of regeneration or discarding it although the capacity or the number of cycle permissible will largely depend on the concentration of uranium in the groundwater to be decontaminated. A specially designed column with 5 cm diameter was fabricated for column operation (Fig. 6.3).

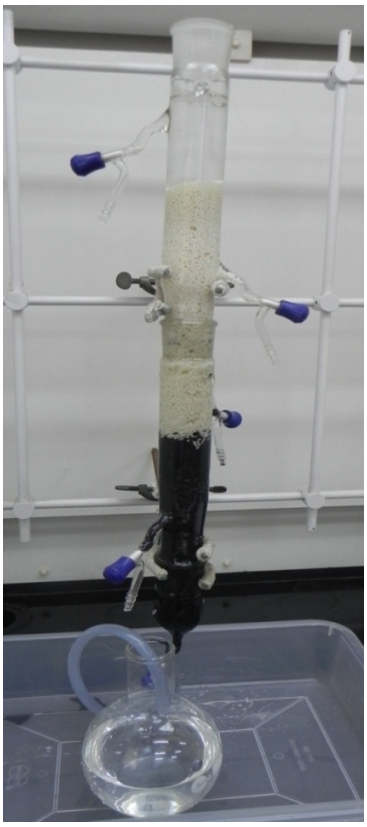

Fig. 6.3: Decontamination of U from groundwater in field condition in column method

It had option for elution from different points at desired heights. One third of the column from the bottom was field with activated charcoal granules the middle portion was field with Cal-Alg-Chi beads and the top portion was kept vacant for the charging of contaminated water. To avoid pH adjustment under field condition, there is a compromise with uptake

capacity. General physicochemical parameters of three groundwater samples used for this study measured before and after treatment with the kit are given in table 6.5. Data are given for both batch and column method. It is clear that due to the treatment with the Cal-Alg-Chi beads no major variation of any physicochemical property. Special care was taken regarding leaching of the components of the beads namely calcium (Ca), chitosan and alginate. No elevated level of concentrations of Ca and DOC (dissolved organic content) was observed in the water after treatment suggesting no leaching of the components of the bead

Table 6.5: Physicochemical parameters groundwater samples before and after treatment with the kit

Parameters	**Before treatment**	**After treatment with Kit (Batch method)**	**After treatment in column method**
pH	5.8-7.9	5.7-7.8	6.1-7.5
Conductance (μ S)	332-418	342-403	278-349
Redox potential (mV)	119-132	125-130	113-128
DOC (mg L^{-1})	6-11	7-11	5-8
Ca (mg L^{-1})	36.2-44.3	36.7-44.5	32.6-41.7
Mg (mg L^{-1})	13.6-16.8	15.4-17.8	14.5-16.1
Na(mg L^{-1})	21.5-29.6	23.1-27.4	21.8-26.0
K (mg L^{-1})	0.6-0.9	0.7-0.9	0.7-0.8
Fe (mg L^{-1})	2.3-3.1	2.4-3.1	1.5-2.7
Cl^{-1} (mg L^{-1})	15.6-22.4	15.2 -20.8	14.5-18.6

6.3.2 Fluoride decontamination kit

Fluoride containing groundwater samples collected from the state of Andhra Pradesh were subjected to treatment with the Cal-Alg-Alu beads developed for removal of fluoride. The table 6.6 gives the concentration of fluoride in three ground water samples. In all the samples collected from Nalgonda district of Andhra Pradesh, the fluoride concentration is higher than

the permissible limit (1.5 μg mL^{-1}). The table also shows the values of fluoride concentration after treatment with the developed Cal-Alg-Alu beads. It is clear from the values that treating the contaminated groundwater, the concentration of fluoride could be brought down to <1 μg mL^{-1}.

Table 6.6: Concentration of F in groundwater samples before and after treatment with the Cal-Alg-Alu beads

Sample identification	**Concentration of fluoride before treatment (μg mL^{-1})**	**Concentration of fluoride after treatment with the Cal-Alg-Alu beads (μg mL^{-1})**
GW-F-1	3.6	<1
GW-F-2	3.2	<1
GW-F-3	4.1	<1

Assessment of drinking water quality after treatment with the beads was carried out. Various physicochemical characteristics of the groundwaters used for study is given in the table-6.7. It also gives the values of the same physicochemical parameters of the ground water samples observed after treatment with the beads for fluoride removal. Table-6.16, which gives the range of minimum and maximum values, it's clear that there is no major variation among these water samples. Ground water samples also did not show elevated levels of concentration of any particular properties after the treatment with the beads assuring the drinkability of the water. Special care has been taken for aluminium (Al) and alginate and no elevated level of Al and DOC was observed in the potable water after the removal of fluoride.

Table 6.7: Physicochemical characteristics of groundwater before and after the treatment with the Cal-Alg-Alu beads

Parameters	**Before treatment**	**After treatment**
pH	7.4-7.8	7.2-7.7
Conductance (µ S)	348-356	360-368
Redox potential (mV)	126-132	122-127
Cl^{-1} (mg L^{-1})	18.9-21.3	17.4-21.0
PO_4^{3-} (mg L^{-1})	0.64-0.66	0.65-0.67
Na^{+}(mg L^{-1})	24.2-27.8	24.4-28.6
K^{+} (mg L^{-1})	0.75-0.82	0.74-0.89
Mg^{2+} (mg L^{-1})	15.3-16.9	15.1-16.8
Ca^{2+} (mg L^{-1})	39.1-42.6	40.2-44.7
Cu^{2+} (µg L^{-1})	5.4-7.3	5.2-6.8
Pb^{2+} (µg L^{-1})	2.8-3.5	2.6-3.0
DOC (mg L^{-1})	9-11	10-11
Fe (mg L^{-1})	1.6-2.0	1.8-2.3
Al (µg L^{-1})	<10	<10

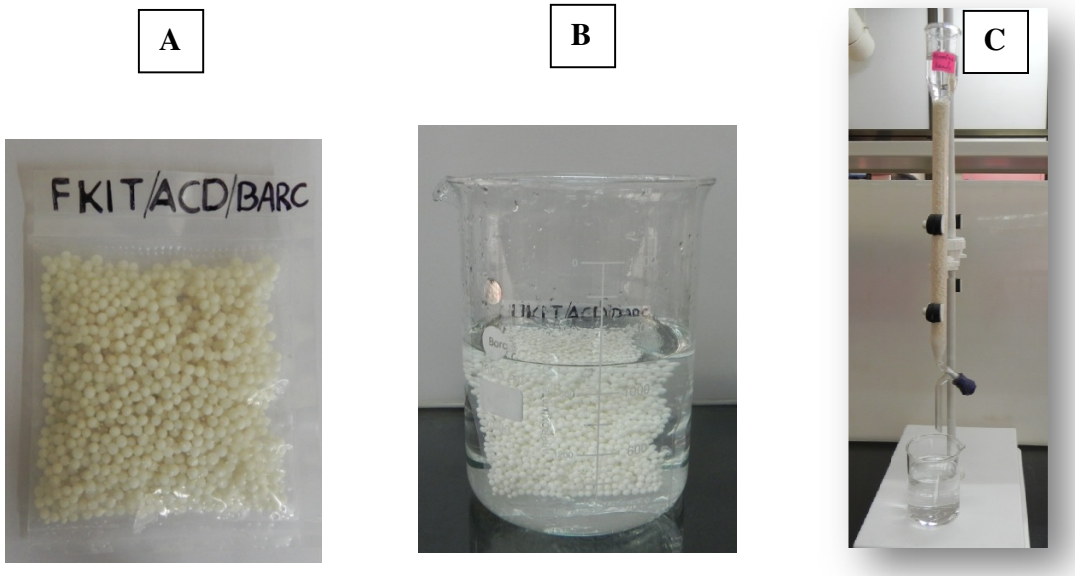

Fig. 6.4: (A) Kit for decontamination of fluoride from groundwater; (B) for batch method; (C) for column method

In-house prepared kit "Cal-Alg-Alu beads in a sealed perforated polythene bag" was prepared as shown in Fig. 6.4A. This kit can be dipped into a container of water (20 Lit approximately) and can be taken out after eight hours and the decontaminated water can be consumed safely (Fig. 6.4B). No pretreatment or pH adjustment is required as the Cal-Alg-Alu beads work most efficiently at pH 6.5-8.5. It is very convenient to be used by a common man. The same operation can also be performed in the column with a residence time of 8 hours (Fig. 6.4C).

6.3.3 Arsenic decontamination kit

Groundwater samples were collected from the arsenic contaminated area of West Bengal, India. The concentrations of As in those samples was in the range of 53-125 ng mL^{-1}. The Cal-Alg-Goe beads were successfully tested for these groundwater samples collected from ambient environment. As discussed in chapter 5, to make sure that arsenic is present in As(V) form, oxidising environment was created by using nitric acid and hydrogen peroxide. For three different samples as discussed, the arsenic concentrations were brought down to 7-18 ng mL^{-1} after treatment with Cal-Alg-Goe beads. The As concentrations both before and after the treatment are given in table 6.8.

A set up for the easy decontamination of arsenic contaminated groundwater samples is demonstrated in laboratory and is shown in Fig. 6.5. After pH adjustment and oxidation, the water is treated with Cal-Alg-Goe beads, then the pH is readjusted. To take care of any added ions for the pretreatment, the water is again passed through the activated charcoal column which has a very good property for the sorption of the excess concentration of metal ions and anions. The final water that comes out of the activated charcoal column is collected.

Table 6.8: Arsenic concentrations in groundwater samples before and after the treatment with the Cal-Alg-Goe beads

Sample identification	**Concentration of As before treatment (ng/mL)**	**Concentration of As after treatment with the beads(ng/mL)**
As-GW-Sample 1	125	18
As-GW-Sample 2	53	7
As-GW-Sample 3	84	11

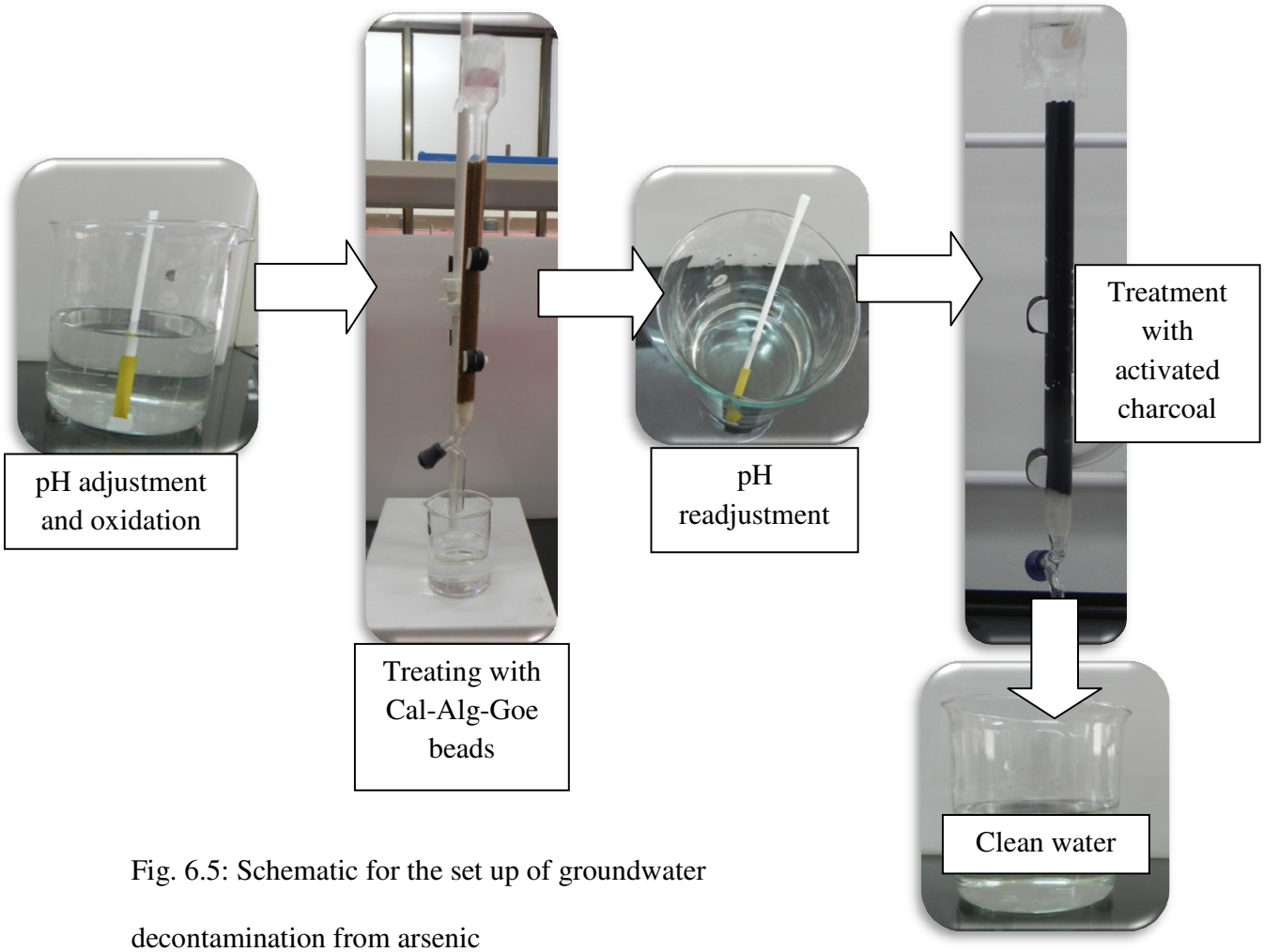

Fig. 6.5: Schematic for the set up of groundwater decontamination from arsenic

Like uranium and fluoride a ready to use kit was also developed for the decontamination of arsenic in batch mode (Fig. 6.6).

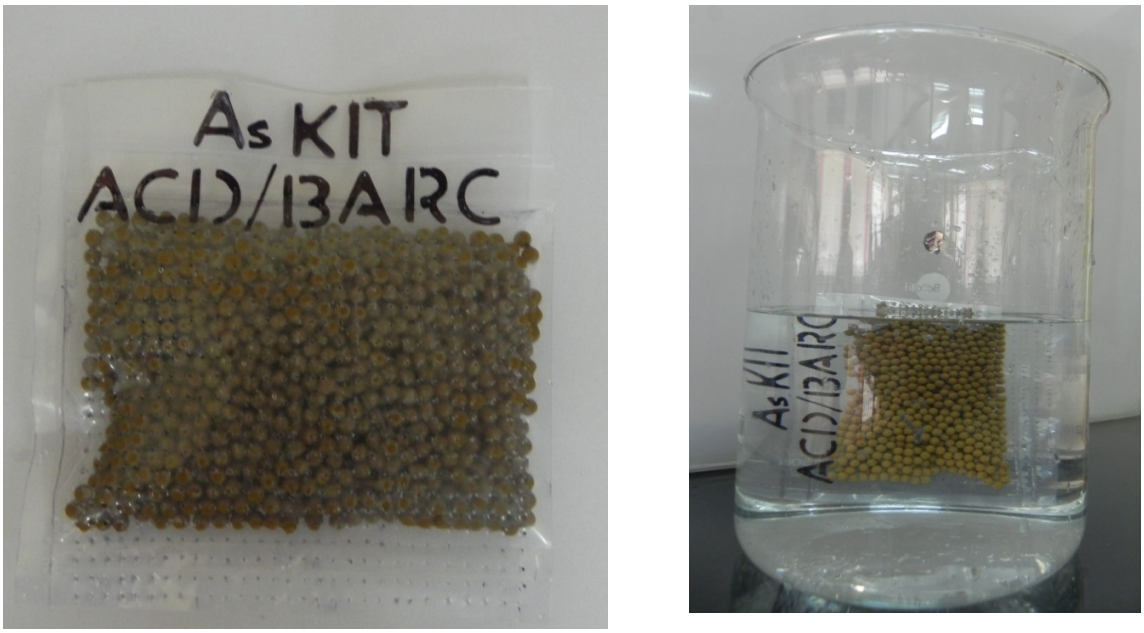

Fig. 6.6: Ready to use kit for arsenic removal from groundwater

Various physicochemical characteristics of groundwater having natural arsenic contamination used for this study are given in the table 6.9. It also gives the values of the same physicochemical parameters of the ground water samples observed after treatment with

Table 6.9: Physicochemical characteristics of groundwater before and after the treatment with Cal-Alg –Goe beads

Parameters	**Before treatment**	**After treatment**
pH	6.5-7.5	6.5-7.5
Conductance (μ S)	348-356	360-368
Redox potential (mV)	126-132	122-127
DOC (mg L^{-1})	9-11	10-12
Cl^{-1} (mg L^{-1})	18.9-21.3	17.4-21.0
PO_4^{3-} (mg L^{-1})	0.64-0.66	0.65-0.67
Na(mg L^{-1})	24.2-27.8	24.4-28.6
K (mg L^{-1})	0.75-0.82	0.74-0.89
Mg (mg L^{-1})	15.3-16.9	15.1-16.8
Ca (mg L^{-1})	39.1-42.6	40.2-44.7
Cu (μg L^{-1})	5.4-7.3	5.2-6.8
Pb (μg L^{-1})	2.8-3.5	2.6-3.0
Fe (mg L^{-1})	1.6-2.0	1.8-2.3

the beads for arsenic removal. From table 6.9, which gives the range of minimum and maximum values, it's clear that there is no major variation among these water samples. Ground water samples also did not show elevated levels of concentration of any particular properties after the treatment with the beads assuring the drinkability of the water. Special care had been taken for iron (Fe), calcium (Ca) and dissolved organic content (DOC). No elevation in the concentrations of Ca, Fe and DOC was observed in the potable water after the removal of arsenic suggesting no leaching of the components from the beads.

6.3.4 ^{241}Am decontamination kit

The hybrid materials developed as discussed above are utilized to demonstrate the field application at a larger scale for decontamination of potable water. After having decontamination of ^{241}Am from the water samples using Cal-Alg beads in a column, solutions were further passed through the activated charcoal column for purification of potable water. The demonstration schematic is given in Fig. 6.7

The important water quality parameters monitored of the potable water collected from three different sources are given in the table 6.10. From this table it is clear that except total hardness which is the measure of concentration of calcium and magnesium carbonate and total dissolved solid (TDS), there is not much variation in concentration of different parameters. There is a slight variation in the concentration of nitrate but still much below than the permissible limit of 10 μg mL^{-1} [63].

In order to verify the ruggedness of the developed Cal-Alg beads, sorption of Am^{3+} from spiked water samples (200 Bq L^{-1} of ^{241}Am) originated from different geochemical environment was tested. The water samples collected from the three different sources having marked variation in the concentration of total hardness and total dissolved content (TDS) as

discussed in table 6.10, were passed through the alginate column having the. Fig. 6.8 shows the sorption profile with time for three different sources of natural water. From this Fig. it is clear that there is no marked variation in case of groundwater and rainwater whereas in case lake water there is slight decrease in Am sorption, this decrease is attributed to the slightly elevated level of DOC in case of lake water which complexes with Am^{3+} and it does not allow the further binding with –OH and –COOH group of alginate.

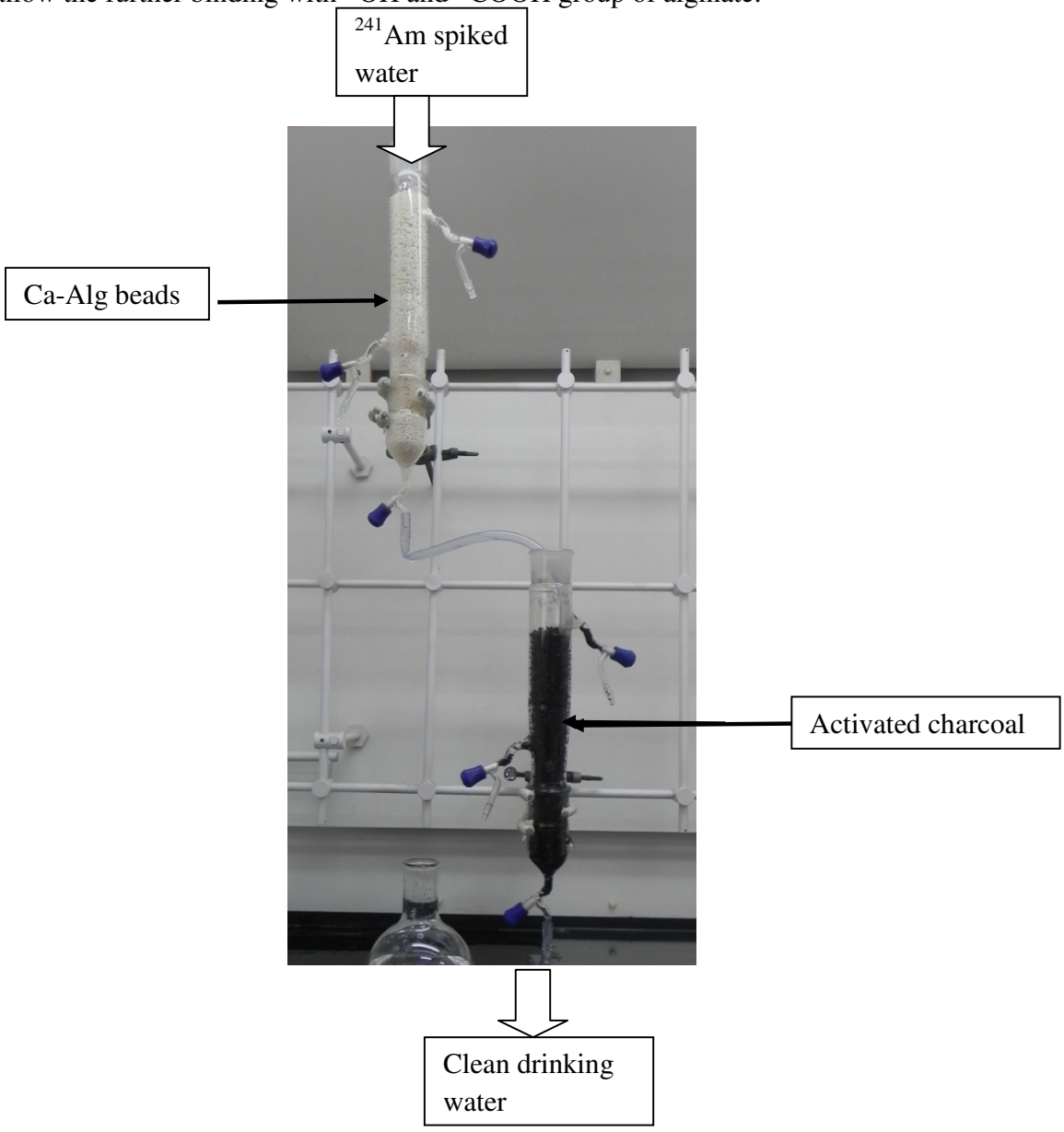

Fig. 6.7: Demonstration of ^{241}Am removal from spiked water samples

Table 6.10: Physicochemical parameters of the collected potable water

Parameters	Average Value (µg L^{-1})		
	Ground Water	**Rain Water**	**Lake Water**
pH	7.8 ± 0.4	4.5 ± 0.3	5.0 ± 0.4
Conductance (µS)	400 ± 30	200 ± 20	240 ± 21
Total Hardness	100 ± 10	70 ± 8.7	72 ± 6.2
HCO_3^-	70 ± 6	30 ± 4	34 ± 2.3
Dissolved organic carbon (DOC)	1.5 ± 0.02	0.8 ± 0.08	2.30 ± 0.12
Total Dissolved Solid	180 ± 20	80 ± 10	100 ± 5
Turbidity (NTU)	7 ± 2	3 ± 1	5 ± 1
PO_4^{3-}	0.45 ± 0.03	0.25 ± 0.08	0.25 ± 0.06
NO_3^-	6 ± 0.8	2.2 ± 0.8	3.8 ± 0.8
F^-	0.09 ± 0.01	0.05 ± 0.01	0.03 ± 0.01
Calcium	39.26 ± 3.20	27 ± 1.7	25 ± 1.4
Mangnesium	17.2 ± 12	15 ± 1.1	15 ± 1.3
Arsenic (ng L^{-1})	<5	<5	<5
Cadmium	<0.01	<0.01	<0.01
Gross alpha (Bq L^{-1})	<0.1	<0.1	<0.1
Gross beta (Bq L^{-1})	<1.0	<1.0	<1.0

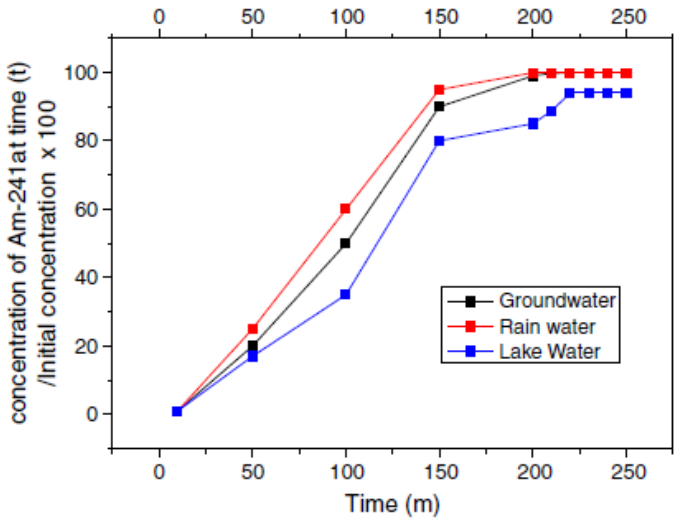

Fig. 6.8: Percentage retention of ^{241}Am by Cal-Alg column with time in case of water samples originated from different sources

The impact of DOC on the aquatic chemistry of transuranic has been discussed elsewhere [173,177,221]. Fig. 6.9 shows the experimentally evaluated ^{241}Am value at different levels of DOC concentration. Experiments at different levels of DOC were conducted keeping the concentration of ^{241}Am as 200 Bq L^{-1}. From this Fig. it is clear that there is decrease in the sorption of ^{241}Am with increase in concentration of DOC in water sample. Experimental results clearly indicate there is linear decrease in the sorption capacity of the column in the DOC range of 1–20 mg L^{-1} and thereafter between 30 and 50 mg L^{-1} only 7–8% ^{241}Am gets sorbed on the column. This phenomenon is again attributed to complexation of ^{241}Am with DOC, which makes ^{241}Am non-feasible to bind with functional groups.

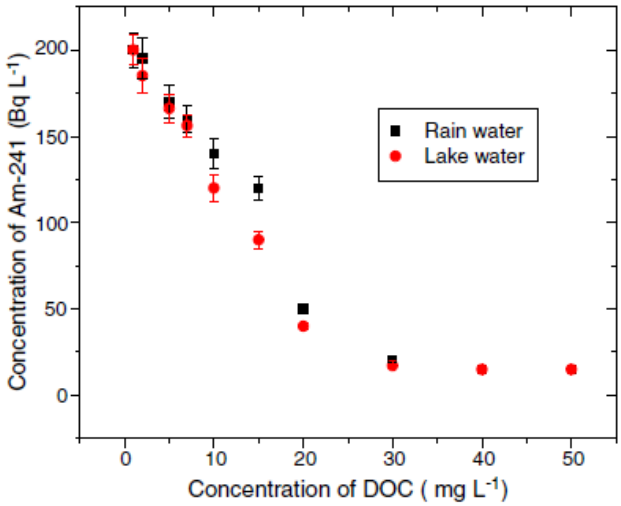

Fig. 6.9: Impact of DOC on sorption of ^{241}Am (200 BqL^{-1}) in Cal-Alg column

Table 6.11 gives the values obtained for various parameters. From the data it is clear that the parameters given in the table 6.10. Small variation in the parameters in both the cases parameters (Ca^{2+}, NO_3^-, Na^+ and Cl^-) are not much different from the original may be due to the absorption at the charcoal column for some of the metal ions.

Table 6.11: Physicochemical parameters of three different waters after passing through Cal-Alg and activated charcoal column

Parameters	Average Value (µg L^{-1})					
	Ground Water		Rain Water		Lake Water	
After passing through-	Calcium alginate column	Activated charcoal column	Calcium alginate column	Activated charcoal column	Calcium alginate column	Activated charcoal column
pH	4.7 ± 0.3	4.8 ± 0.4	4.5 ± 0.3	4.5 ± 0.3	5.0 ± 0.4	5.0 ± 0.4
Conductance (µS)	230 ± 25	220 ± 30	200 ± 20	180 ± 20	175 ± 21	175 ± 21
Total Hardness	70 ± 10	65 ± 10	78 ± 87	55 ± 8.7	62 ± 6.2	62 ± 6.2
HCO_3^-	55 ± 6	55 ± 6	35 ± 1.3	35 ± 1.3	30 ± 1.3	30 ± 1.3
Dissolved organic carbon (DOC)	1.0 ± 0.02	1.0 ± 0.02	0.8 ± 0.08	0.8 ± 0.08	1.30 ± 0.12	1.30 ± 0.12
Total Dissolved Solid	112 ± 20	110 ± 20	92 ± 10	78 ± 10	76 ± 5	76 ± 5
Turbidity (NTU)	3 ± 2	3 ± 2	3 ± 1	3 ± 1	5 ± 1	5 ± 1
Ca^{2+}	47.26 ± 3.20	39.26 ± 3.20	39 ± 1.7	27 ± 1.7	25 ±1.4	25 ± 1.4
NO_3^-	10.0 ± 0.8	6 ± 0.8	12.2 ± 0.8	2.2 ± 0.8	3.8 ± 0.8	3.8 ± 0.8
Cl^-	290	250	600	500	650	590
Na^+	450×10^3	250×10^3	390×10^3	290×10^3	360×10^3	300×10^3
Dissolved Oxygen	7 ± 1.9	7 ± 1.9	6.67 ± 1.1	6.9 ±1.1	6.4 ± 1.7	65 ±1.7
Gross alpha (Bq L^{-1})	<0.1	<0.1	<0.1	<0.1	<0.1	<0.1
Gross beta (Bq L^{-1})	<1.1	<1.1	<1.1	<1.1	<1.1	<1.1

6.3.5 TiO_2 NP decontamination kit

Lake & groundwater samples used for the study were collected in one litre polypropylene bottles and filtered through 0.45µm filter paper attached to suction filtration assembly (Millipore) before use. Different physicochemical properties were measured before and after contamination. They were used for spiking with TiO_2 NP. These water samples were spiked with TiO_2 NP and the beads were successfully tested to decontaminate. Table 6.12 gives the concentrations of TiO_2 NP before and after treatment with Cal-Alg-SM beads.

Table 6.12: Decrease in concentration of TiO_2 NP after the treatment in four different samples

Sample identification	**Spiked concentration of TiO_2 NP (ng mL^{-1})**	**Concentration of TiO_2 NP after treatment with the beads (ng mL^{-1})**
Groundwater -1	1000	32
Groundwater -2	1000	17
Groundwater-3	1000	26
Lake water	1000	Below detection limit (<10)
Experimental conditions: Sorbent dose: 5 mg mL^{-1}, Time: 8h, pH:4-5, Temperature: 25-30ºC.		

Table-6.13 shows various physicochemical characteristics of groundwater samples used for this study, both before and after the treatment with the Cal-Alg-SM beads for removal of TiO_2 NP. It was clear from table-6.8, which gives the range of the physicochemical parameters, that no major variation of any particular property was observed due to the treatment with the beads.

Table 6.13: Physicochemical characteristics of lake and groundwater before and after removal of TiO_2 NP using Cal-Alg-SM beads

Parameters	**Before treatment**	**After treatment**
pH	5.5-7.6	5.7-7.7
Conductance (µ S)	321-406	346-398
Redox potential (mV)	118-125	121-129
DOC (mg L^{-1})	8-10	9-12
Cl^{-1} (mg L^{-1})	17.5-20.6	18.1 -20.9
PO_4^{3-} (mg L^{-1})	0.52-0.57	0.52-0.57
Na(mg L^{-1})	23.2-28.2	23.4-28.7
K (mg L^{-1})	0.85-0.90	0.78-0.89
Mg (mg L^{-1})	14.4-15.9	15.3-16.4
Ca (mg L^{-1})	40.1-43.7	39.8-43.9
Cu (µg L^{-1})	5.5-8.6	5.3-7.9
Fe (mg L^{-1})	1.5-2.1	1.6-2.1
Si (mg L^{-1})	38.3-51.6	39.1-51.7
Experimental conditions: Sorbent dose: 5 mg mL^{-1}, Time: 8h, Initial TiO_2 NP concentration: 10 µg mL^{-1}, Temperature: 25-30ºC.		

No elevated level of concentration after the treatment, assures the drinkability of the water. Special care was taken for calcium (Ca), silica (Si) and alginate which are the components of the beads. Results showed no elevated level of concentrations of Ca, Si and DOC (dissolved organic content) in the water after treatment, suggesting no leaching of any of the components from the beads.

6.3.6 Ready to use suspension for decontamination of $^{239+240}$Pu and ^{241}Am

Humic acid coated goethite suspension which is a different kind of hybrid material can also be used in the suspension form for the decontamination of $^{239+240}$Pu and ^{241}Am as discussed in details in chapter 3. Uptake was checked in the spiked ground water samples. From table 6.14, it is clear that more than 99% of the spiked $^{239+240}$Pu and ^{241}Am were carried away with humic acid coated goethite suspension. Experimental results also showed that variation in the concentration of other metal ions like Ca, Mg, K and Na does not have any impact on the decontamination process as in all three groundwater extent of decontamination is same.

Table 6.14: Decontamination of $^{239+240}$Pu and ^{241}Am from the three groundwater samples

	Radionuclide					
	$Pu^{239+240}$			**Am^{241}**		
Initial Contamination (Bq L^{-1})	10	50	100	10	50	100
Concentration after treatment with HA coated goethite suspension(Bq L^{-1})						
Ground Water 1	< 0.1	< 0.1	< 0.1	< 0.1	< 0.1	< 0.1
Ground Water 2	< 0.1	< 0.1	< 0.1	< 0.1	< 0.1	< 0.1
Ground Water 3	< 0.1	< 0.1	< 0.1	< 0.1	< 0.1	< 0.1

Groundwater sample is subjected to ultrafiltration cell in filtration mode (allow all the solution to pass through the membrane) having a membrane of 500 NMWL to remove the humic coated goethite suspension. Table 6.15 shows the concentration of various elements

including concentration of DOC, Fe. From this table it is evident that there is no elevation in the concentration of any of these elements.

Table 6.15: Characteristics of the water samples after decontamination of $^{239+240}$Pu and ^{241}Am and after passing through the ultrafiltration membrane of 500 D NMWL

Parameters	**Average Value (μg L^{-1})**		
	Ground Water I	**Ground Water II**	**Ground Water III**
pH	7.2 ± 0.2	7.3 ± 0.3	7.2 ± 0.1
Conductance (μS)	390 ± 10	400 ± 18	390 ± 30
Total Hardness	110 ± 11	120 ± 14	110 ± 15
HCO_3^-	75 ± 6	82 ± 5	62 ± 3
Dissolved organic carbon(DOC)	1.8 ± 0.02	1.2 ± 0.08	1.3 ± 0.07
Total Dissolved Solid	160 ± 15	180 ± 11	140 ± 1.4
Turbidity (NTU)	4 ± 1	5 ± 1	3 ± 2
Dissolved oxygen	6.7 ± 1.3	6.2 ± 0.8	6.8 ± 1.9
PO_4^{3-}	0.34 ± 0.01	0.21 ± 0.03	0.26 ± 0.03
NO_3^-	10 ± 0.8	8 ± 0.8	7 ± 0.8
F^-	0.02 ± 0.01	0.04 ± 0.01	0.04 ± 0.01
Calcium	33.16 ± 2.08	31.16 ± 1.80	30.26 ± 1.67
Magnesium	14.2 ± 1.6	17.2 ± 1.2	15.2 ± 1.1
Arsenic (ng L^{-1})	<5	<5	<5
Cadmium	<0.01	<0.01	<0.01
Gross alpha (Bq L^{-1})	<0.1	<0.1	<0.1
Gross beta (Bq L^{-1})	<1.0	<1.0	<1.0

Chapter 7

Work summary

7. Work summary

Hybrid material has emerged to be the alternative material and going to revotionalize the technologies involve in removing various kind of contaimants from drinking water. The motivation of this dissertation was to develop new and highly efficient hybrid materials which are economical, easy to use and free from from excessive use of chemicals. Hybrid materials require only one unit operation system compared to the conventional process (e.g. coagulation–flocculation). An ideal hybrid material will have good stability, less pH and dosage dependency and it should be able to treat various type of wastewater. The unit or kit developed for decontamination using hybrid materials should operate without electricity to make it acceptable to a wider population. It is suggested that inorganic–organic hybrid materials are the most ideal combination among the hybrid systems. However, in anticipation of the demand on the environmental friendly materials in treating groundwater, inorganic–natural polymer hybrid materials could be the potential hybrid combinations. Natural polymers like alginate, chitosan could be easily obtained from the natural environment and are relatively less toxic and environmental friendly.

In this thesis work, hybrid materials were synthesized using ionotropic gelation method (e.g. alginate based beads) involving displacement reaction and sol gel method (e.g. silica microspheres). The synthesized materials have been characterized for size, zeta potential, surface morphology and chemical composition. Surface morphology and presence of various functional groups on the developed materials were characterized by using scanning electron microscope hyphenated with energy dispersive spectrometer (SED-EDS) and attenuated total reflectance Fourier transform infra red spectrometry (ATR-FTIR) respectively. The developed materials were used for removal of contaminants from aquatic

stream. The contaminants studied in this thesis are classified as radioactive (uranium, thorium, americium, plutonium), new generation nano particle contaminant (TiO_2 nano particles) and conventional (arsenic and fluoride). Various parameters (e.g. pH, contact time) for uptake were optimised. Isotherm, kinetics were tested for all the developed materials. The drinkability of the water was ensured and a separate chapter has been dedicated for the discussion on the impact on water quality parameters. It also demonstrate the use of the developed hybrid materials for decontamination of uranium, arsenic and fluoride from groundwater samples under field condition without disturbing the water quality parameters. The major results on these materials have been presented at the end of the corresponding Chapters in which they are described in. The uptake capacities of various hybrid materials investigated in the present thesis are summarized in Fig. 7.1.

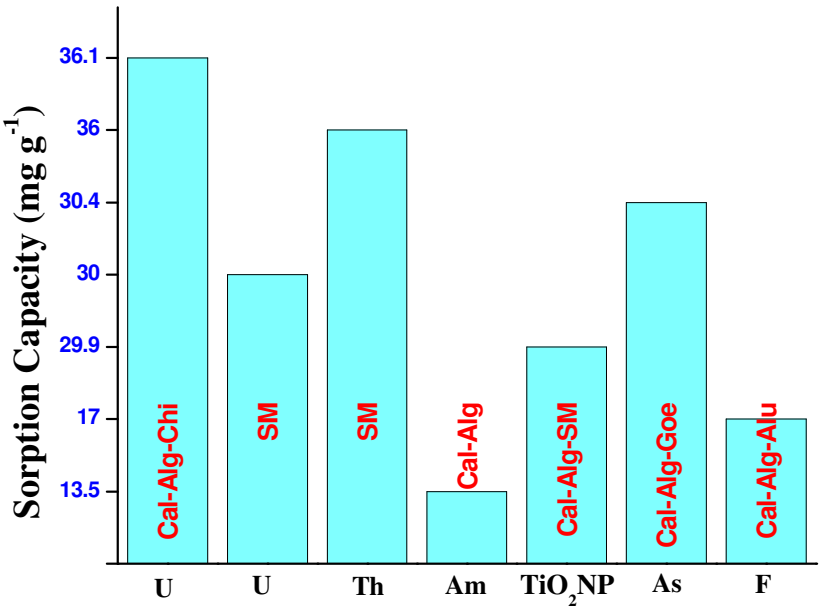

Fig. 7.1: Uptake capacities of various hybrid materials developed in this thesis

The following hybrid materials were synthesised and the results of the contaminants removal are summarised below.

(i) **Cal-Aig-Chi beads:** The developed hybrid material (Cal-Alg-Chi beads: 7% chitosan in 4% Calcium alginate) using two biogenic materials efficiently reduced the elevated levels of uranium in potable water to acceptable level (<15 ng mL^{-1}). The sorption capacity of the material was 36.04 mg g^{-1} for uranium at 25 – 35^{O} C. Reduction in uranium concentration was carried out without compromising quality of potable water. The beads were utilized for cleaning of uranium contaminated groundwater samples under field condition. Experimental evidence clearly indicates the interaction of uranyl ions with carbonyl and hydroxyl groups in chitosan. The blue shift in the vibration band of carbonyl groups of the amide group in FTIR spectrum of uranium sorbed Cal-Alg-Chi beads, validate the above observation. Sorbed uranium from Cal-Alg-Chi beads was efficiently recovered using 0.1N HNO_3.

(ii) **Silica microspheres:** Silica microspheres were synthesized using PVP and TEOS and applied as an effective sorbent for the removal of uranium and thorium from potable water in a batch process. The microspheres were characterized for their size by using dynamic light scattering, and presence of silicate structure is verified by recording their attenuated total reflectance-Fourier transform infrared spectrum. The surface morphologies of the prepared silica microspheres were studied by using scanning electron microscope. The results of this study clearly showed the potential of this material to decontaminate various aquatic streams from U and Th. Ultra-filtration technique was used to isolate the microsphere from the water samples. Equilibrium sorption follows Langmuir isotherms and the maximum U, and Th uptake was 30 and

36 mg g-1, respectively. Major physicochemical characteristics of the water were monitored before and after the decontamination process. Experimental results show no significant variations in any of the measured parameters.

(iii) **Cal-Alg beads:** The decontamination of ^{241}Am from potable water was successively achieved without disturbing the variouswater quality parameters by using calcium alginate beads. 60–98% Am was sorbed in the beads with a maximum observed at pH 4±0.2. Control on the concentration of Ca^{2+}, NO_3^{-1}, Na^+ and Cl^- was achieved by using activated charcoal column in conjugation with alginate column. It was observed that the variation of carbonate, bicarbonate, does not influence the sorption capacity (13.5 mg g^{-1}) of calcium alginate whereas the DOC decreased the sorption capacity in the range of 40–93% depending on DOC concentration. The mechanism of interaction of Am with calcium alginate is proposed based on attenuated total reflectance-Fourier transform infrared spectroscopy.

(iv) Humic coated nano goethite: Humic coated goethite suspension was successfully utilized to remove the $^{239+240}Pu$ and ^{241}Am from groundwater samples without compromising on the quality of drinking water. Polydispersive colloids of goethite were generated by controlled oxidation of $FeSO_4$ in the presence of NaOH. Size characterization, morphology and elemental profiling of goethite suspension and their aggregation with increase in the concentration of humic acid was studied by using dynamic light scattering and scanning electron microscope hyphenated with energy dispersive spectrometry. Experimental results clearly indicate that optimum size for goethite suspension is 30 nm for maximum uptake of $^{239+240}Pu$ and ^{241}Am. This selectivity was further enhanced when goethite suspension was treated with a humic

acid solution having a concentration of 60 μg mL^{-1}. Goethite suspension was separated from the groundwater using ultra filtration cell with membrane having 500 NMWL (nominal molecular weight limit).

(v) Cal-Alg-SM beads: The optimum composition of the developed hybrid material was 10% loading of silica microspheres into 4% Ca-alginate matrix. The results from the uptake study exhibit the potential of Cal-Alg-SM beads for TiO_2 nanoparticles removal from potable water at pH 3-5 without disturbing the water qualities. The sorption capacity of the beads for TiO_2 nanoparticles was evaluated as 29.9 mg g^{-1} at 25–35^{O} C from Langmuir isotherm model and this matched well with the experimentally determined value. The kinetics followed pseudo second order rate law. The FTIR and SEM-EDS analysis provided an understanding of the interaction between TiO_2 NP and silica microspheres impregnated into Ca-alginate. Mechanism of sorption could be proposed based on the zeta potential values of both silica microspheres and TiO_2 nanoparticles at different pH. Beads were successfully tested with lake and groundwater samples spiked with TiO_2 nanoparticles.

(vi) Cal-Alg-Goe beads: The results from the thesis work exhibit the potential of Cal-Alg-Goe beads (18% goethite in 4% alginate) for arsenic removal for a wide range of pH (3.0-7.5) from potable water without disturbing the water qualities. The sorption capacity of the beads for arsenic was found to be 30.44 mg g^{-1}. The sorption capacity determined experimentally matches well with the maximum sorption capacity obtained by fitting the data in the Langmuir model. Kinetic analyses indicate that the sorption process followed pseudo-first-order kinetics under the selected concentration range. The FTIR and XRF results provide an evidence of the interaction between

arsenic and goethite moieties resulting in both adsorption of different species of arsenic (H_3AsO_3, $H_3AsO_3^{2-}$, H_3AsO_4, $H_3AsO_4^{-}$,$H_3AsO_4^{2-}$, AsO_4^{3-}etc.) and inner sphere complexation with the iron. No change of the drinking water quality parameters was observed due to the treatment with the beads. Beads were successfully tested for real groundwater samples having elevated levels of arsenic collected from West Bengal, India.

(vii) Cal-Alg-Alu beads: The optimal condition for synthesis of calcium alginate alumina (Cal-Alg-Alu) beads was 2 % (wt/vol) alginate having alumina loading 22 % (wt/vol) alumina, stirring time: 1 h, drying temperature: 60 °C for 8 h. Works carried out in this thesis showed the potential of Cal-Alg-Alu beads for fluoride removal from contaminated potable water collected from fluoride affected area, without disturbing the water qualities. The sorption of fluoride on Cal-Alg-Alu was found to be free from pH dependency in the pH range 3.5 -9. Kinetic analyses indicate that the sorption process followed pseudo-second-order kinetics under the selected concentration range. The sorption capacity of alumina for fluoride was found to be 17.0 mg g^{-1} at 25 - 35 ^{O}C. The sorption isotherm was fitted well with Langmuir model. The FTIR and EDX results provide an evidence of the interaction between fluoride and alumina moieties resulting in the formation of aluminum-fluoro complexes. Fluoride sorption was not influenced by the presence of Na^+, K^+, Ca^{2+}, Cl^-, I^-, Mg^{2+}, CO_3^{2-}, SO_4^{2-} and PO_4^{3-} ions.

To sum up, the development of highly efficient hybrid materials to be used under field condition requires competence at multidisciplinary sciences (i.e. chemistry, biology,

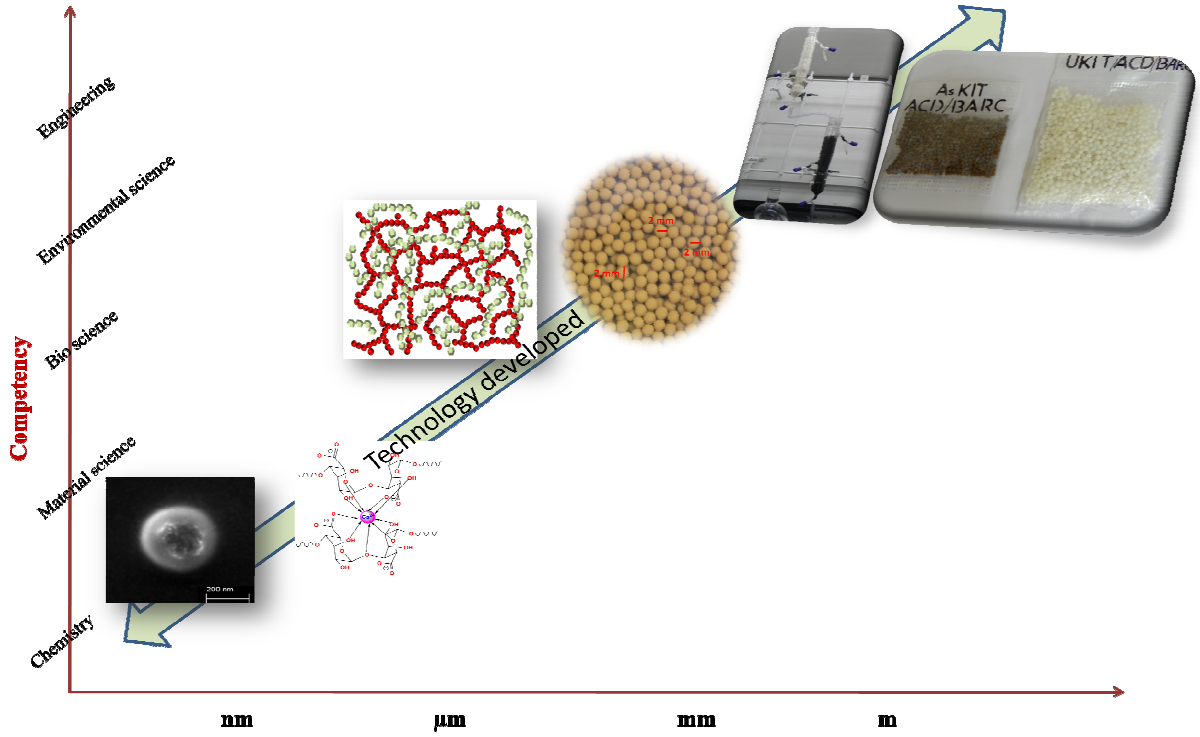

Fig. 7.2: Involvement of multidisciplinary science for the development of hybrid material with dimension scale

physics, materials science and engineering) at different length scales, as schematically shown in Fig. 7.2. To an extent, this thesis has been successful in demonstrating the development of novel hybrid materials with sufficient sorption capacities. This thesis also opens up following work in the future:

(i) How to efficiently and costly regenerate the exhausted hybrid materials still remains an interesting but challenging task. Development of more facile processes for the long-term performance of the hybrid sorbents, as well as their field application in contaminated water treatment has to be considered. To avoid hazards of the recovered contaminants and toxicology of used hybrid materials,

the hybrid material development should be accompanied by eco-friendly waste management methods.

(ii) The batch mode sorption conditions should be transferred to column operations so that hyrid material technology can be utilized for the welfare of human beings.

(iii) The newly developed hybrid sorbents seems to be an effective approach to respond to many technical problems for field operation. For more convenient and economic field application, the requirement of pH adjustment has to be avoided.

(iv) Still there is a need for further research on nanoparticles based hybrid materials with increased affinity, capacity, selectivity, faster kinetics and capability to work at column operations for water treatment on a large scale.

To the best of my knowledge and experimental finding, the future of hybrid material in water treatment is quite bright, but it needs to be complemented with the collaborative efforts of research, development and industry to materialize a dream of feasible and economical water treatment technology. By working together, it will be possible to resolve water contamination globally.

References

1. Frank Hoffmann, Maximilian Cornelius, Jurgen Morell and Michael Froba, Angew. Chem. Int. Ed. 45 (2006) 3216 – 3251.
2. N.D. Tzoupanos and A.I. Zouboulis, Water Res. 45 (2011) 3614–3626.
3. H. Tang and B. Shi, Editors: H.H. Hahn, E. Hoffmann, Proceedings of the 10th Gothenburg Symposium 2002, Gothenburg, Sweden, (2002) 17–28.
4. W.Y. Yang, J.W. Qian and Z.Q. Shen, J. Colloid Interf. Sci. 273 (2004) 400–405.
5. B. Gao, Q. Yue and J. Miao, Water Sci. Technol. 47 (2003) 127–132.
6. B.Y. Gao, H.H. Hahn and E. Hoffmann, Water Research 36 (2002) 3573–3581.
7. H. Zhao, J. Peng, A. Xue and J. Ni, Compos. Sci. Technol. 69 (2009) 1629–1634.
8. Y. Dong, A. Deng, H. Guo and X. Tang, Huanjing Kexue Xuebao/Acta Scientiae Circumstantiae 29 (2009) 2385–2392.
9. K.E. Lee, T.T. Teng, N. Morad, B.T. Poh and Y.F. Hong, Sep. Purif. Technol. 75 (2010) 346–351.
10. K.E. Lee, T.T. Teng, N. Morad, B.T. Poh and M. Mahalingam, Desalination 266 (2011) 108–113.
11. T. S. Srivatsan, Materials and Manufacturing Processes 24 (2009) 1231-1231.
12. M. Nanko, AZojomo 6 (2009) 1–8.
13. Guido Kickelbick, Prog. Polym. Sci. 28 (2003) 83–114.
14. P.A. Moussas and A.I. Zouboulis, Water Res. 43 (2009) 3511–3524.
15. Khai Ern Lee, Norhashimah Morad, Tjoon Tow Teng and Beng Teik Poh, Chemical Engineering Journal 203 (2012) 370–386.
16. Achintya N. Bezbaruah, Sita Krajangpana, Bret J. Chisholmb, Eakalak Khan and Juan J. Elorza Bermudez, Journal of Hazardous Materials 166 (2009) 1339–1343.

17. Mingwei Zhang, Kegong Fang, Minggui Lin, Bo Hou, Liangshu Zhong,Yan Zhu, Wei Wei and Yuhan Sun, J. Phys. Chem. C 117 (2013) 21529−21538.
18. Thomas A. Davis, Bohumil Volesky and Alfonso Mucci, Water Research 37 (2003) 4311–4330.
19. Ming Hua, Shujuan Zhang, Bingcai Pan, Weiming Zhang, Lu Lv and Quanxing Zhang, Journal of Hazardous Materials 211– 212 (2012) 317– 331.
20. Richard Hayes, Adham Ahmed, Tony Edge and Haifei Zhang, Journal of Chromatography A 1357 (2014) 36–52.
21. G. Guiochona and F. Gritti, J. Chromatogr. A 1218 (2011) 1915.
22. R.W. Brice, X. Zhang and L.A. Colón, J. Sep. Sci. 32 (2009) 2723.
23. Hua Zou, Shishan Wu, Qianping Ran and Jian Shen, J. Phys. Chem. C 112 (2008) 11623–11629.
24. F. Caruso, Adv. Mater. 13 (2001) 11.
25. E. Bourgeat-Lami, J. Nanosci. Nanotechnol. 2 (2002) 1.
26. G. Kickelbick and L. M. Liz-Marza´n, In Encyclopedia of Nanoscience and Nanotechnology; H. S. Nalwa, Ed.; American Scientific Publishers: Stevenson Ranch, CA, 2 (2004) 199-220.
27. Mark M. Benjamin, Ronald S. Sletten, Robert P. Bailey and Thomas Bennett, Wat. Res. 30 (11) (1996) 2609-2620.
28. Yanhui Li, Fuqiang Liu, Bing Xia, Qiuju Du, Pan Zhang, Dechang Wang, Zonghua Wang and Yanzhi Xia, Journal of Hazardous Materials 177 (2010) 876–880.
29. Siddhesh N. Pawar and Kevin J. Edgar, Biomaterials 33 (2012) 3279-3305.
30. T. J. Painter, O. Smidsrød and A. Haug, Acta Chem Scand 22 (1968) 1637-48.

31. B. Larsen, O. Smidsrød, T.J. Painter and A. Haug, Acta Chem Scand 24 (1970) 726-728.
32. O. Smidsrod and S. G.Whittington, Macromolecules 1969;2 (1969) 42-4.
33. A. Penman and G. R. Sanderson, Carbohydr Res 25 (1972) 273-82.
34. H. Grasdalen, B. Larsen and O. Smidsrød, Carbohydr Res 68 (1979) 23-31.
35. K. I. Draget, Alginates. In: G. O. Phillips, P. A. Williams, editors. Handbook of hydrocolloids, (2009) 379-95.
36. J. S. Boateng, K. H. Matthews, H. N. E. Stevens and G. M. Eccleston, J Pharm Sci 97 (2008) 2892-923.
37. P. Sikorski, F. Mo, G. Skjåk-Bræk and B. T. Stokke, Biomacromolecules 8 (2007) 2098-103.
38. I. Donati, S. Holtan, Y. A. Mørch, M. Borgogna, M. Dentini and G. Skjåk-Bræk, Biomacromolecules 6 (2005) 1031-40.
39. S. N. Pawar and K. J. Edgar Biomacromolecules 12 (2011) 4095-103.
40. Rajan S. Bhattarai, Nagasamy Venkatesh Dhandapani and Ayush Shrestha, Chronicles of Young Scientists 2(4) (2011) 192-196.
41. Imran Ali, Chem. Rev. 112 (2012) 5073−5091.
42. N. Nemerow and A. Dasgupta, Industrial and Hazardous Waste Treatment, Van Nostrand Reinhold: New York (1991).
43. G. Tchobanoglous and L. B. Franklin, Wastewater Engineering: Treatment, Disposal and Reuse; McGraw Hill, Inc.: New York (1991).
44. E. A. Laws, Aquatic Pollution: An Introductory Text, 3rd ed.; John Wiley & Sons: New York, (2000).

45. D. Z. John, Handbook of Drinking Water Quality: Standards and Controls, Van Nostrand Reinhold: New York, (1990).
46. R. L. Droste, Theory and Practice of Water and Wastewater Treatment; John Wiley & Sons: New York, (1997).
47. J. H. Duffus, Pure Appl. Chem. 74 (2002) 793.
48. I. Ali, and H. Y. Aboul-Enein, Instrumental Methods in Metal Ions Speciation: Chromatography, Capillary Electrophoresis and Electrochemistry; Taylor & Francis Ltd.: New York (2006).
49. I. Ali, H. Y. Aboul-Enein and V. K. Gupta, Nano Chromatography and Capillary Electrophoresis: Pharmaceutical and Environmental Analyses; John Wiley & Sons: Hoboken, NJ (2009).
50. J. L. Wang and C. Chen, Biotechnol Adv 24 (2006) 427–51.
51. Jianlong Wang and Can Chen, Biotechnology Advances 27 (2009) 195–226.
52. E. R. Kisin, A. R. Murray, M. J. Keane, X. C. Shi, D. Schwegler-Berry, O. Gorelik, S. Arepalli, V. Castranova, W. E. Wallace, V. E. Kagan and A. A. Shvedova, J. Toxicol. Environ. Health A, 70 (2007) 2071–2079.
53. T. A. Robertson, W. Y. Sanchez and M. S. Roberts, J. Biomed. Nanotechnol., 6 (2010) 452–468.
54. H. Shi, R. Magaye, V. Castranova and J. Zhao, Part. Fibre. Toxicol., 10 (2013) 15.
55. S. M. Gupta and M. Tripathi, Chin. Sci. Bull, 56 (2011) 1639–1657.
56. J. Riu, A. Maroto and F. X. Rius, Talanta, 69 (2006) 288–301.
57. M. J. Z. Ruth, B. Linda and D. Min, Exp. Ther. Med., 4 (2012) 551–561.
58. P. Z. Ray and H. J. Shipley, RSC Adv., 5 (2015) 29885- 29907.

59. R. A. Meyers, Ed. Encyclopedia of Environmental Pollution and Clean-up; John Wiley & Sons: New York (1999).

60. B. Damià, Ed. Emerging Organic Pollutants in Waste Waters and Sludge; Springer: New York (2005).

61. I. Ali, and H. Y. Aboul-Enein, Chiral Pollutants: Distribution, Toxicity and Analysis by Chromatography and Capillary Electrophoresis; John Wiley & Sons: Chichester, UK (2004).

62. Guidelines for Drinking-Water Quality, Forth Edition, World Health Organization ISBN 978924154851 (2011).

63. Guidelines for Drinking-water Quality, Third edition, World Health Organization ISBN: 9789241547611 (2008) 7–300.

64. Guidelines for drinking-water quality [electronic resource]: incorporating first addendum (vol. I) recommendations. World Health Organization (2006) 375–377, 448–1456.

65. C. Gok and S. J. Aytas, Hazard Mater 168 (2009) 369–375.

66. I. Ali, Sepn. Purfn. Rev. 43 (2014) 175–205.

67. J. Singh, L. Singh and S. Singh, J. Environ. Radioact. 76 (1995) 217–222.

68. S. Singh, A. Kumar and B. Singh, Environment International 28 (2002) 97–101.

69. Threshold limit values and biological exposure indices for 1992–1993. Cincinnati: Ohio: American Conference of Governmental industrial hygienists (1992).

70. Participants IRSIW: A workshop consensus report, Inhal Toxicol 12 (2000) 1–17.

71. M. Ortlieb, GIT Lab. J. Eur. 14 (2010) 42–43.

72. R. K. Shukla, V. Sharma, A. K. Pandey, S. Singh, S. Sultana and A. Dhawan, Toxicol. In Vitro 25 (2011) 231–241.

73. J. J. Wang, B. J. Sanderson and H. Wang, Mutat. Res. 628 (2007) 99–106.

74. R. Baan, K. Straif, Y. Grosse, B. Secretan, F. Ghissassi El and V. Cogliano, Lancet. Oncol. 7 (2006) 295–296.

75. T. Kaida, K. Kobayashi, M. Adachi and F. Suzuki, J. Cosmet. Sci. 55 (2004) 219–220.

76. R. Wolf, H. Matz, E. Orion and J. Lipozencic, Acta Dermatovenerol Croat 11 (2003) 158–162.

77. A. D. Maynard and E. D. Kuempel, J. Nanopart. Res. 6 (2005) 587–614.

78. J. S. Tsuji, A. D. Maynard, P. C. Howard, J. T. James, C. W. Lam, D. B. Warheit and A. B. Santamaria, Toxicol. Sci. 89 (2006) 42–50.

79. J. Zhao, L. Bowman, X. Zhang, V. Vallyathan, S. H. Young, V. Castranova and M. Ding, J. Toxicol. Environ. Health A 72 (2009) 1141–1149.

80. K. P. Lee, H. J. Trochimowicz and C. F. Reinhardt, Toxicol. Appl. Pharmacol. 79 (1985) 179–192.

81. E. Fabian, R. Landsiedel, L. Ma-Hock, K. Wiench, W. Wohlleben and B. van Ravenzwaay, Arch. Toxicol. 82 (2008) 151–157.

82. G. Oberdorster, Int. Arch. Occup. Environ. Health 74 (2001) 1–8.

83. G. Oberdorster, J. Ferin and B. E. Lehnert, Environ. Health Perspect 102 (Suppl 5) (1994) 173–179.

84. T. M. Sager, C. Kommineni and V. Castranova, Part Fibre. Toxicol. 5 (2008) 17.

85. IARC, Sci Publ. (2006) 86.

86. T. C. Long, J. Tajuba, P. Sama, N. Saleh, C. Swartz, J. Parker, S. Hester, G. V. Lowry and B. Veronesi, Environ. Health Perspect. 115 (2007) 1631–1637.

87. B. K. Mandal and K. T. Suzuki, Talanta 58 (2002) 201–235.

88. W. R. Cullen and K. J. Reimer, Chemical Reviews 89 (1989) 713–764.

89. S. Goldberg and C. T. Johnston, Journal of Colloid and Interface Science 234 (2001) 204–216.

90. P. L. Smedley and D. G. Kinniburgh, Applied Geochemistry 17 (2002) 517–568.

91. M. M. Ghosh and J. R. Yuan, Environmental Progress 6 (1987) 150.

92. D. G. Brookins, Eh–pH diagrams for geochemistry (1988) Berlin: Springer.

93. S. Wang and C. N. Mulligan, Science of the Total Environment 366 (2006) 701–721.

94. S. K. Gupta and K. Y. Chen 50(3) (1978) 493–506.

95. USEPA: Arsenic treatment technology evaluation handbook for small system. EPA 816-R-03-014 (2000) Washington, DC.

96. M. Dinesh and C. U. Jr. Pittman, Journal of Hazardous Materials 142 (2007) 1–53.

97. Guidelines for drinking water quality recommendations, World Health Organization, (1993), Geneva.

98. P. T. C. Harrison, Journal of Fluorine Chemistry 126 (2005) 1448–1456.

99. V. K. Saxena and S. Ahmed, Environmental Geology 49(9) (2001) 1084–1087.

100. D. K. Nordstrom, J.W. Ball, R. J. Donahoe and D. Whittemore, Geochimica et Cosmochimica Acta 53 (1989) 1727–1740.

101. N. V. R. Rao, N. Rao, K. S. P. Rao and R. D. Schuiling, Environmental Geology 21 (1993) 84–89.

102. D. K. Nordstrom and E. A. Jenne, Geochimica et Cosmochimica Acta 41 (1977) 175–188.

103. W. Binbin, Z. Baoshan, W. Hongying, P. Yakun and T. Yuehua, Environmental Geochemistry and Health 27 (2005) 285–288.

104. M. Meenakshi and R. C. Maheshwari, Journal of Hazardous Materials B 137 (2006) 456–463.

105. K. Rankama and G. Edgington, Soil Science 61 (1946) 341–353.

106. E. J. Reardon and Y. Wang, Environmental Science and Technology 34 (2000) 3247–3253.

107. V.K. Gupta, I. Ali, T.A. Saleh, A. Nayak and S. Agarwal, RSC Advances 2 (16) (2012) 6380–6388.

108. International Desalination Association (IDA), Desalination in 2008 global marker snapshot, 21st GWI/International Desalination Association Worldwide Desalting Plant Inventory (2008).

109. M.M. Pendergast and E.M. Hoek, Energy Environ. Sci. 4 (6) (2011) 1946–1971.

110. T.N. Carter, Desalination andmembrane technologies: federal research and adoption issues, Available at http://www.fas.org/sgp/crs/misc/R40477.pdf 2013.

111. P.S. Goh, A.F. Ismail and B.C. Ng, Desalination 308 (2013) 2–14.

112. Rasel Das, Md. Eaqub Ali, Sharifah Bee Abd Hamid, Seeram Ramakrishna and Zaira Zaman Chowdhury, Desalination 336 (2014) 97–109.

113. H. Y. Yang, Z. J. Han, S. F. Yu, K. L. Pey, K. Ostrikov and R. Karnik, Nat. Commun. 4 (2013) http://dx.doi.org/10.1038/ncomms3220 (Article number: 2220).

114. M. Jang, W. Chen and F. S. Cannon, Environ. Sci. Technol. 42(9) 2008 3369–3374.

115. V. Kumar, N. Talreja, D. Deva, N. Sankararamakrishnan, A. Sharma and N. Verma, Desalination 282 (2011) 27–38.

116. Phoebe Zito Raya and Heather J. Shipley, RSC Adv. 5 (2015) 29885.

117. G. M. Gadd, Phytologist 124 (1993) 25–60.

118. H. Mimura, H. Ohta, H. Hoshi, K. Akiba, Y. Wakui and Y. Onodera, J. Radioanal. Nucl. Chem. 247 (2001) 33–38.

119. R.K. Singhal, S. Joshi, K. Tirumalesh and R.P. Gurg, J. Radioanal. Nucl. Chem. 261 (1) (2004) 73–78.

120. A. Banerjee and D. Nayak, Bioresour. Technol. 98 (2007) 2771–2774.

121. Y. Konishi, S. Asai, Y. Midoh and M. Oku, Sep. Sci. Technol. 28 (1993) 1691–1702.

122. J.H. Min and J.G. Hering, Water Res. 32 (1998) 1544–1552.

123. L.K. Jang, D. Nguyen and G.G. Geesey, Water Res. 33 (1999) 2817–2825.

124. D. Nayak and S. Lahiri, J. Radioanal. Nucl. Chem. 267 (2006) 59–65.

125. M. N. V. R. Kumar, Reactive and Functional Polymers 46 (2000) 1–2.

126. M. Rinaudo, Prog. Polym. Sci. 31 (2006) 603–632.

127. W. S. W. Ngaha, L. C. Teonga and M. A. K. M. Hanafiah, Carbohydrate Polymers 83(2011) 1446–1456.

128. V. Bansal, P. K. Sharma, N. Sharma, O. P. Pal and R. Malviya, Advances in Biological Research 5 (2011) 28-37.

129. J. M. Wu and Y. Y. Wang, J. Environ. Sci. (China) 15 (2003) 633.

130. D. Kratochvil and B. Volesky, Trends Biotechnol. 16 (1998) 291.

131. Fengna Xi and Jianmin Wu, Journal of Chromatography A 1057 (2004) 41–47.

132. P. J. Hagrman, D. Hagrman and J. Zubieta, Angew. Chem. Int. Ed. 38 (1999) 2638 - 2684.

133. M. Outokesh, H. Mimura, Y. Niibori and K. Tanaka, J. Microencapsulation 17 (2006) 291–301.

134. L. Guangyu, H. Zhang, X. Yang and Y. Wang, Polymer 48 (2007) 5896–5904.

135. M. Emadi, E. Shams and M. K. Amini, Journal of Chemistry (2013) Article ID 787682.

136. J. Qu, W. Li, C. Y. Cao, X. J. Yin, Liang Zhao, J. Bai, Z. Qinc and W. G. Song, J. Mater. Chem. 22 (2012) 17222-17226.

137. H. Basu, R. K. Singhal, M. V. Pimple, Manisha V., M. K. T. Bassan, A. V. R. Reddy and T. Mukherjee, J. Radioanal. Nucl. Chem. 289 (2011) 231–237.

138. H. Li, W. Li, Y. Zhang, T. Wang, B. Wang, W. Xu, L. Jiang, W. Song, C. Shu and C. Wang, J. Mater. Chem. 21 (2011) 7878-7881.

139. H. Basu, R.K. Singhal, M. V. Pimple, A. Kumar and A. V. R. Reddy, J. Radioanal. Nucl. Chem. 303 (2014) 2283–2291.

140. T. Zhang, J. Ge, Y. Hu, Q. Zhang, S. Aloni and Y. Yin, Angew Chem. 120 (2008) 5890–5895.

141. H. Zou, S. Wu, Q. Ran and J. Shen, J. Phys. Chem. C 112 (2008) 11623–11629.

142. W. Li, C. Y. Cao, L. Y. Wu, M. F. Ge and W. G. Song, J. Hazard. Mater. 198 (2011) 143-150.

143. R. Naseem and S. S. Tahir, Water Res. 35 (2001) 3982–3986.

144. C. Rosaria, M. Sciortino, G. Alonzo, A. D. Schrijver and M. Pagliaro, Chem. Rev., 111 (2011) 765–789.

145. W. Li , F. Xia, J. Qu, P. Li , D. Chen , Z. Chen , Y. Yu , Y. Lu , R. A. Caruso and W. Song, Nano Res., **7** (2014) 903-916.

146. W. Li, D. Chen, F. Xia, J. Z. Y. Tan, P. P. Huang, W. G. Song, N. M. Nursam and R. A. Caruso, Environ. Sci.: Nano (2016) Advance Article, DOI: 10.1039/C5EN00171D.

147. R. W. Buddemeier and J. R. Hunt, Applied Geochemistry 3 (1988) 535.

148. C. Degueldre, B. Baeyens, W. Goerlich, J. Riga, J. Verbist and P. Stadelmann, Geochimica et Cosmochimica Acta, 53 (1989) 603–610.

149. J. F. McCarthy and C. Degueldre, In J. Buffle & H. P. van Leeuwen (Eds.), Environmental particles 2 (1993) 247–315 Boca Raton: Lewis.

150. B. A. Manning and S. Goldberg, Soil Science Society of America Journal, 60 (1996) 121–131.

151. K. A. Sullivan, and R. C. Aller, Geochimica et Cosmochimica Acta, 60 (1996) 1465–1477.

152. B. A. Manning, S. E. Fendorf and S. Goldberg, Environmental Science and Technology 32 (1998) 2383–2388.

153. E. Kumar, A. Bhatnagar, U. Kumar and S. Mika, Journal of Hazardous Materials 186 (2011) 1042–1049.

154. G. Moges, F. Zewge and M. Socher, Journal of African Earth Sciences 21 (1996) 479–482.

155. Y. Wang and E. J. Reardon, Applied Geochemistry 16 (2001) 531–539.

156. D. S. Bhargava and D. J. Killedar, Water Research 26 (1992) 781–788.

157. M. S. Onyango, Y. Kojima, A. Kumar, D. Kuchar, M. Kubota and H. Matsuda, Separation Science and Technology 41 (2006) 683–704.

158. A. Kumar, M. Bhatnagar, W. Ji Jung, S. Lee, S. J. Kim, G. Lee, H. Song, J. Y. Choi, J. Yang, and B. H. Jeon, Water Research 43 (2009) 490–498.

159. D. Thakre, S. Jagtap, A. Bansiwal, N. Labhsetwar and S. Rayalu, Journal of Fluorine Chemistry 131 (2010) 373–377.

160. X. Wu, Y. Zhang, X. Dou and M. Yang, Chemosphere 69 (2007) 1758–1764.

161. M.Yang, T. Hashimoto, N. Hoshi and H. Myoga, Water Research 33 (1999) 3395–3402.

162. H. Bamnolker, B. Nitzan, S, Gura and S. Margel, J. Mater. Sci. Lett. 16 (1997) 1412.

163. I. Tissot, C. Novat, F. Lefebvre and E. Bourgeat-Lami, Macromolecules 34 (2001) 5737.

164. X. F. Ding, K. F. Yu, Y. Q. Jiang, Hari-Bala, H. B. Zhang and Z. C. Wang, Mater. Lett. 58 (2004) 3618.

165. Y. W. Chen, E. T. Kang, K. G. Neoh and A. Greiner, AdV. Funct. Mater. 15 (2005) 113.

166. J. X. Yang, D. D. Hu, Y. Fang, C. L. Bai and H. Y. Wang, Chem. Mater. 18 (2006) 4902.

167. Y. Lu, J. McLellan and Y. N. Xia, Langmuir 20 (2004) 3464.

168. J. J. L. M. Cornelissen, E. F. Connor, H. C. Kim, V. Y. Lee, T. Magibitang, P. M. Rice, W. Volksen, L. K. Sundberg and R. D. Miller, Chem. Commun. (2003) 1010.

169. M. Chen, L. M. Wu, S. X. Zhou and B. You, Adv. Mater. 18 (2006) 801.

170. L. L. Hench and J. K.West, Chem. Rev. 90 (1990) 33–72.

171. C. Frank, R. A. Caruso and H. Mohwald, Science 282 (1998) 1111–1118.

172. L. Guangyu, H. Zhang, X. Yang and Y. Wang, Polymer 48 (2007) 5896–5904.

173. R. K. Singhal, J. Preetha, Rupali Karpe, P. Hema, A. Kumar, V. M. Joshi, A. K. Ranade and A. G. Hegde, J Radioanal Nucl Chem 279–1 (2009) 301-306.

174. R. K. Singhal, S. N. Joshi and A. G. Hegde, J Radioanal Nucl Chem 261(2) (2004) 263–267.

175. J. Guogang, G.Torri and P. Innocenzi, J Radioanal Nucl Chem 262–2 (2004) 433.

176. R. K. Singhal, R. Karpe, K. P. Muthe and A. V. R. Reddy, J Radioanal Nucl Chem 278 (2009) 214.

177. R. K. Singhal, R. Karpe, A. Kumar, J. Preetha and A. G. Hegde, Ann Nucl Energy 35 (2008) 1314.

178. S.M.L. Silva, C.R.C. Braga, M.V.L. Fook, C.M.O. Raposo, L.H. Carvalho and E. L. Canedo, Application of Infrared Spectroscopy to Analysis of Chitosan/Clay Nanocomposites, Infrared Spectroscopy-Materials Science, Engineering and Technology, Prof. Theophanides Theophile (Ed.), InTech. ISBN: 978-953-51-0537-4. (2012).

179. K. Xu, M. Kim Hanna and D. Nag, Industrial Crops and Products 21 (2005) 185–192.

180. T. Tsuchida, Solid State Ionics, 63 (1993) 464–470.

181. M. Zhareslu, P. M. Crisan, V. Fruth and S. Preda, Journal of Optoelectronics and Advanced Materials 5 (2003) 1411–1416.

182. S. Lagergren and Handlingar, 24(4) (1898) 1–39.

183. D. G. Lewis and V. C. Farmer, Clay Miner 21 (1986) 93.

184. G. Lefevre, Adv Colloid Interface Sci 107 (2004) 109.

185. G. Limousin, J.-P. Gaudet, L. Charlet, S. Szenknect, V. Barthe`s and M. Krimissa, Applied Geochemistry 22 (2007) 249–275.

186. V. K. Gupta, S. Sharma, I. S. Yadav and M. Dinesh, J. Chem. Technol. Biotechnol. 71 (1998) 180–186.

187. M. C. Kimling, N. Scales, T. L. Hanley and R. A. Caruso, Environ. Sci. Technol. 46 (2012) 7913–7920.

188. Y. S. Ho and G. McKay, Process Biochem. 34 (1999) 451–465.

189. T. J. Wolery, Report UCRLMA-110662 part 1. Lawrence Livermore National Laboratory, California. (1992).

190. S. Reza, Y. Seyed, J. Ahmadib, F. Shemirania, M.R. Jamalic and M.S. Niasari, Talanta 80 (2009) 212–217.

191. R. K. Singhal, P. K. Sharma, M. K. T. Bassan H. Basu and A. V. R. Reddy, J Radioanal Nucl Chem 288 (2011) 149–156.

192. G. Meinrath, JRadioanal Nuc Chem 211 (1996) 349–362.

193. G. Meinrath, J Radioanal Nuc Chem 224 (1997) 119–126.

194. H. A. Elliot, M. R. Liberati and C. P. Huang, J Environ Qual 15 (1986). 214–219.

195. E. Erdem, N. Karapinar and R. Donat, J Colloid Interface Sci 280 (2004) 309–314.

196. Guido Kickelbick, Hybrid Materials: Synthesis, Characterization, and Applications, ISBN: 978-3-527-61048-8 (2007).

197. E. Osthols (1995) Geochim Cosmochim Acta 59 (1995) 1235–1249.

198. E. Osthols, A. Manceau, F. Farges and L. Charlet, J Colloid Interface Sci 194 (1997) 10–21.

199. M. Quigley, B. D. Honeyman and P. H. Santschi, Aquat Geochem 1 (1996) 277–301.

200. R. Donat, A. Akdogan, E. Erdem and H. Cetisli, J Colloid Interface Sci 268(1) (2005) 43–52.

201. F. Barbier, G. Duc and R. M. Petit, Colloids Surf A Physicochem Eng Aspects 166(1–3) (2000) 153–159.

202. H. Chen, F. Tendeyong and S. Yiacoumi, Environ. Sci. Technol. 31 (1997) 1433–1439.

203. L.B. Asprey and R.A. Penneman, J. Am. Chem. Soc. 83 (1961) 2200–2206.

204. L.B. Asprey and R.A. Penneman, Inorg. Chem. 1 (1962) 134–140.

205. Y. Wu, H. Mimuraand and Y. Niibori, J. Ion Exch. 18 (4) (2007) 396–401.

206. P. Yong and L.E. Macaskie, J. Chem. Technol. Biotechnol. 7 (1998) 15–26.

207. L.K. Jang, S.L. Lopez, S.L. Eastman and P. Pryfogle, Biotechnol. Bioeng. 37 (1991) 266–273.

208. S. Schiewer and B. Volesky, Environ. Sci. Technol. 30 (1996) 2921–2927.

209. L. Cao, D. Chen, W. Li and R. A. Caruso, ACS Appl. Mater. Interfaces 6 (2014) 13129–13137.

210. Y. Yu, C. Cao , W. Li , P. Li, J. Qu and W. Song, Nano Res. 5 (2012) 434-442.

211. I. Puigdom'enech, (2004) MEDUSA. http://www.w1.156.telia.com/ u15651596.

212. J. Gim'enez, M. Mart'ınez, J. de Pablo, M. Rovira and L. Duro, Journal of Hazardous Materials 141 (2007) 575–580.

213. M. Streat, K. Hellgardt and N. L. R. Newton, Process Safety and Environmental Protection 86 (2008) 21– 30.

214. M. P. Asta, J. Cama, M. Martinez and J. Gimenez, Journal of Hazardous Materials, 171 (2009) 965–972.

215. M. Lezehari, M. Baudu, O. Bouras and J. P. Basly, Journal of Colloid and Interface Science 379(1) (2012) 101–106.

216. C. Y. Hu, S. L. Lo and W. H. Kuan, Journal of Colloid and Interface Science 283 (2005) 472–476.

217. W. Zhang, M. Sun and R. Prins, The Journal of Physical Chemistry B 106 (2002) 11805–11809.

218. Guidelines for drinking-water quality Volume 3 Surveillance and control of community supplies, World Health Organization, Geneva (1997) ISBN 92 4 154503 8 (v. 3).

219. Indian Standard for Drinking Water Specification, IS 10500 (2012).

220. Indian Standard for Drinking Water Specification, IS 10500 (1991).

221. J. Chen and S. Yiacoumi, Sep. Sci. Technol. 32 (1997) 51–69.

222. Status of groundwater quality in India, Part-I, Groundwater quality series, Central Pollution Control Board, GWQS/ 09/2006-2007.

223. Guidelines for Water Quality Monitoring, Central Pollution Control Board, MINARS/27/2007-08.

224. U. K. Chowdhury, B. K. Biswas, T. R. Chowdhury, G. Samanta, B. K. Mandal, G. C. Basu, C. R. Chanda, D. Lodh, K. C. Saha, S. K. Mukherjee, S. Roy, S. Kabir, Q. Quamruzzaman and D. Chakraborti, Environ Health Perspect. 108(5) (2000) 393–397.

225. R. T. Nickson, J. M. McArthur, P. Ravenscroft, W. G. Burgess and K. M. Ahmed Applied Geochemistry, 15(4) (2000) 403–413.

226. Dipankar Chakraborti, Subhash C Mukherjee, Shyamapada Pati, Mrinal K Sengupta, Mohammad M Rahman, Uttam K Chowdhury, Dilip Lodh, Chitta R Chanda, Anil K Chakraborti and Gautam K Basu, Environ Health Perspect. 111(9) (2003) 1194–1201.

227. K. Brindha, R. Rajesh, R. Murugan and L. Elango, Environmental Monitoring and Assessment 172(1) (2011) 481-492.

228. N. Kundu, M. Panigrahi, S. Tripathy, S. Munshi, M. Powell and B. Hart, Environmental Geology 41(3) (2001) 451–460.

229. N. Janardhana Raju, Sangita Dey and Kaushik Das, Current Science 96(7) (2009) 979-985.

230. M. Alrakabi, G. Singh, A. Bhalla, S. Kumar, S. Kumar, A. Srivastava, B. Rai, N. Singh, J. S. Shahi and D. Mehta, J Radioanal Nucl Chem 294 (2012) 221–227.